NOTICE

The quality of this microfiche is heavily dependent upon the quality of the original thesis submitted for microfilming. Every effort has been made to ensure the highest quality of reproduction possible.

If pages are missing, contact the university which granted the degree.

Some pages may have indistinct print especially if the original pages were typed with a poor typewriter ribbon or if the university sent us a poor photocopy.

Previously copyrighted materials (journal articles, published tests, etc.) are not filmed.

Reproduction in full or in part of this film is governed by the Canadian Copyright Act, R.S.C. 1970, c. C-30. Please read the authorization forms which accompany this thesis.

THIS DISSERTATION
HAS BEEN MICROFILMED
EXACTLY AS RECEIVED

AVIS

La qualité de cette microfiche dépend grandement de la qualité de la thèse soumise au microfilmage. Nous avons tout fait pour assurer une qualité supérieure de reproduction.

S'il manque des pages, veuillez communiquer avec l'université qui a conféré le grade.

La qualité d'impression de certaines pages peut laisser à désirer, surtout si les pages originales ont été dactylographiées à l'aide d'un ruban usé ou si l'université nous a fait parvenir une photocopie de mauvaise qualité.

Les documents qui font déjà l'objet d'un droit d'auteur (articles de revue, examens publiés, etc.) ne sont pas microfilmés.

La reproduction, même partielle, de ce microfilm est soumise à la Loi canadienne sur le droit d'auteur, SRC 1970, c. C-30. Veuillez prendre connaissance des formules d'autorisation qui accompagnent cette thèse.

LA THÈSE A ÉTÉ
MICROFILMÉE TELLE QUE
NOUS L'AVONS REÇUE

CRACK PROPAGATION

IN

ISOTROPIC LINEARLY ELASTIC SOLIDS

By

S. J. Mshana

A thesis submitted to the School of Graduate Studies of the University of Ottawa in Partial fulfillment of the requirements for the degree of

MASTER OF APPLIED SCIENCE

IN

MECHANICAL ENGINEERING

University of Ottawa
Ottawa, Ontario, CANADA

August, 1979

Crack Propagation in Isotropic Linearly Elastic Solids

ABSTRACT

1. The kinetics theory of thermally activated time dependent fracture propagation was extended to describe the crack size distribution in homogeneous isotropic linearly elastic solids. In the theory the crack propagation process is represented by a differential equation that describes the crack size distribution as a function of time for single step processes. Because of the essential physical similarity of crack propagation with diffusion and heat transfer, the functional solution of the fracture equation can be developed advantageously by utilizing the mathematical theory of diffusion and heat transfer. The results describe the crack-size distribution as a function of the surface free energy (bond energy), temperature, time, as well as the loading and geometrical boundary conditions of the test specimen.

2. A complete kinetics analysis is carried out for the description of the kinked crack front propagation rate over the consecutive energy-barrier system of the crystal lattice. The steady state kink concentration distribution and the crack propagation velocity are determined by using discrete analysis approach and by a continuous function description. The analysis shows that the two methods give the same results except when the rate of bond breaking is less than the rate of bond healing. The crack propagation velocity and the kink concentration distribution are expressed as functions of the applied stress,

temperature, the surface free energy (bond energy) and the defective nature of the material. There is a good agreement between Region I of stress corrosion cracking for porcelain in water and the steady state crack front spreading analysis. The threshold stress intensity appears to be controlled by the material properties, the crack geometry and the chemical environment.

3. The kinetics analysis of non-steady state crack propagation is carried out to describe the crack size distribution in stress corrosion cracking. The analysis shows that the crack size distribution is a function of the applied stress, temperature, time, the activation free energy of the corroded material and the chemical environment. Typical calculation results show that steady state is reached within a small fraction of a second.

Table of Contents

ACKNOWLEDGEMENTS

The author would like to express his gratitude to his advisor, Dr. A.S. Krausz, for his help throughout every stage of this thesis; his suggestions and encouragement were much appreciated.

The scholarship provided by the Government of Switzerland through the University of Dar-es-Salaam is very much acknowledged.

Finally, the author would like to express his appreciation to Mrs. Lee Sprouse and Mrs. Denise Champion-Demers for the skillful typing of the thesis.

Nomenclature

a_x	interatomic distance in the x-direction
a_y	interatomic distance in the y-direction
a_o	equilibrium interatomic distance
a_{int}	critical interatomic distance
b	semiaxis of an elliptical crack
	distance between two atomic planes
C	crack length
C_{cr}	critical crack length
h	Plank's constant
i	counter
j	counter
k	Boltzmann's constant
k_b	rate constant for the bond breaking process
k_h	rate constant for the bond healing process
k^+	sum of the bond breaking and bond healing rate constants
k^-	difference between the rate of bond breaking and the rate of bond healing
${}_1k_1$	combined rate constant for the threshold region
ℓ	distance between two adjacent kinks
n_c, n_p	number of bonds broken or healed per unit activation
n_t	total number of specimens
n(x,t)	reduced crack tip concentration
r_p	diameter of the crack tip plastic zone
t	time
v_x, v_c, v	crack propagation velocity

X	crack size
A	cross section area
ΔE_b	potential energy change associated with the bond breaking process
ΔE_h	potential energy change associated with the bond healing process
E	Young's modulus of elasticity
F	applied force
F_o	maximum applied force
F_i	the net flow of crack tips over the i-th barrier
F_{ss}	steady state flow of crack tip
G	crack driving force
G_{IC}	critical crack driving force for mode I crack propagation
ΔG	apparent free energy
$\Delta G^{\ddagger}_b$	free energy of activation for the bond breaking process
$\Delta G^{\ddagger}_h$	free energy of activation for the bond healing process
J_{IC}	critical energy release due to mode I crack propagation
K_I	stress intensity for mode I crack propagation
K_{IC}	critical stress intensity for mode I crack propagation
N_A	number of bonds intersecting unit area of the crack plane
N_i	number of intact bonds initially present in the cross section
	number of crack tips in the i-th valley
N	concentration of crack tips
N_o	total number of bonds initially present in the cross section
N_w	number of bonds per unit width of the crack front

N_w^*	equilibrium kink concentration
N_t	total number of specimens
$Q^{\ddagger}$	partition function taken with respect to the ground level
Q_r	partition function for the reactant state
T	temperature
U_E	elastic strain energy
U_s	surface energy
U	total energy of the crack system
W_b	mechanical energy absorbed during the bond breaking process
W_h	mechanical energy absorbed during the bond healing process
α	proportionality constant
n	number of molecules
Γ	surface energy per unit area
Γ_p	plastic work in forming a unit surface area of the crack
κ_b	transmission coefficient for the bond breaking process
κ_h	transmission coefficient for the bond healing process
μ	chemical potential
ξ	generalized coordinate
ρ	concentration of crack tips
	crack tip radius
σ	applied normal stress
σ_e	normal stress at the end of a crack
σ_{yp}	yield stress
σ_{yy}	normal stress in the y-direction
τ_o	h/kT

Chapter 1

Introduction

Modern fracture mechanics was established in 1921 when Griffith [1] developed the classical theory of crack propagation. His theory was based on two conditions. First, that the material is an isotropic linear elastic continuum and secondly that crack propagation will occur if the total mechanical energy composed of the stored elastic energy and the work done by the applied load is sufficient to provide the energy that is required for crack growth.

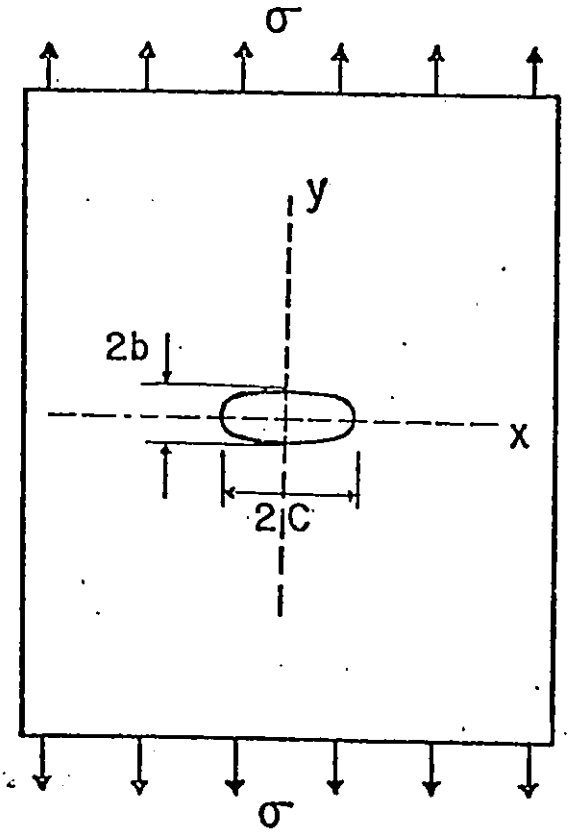

Figure 1.1 Plate containing an elliptical hole and subjected to uniform tension.

To confirm the theory experimentally Griffith used glass, a material which obeys Hooke's law closely at all stress levels.

According to Inglis [2] the total mechanical energy released when an elliptical crack is created in a thin plate subjected to a constant applied stress (Fig. 1.1) is expressed as

$$U_E = \frac{-\pi C^2 \sigma^2}{E} \tag{1.1}$$

for unit thickness of the plate. The potential energy of the surface of the crack, also per unit thickness of the plate is

$$U_s = 4 C \Gamma \tag{1.2}$$

Hence the total free energy of the crack system is

$$U = 4 C \Gamma - \frac{\pi C^2 \sigma^2}{E} \tag{1.3}$$

The Griffith equilibrium condition is

$$\frac{\partial U}{\partial C} = 0 \tag{1.4}$$

or

$$4\Gamma - \frac{2 \pi C \sigma^2}{E} = 0 \tag{1.5}$$

For a given stress σ, therefore, the equilibrium half crack size C_{cr} is

$$C_{cr} = \frac{2 \Gamma E}{\sigma^2 \pi} \tag{1.6}$$

Consequently, (Fig. 1.2) cracks smaller than C_{cr} will reduce in size while those greater than C_{cr} will grow, at a stress σ.

Orowan [3] extended this theory for the atomic scale description of crack initiation and propagation process. He suggested that when a crack opens up and the material separates locally, the bonds are broken and the interatomic forces vary according to Fig. 1.3. When the interatomic force F is maximum, F_o, the atoms are displaced to the critical distance a_{int} and further separation could take place at a smaller force. The area below the curve is the work of fracture (equal to $2a_o^2 \Gamma$).

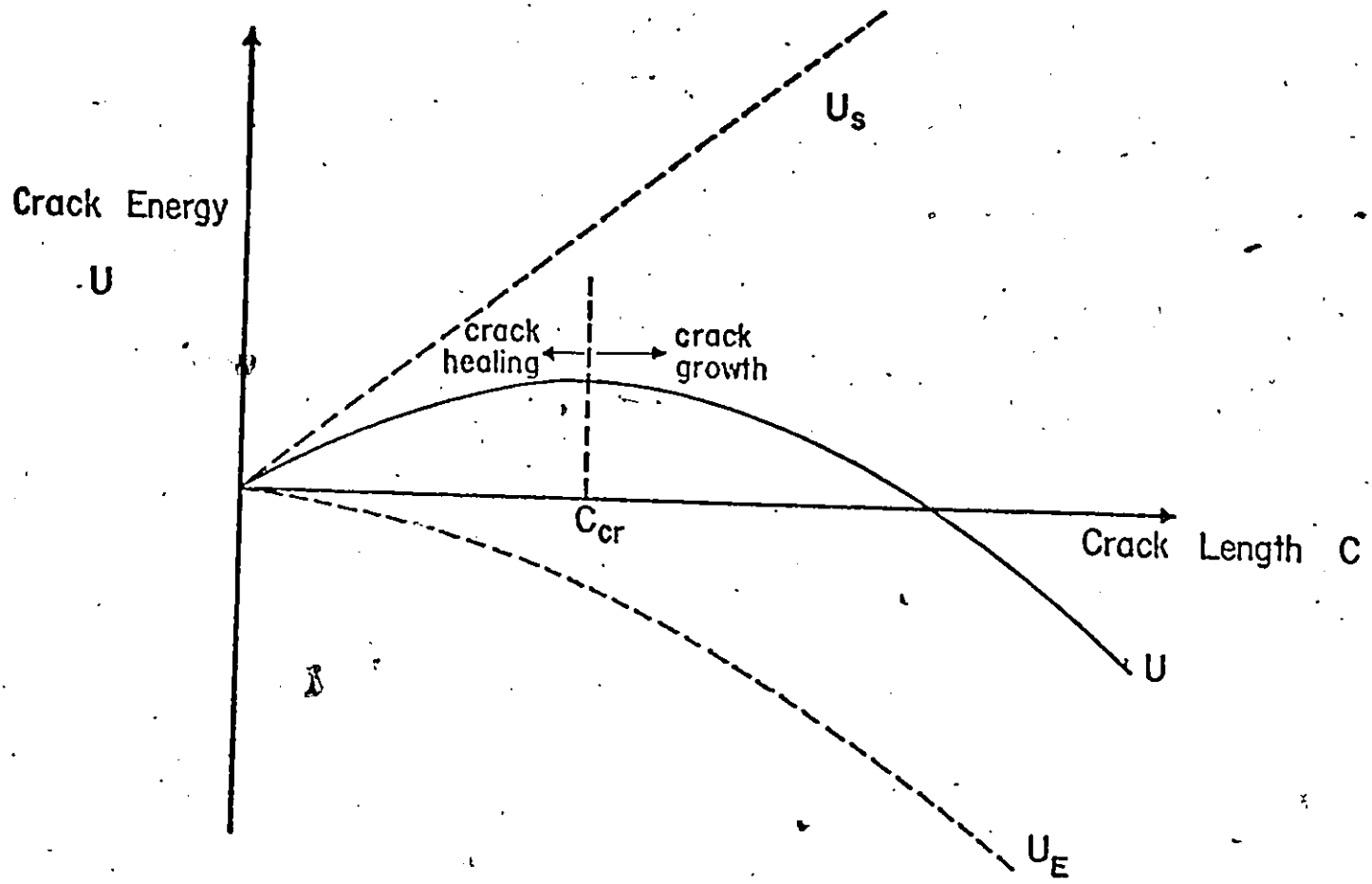

Figure 1.2 Energetics of Griffith crack in uniform tension σ.

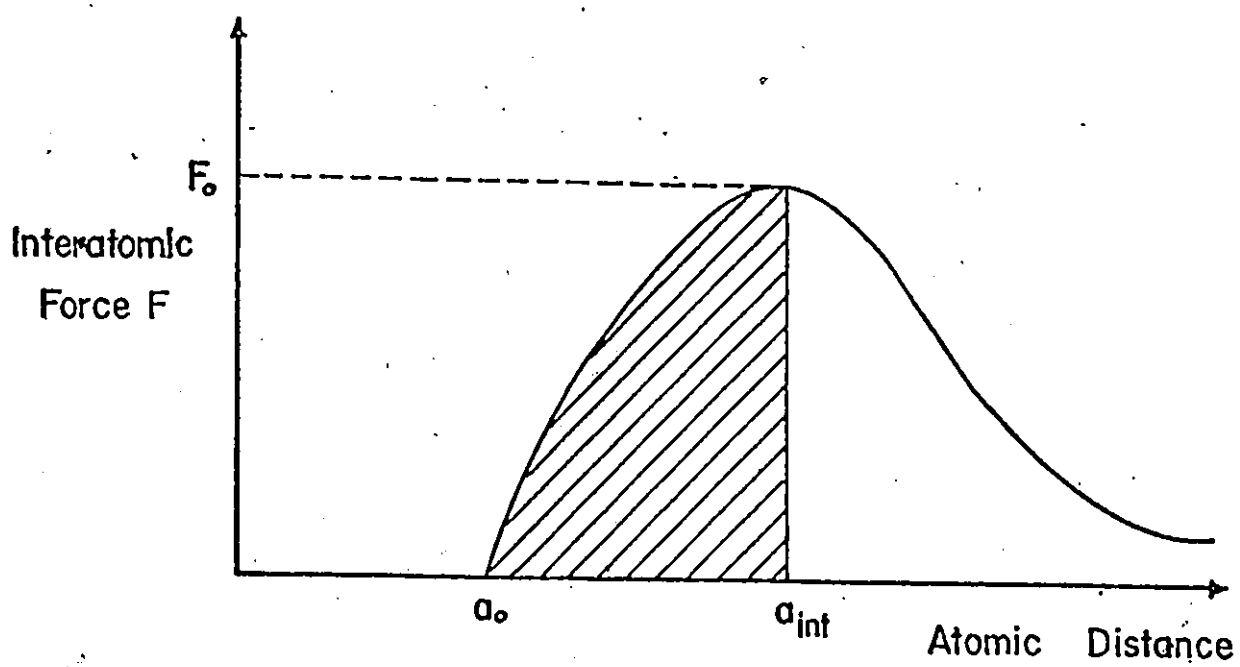

Figure 1.3 The interatomic force acting between two atoms as a function of the interatomic distance.

At the maximum of the curve in Fig. 1.3, the amount of energy represented by the shaded area below the curve must be present between all neighbouring pairs of molecular (or atomic) planes perpendicular to the force. If Hooke's law is assumed to be valid up to the theoretical maximum stress, σ_{max}, then

$$\sigma_{max} = F_o \times \text{number of bonds per unit area} \tag{1.7}$$

The elastic strain energy stored in a volume, having a unit area and a height equal to the distance b between two atomic planes is then of the order of

$$\frac{b\,\sigma^2_{max}}{2E} \tag{1.8}$$

If it is assumed that the shaded area is about one half of the total area below the curve and, therefore, approximately equal to $a_o\Gamma$, the relationship

$$\frac{b\,\sigma^2_{max}}{2E} \simeq \Gamma \tag{1.9}$$

gives the order of magnitude of the critical molecular stress as

$$\sigma_{max} = \left(\frac{2\,E\,\Gamma}{b}\right)^{\frac{1}{2}} \tag{1.10}$$

In the case of an elliptical crack (Figure 1.1) Inglis [2] calculated the stress at the end of the crack to be

$$\sigma_e = 2\,\sigma\,(C/\rho)^{\frac{1}{2}} \tag{1.11}$$

where ρ is the crack tip radius. Orowan's condition for the crack extension then is $\sigma_{max} = \sigma_e$ so that

$$\sigma = \left[\frac{E\,\Gamma}{2C}\left(\frac{\rho}{b}\right)\right]^{\frac{1}{2}} \tag{1.12}$$

This relationship is Orowan's version of the Griffith criterion for crack growth (Eq. (1.6)). Both the Griffith and Orowan relations lead to the same fracture stress when the radius of curvature at the crack root is

$\rho = \frac{4}{\pi} b$. For very sharp cracks ($\rho < \frac{4}{\pi} b$), the Griffith's criterion (strain energy criterion) should control the crack advance, whereas for cracks with $\rho > \frac{4}{\pi} b$, Orowan's relationship should be used to determine the stress at which crack propagation occurs.

Irwin [4] introduced the concept of stress intensity. For the case of a crack in an elastic plate where the stress components ahead of the crack correspond to a condition of plane stress, the stress intensity K_I is defined as

$$K_I = \sigma \sqrt{\pi C} \tag{1.13}$$

When the applied stress σ is increased so that the crack is able to move rapidly, the stress intensity is critical. Equation 1.13 is then written as

$$K_{IC} = \sigma \sqrt{\pi C} \tag{1.14}$$

From Equation (1.6) it follows that

$$K_{IC}^2 = 2E\Gamma = \sigma^2 \pi \tag{1.15}$$

Thus, the critical stress intensity can be measured from the material properties. Irwin defined the crack extension force G as

$$G = \frac{dU_E}{dC} = \frac{\pi \sigma^2 C}{E} \tag{1.16}$$

This is the force required to move the edge of the crack through the plate. Comparing Eq. (1.16) to the Griffith's relationship (Eq. (1.6)), the critical crack driving force is expressed as

$$G_{IC} = \frac{\sigma^2 \pi C}{E} = 2\Gamma \tag{1.17}$$

The crack will, therefore, propagate only if the crack driving force is greater than twice the surface energy per unit area. Both the critical stress intensity and the critical crack driving force may be considered

to be parameters (determined by the material constants) that measure the resistance of the material to crack extension.

When the maximum stress at the tip of an equilibrium crack corresponds to the theoretical strength of the material, the force-separation relationship for the atomic bonds, as Griffith noted, may become non-linear. In such conditions Hooke's law may hardly be assumed to hold. Furthermore, Griffith's model was based on a reversible thermodynamic system in which the creation of the new fracture surface by the rupture of the interatomic bonds provided the sole mode of absorbing the mechanical energy. Indeed this may be taken as the definition of an ideally brittle material but in semi-brittle and non-brittle materials irreversible processes inevitably accompany crack growth and substantially greater amount of mechanical energy may be consumed in the process of separating the material.

Linear elastic stress field analysis of the crack [5,6] predict an infinitely large stress value at the crack tip when the crack tip radius is zero. Most materials, however, exhibit a yeild stress above which they deform plastically. Consequently, (Fig. 1.4) there is a region in front of the crack tip where plastic deformation occurs. Irwin [4,7], Dugdale [8] and others [9,10], have attempted to calculate the size of the plastic region using, among other techniques, the crack opening displacement (COD) method. Mechanical energy is absorbed during plastic deformation. In problems where the movement of the crack involves plastic deformation Eq. (1.17) becomes

$$G_{IC} = 2\,(\Gamma + \Gamma_p) \tag{1.18}$$

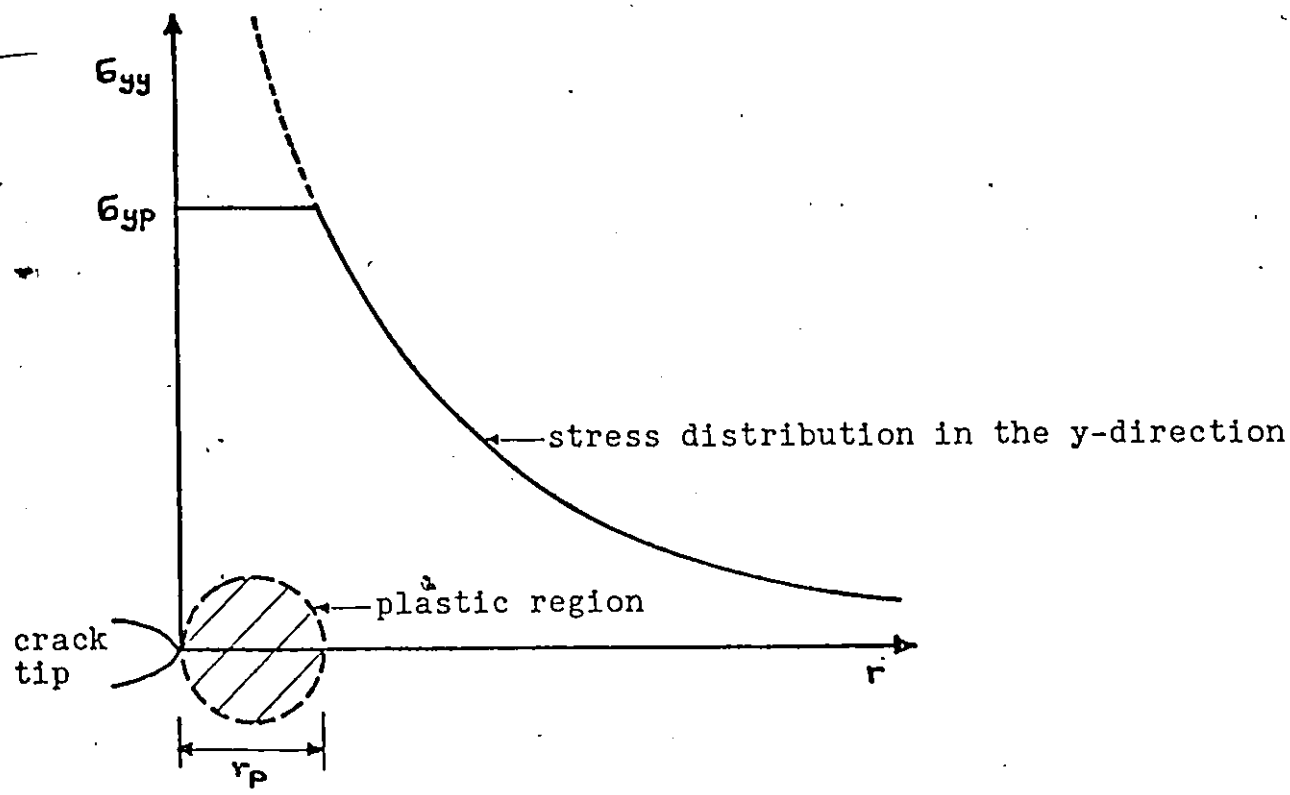

Figure 1.4 Schematic diagram of the stress distribution and the plastic region in front of the crack tip. The dashed line indicates the stress distribution determined from linear elastic stress analysis approach while the solid line shows the actual stress distribution for an elastic ideally plastic solid.

where r_p is the plastic work in forming a unit surface area of the crack. This is the so-called Orowan-Irwin generalization of Griffith's equilibrium condition. The fracture toughness K_{IC} and hence the critical crack driving force has now been accepted as a reliable safety criterion in engineering design. However, the fracture toughness design criterion is restricted to crack initiation [73].

Although some of the accidents due to component failures are certainly due to poor design, it has been discovered gradually that material defects in the form of pre-existing flaws could induce fracture. Furthermore, Anderson [16] and Biggs [17] observed that many failures occur under low stress conditions and were accompanied by very little or no plastic deformation. Consequently, the conventional design criteria based on the tensile strength, yield strength and the buckling stress are insufficient because there are always existing flaws in the material that act as stress raisers and initiate crack growth, the rate of which is sensitive to such variables as temperature, the applied load and the concentration of the chemical environment [18]. Brittle fracture is, therefore, a thermally activated and hence time dependent process.

Thomson, R., C. Hisieh and V. Rana [19,20] used the lattice trapping theory to review Griffith's continuum model for the physically more realistic discrete conditions. In this theory the material is considered to be composed of atoms interconnected by linear or non-linear interatomic bonds. The nature of the atomic bonds or springs depends on the material as shown in Table 1.1. Figures 1.5 and 1.6 show one and two dimensional models of the crack tip. Because of the periodic nature of the material the surface energy field is also periodic. The Griffith model was modified to take into account the periodic surface energy. Figure 1.7 (a) shows the modified surface energy as a function of the crack length. The linear function is the continuum approximation while the periodic functions (step or sine functions) are the superimposed effect of the periodic crystal lattice. Figure 1.7 (b) shows the change in the stored elastic energy as a function of the crack length while Figure 1.7 (c) shows the apparent free energy

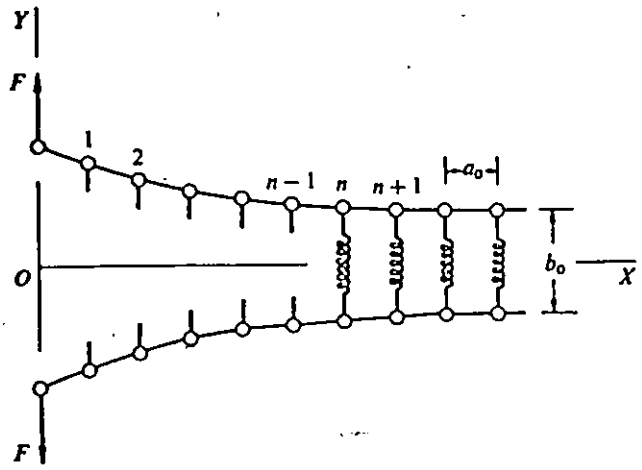

Figure 1.5 Lattice model of a quasi one dimensional crack. |38|

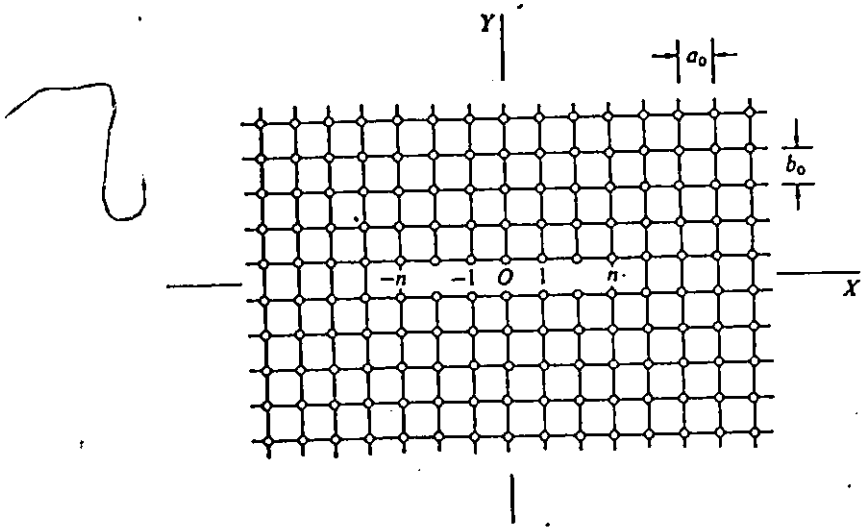

Figure 1.6 Two dimensional crack model consisting of infinite square lattice loaded along OY. The crack propagates along OX. |38|

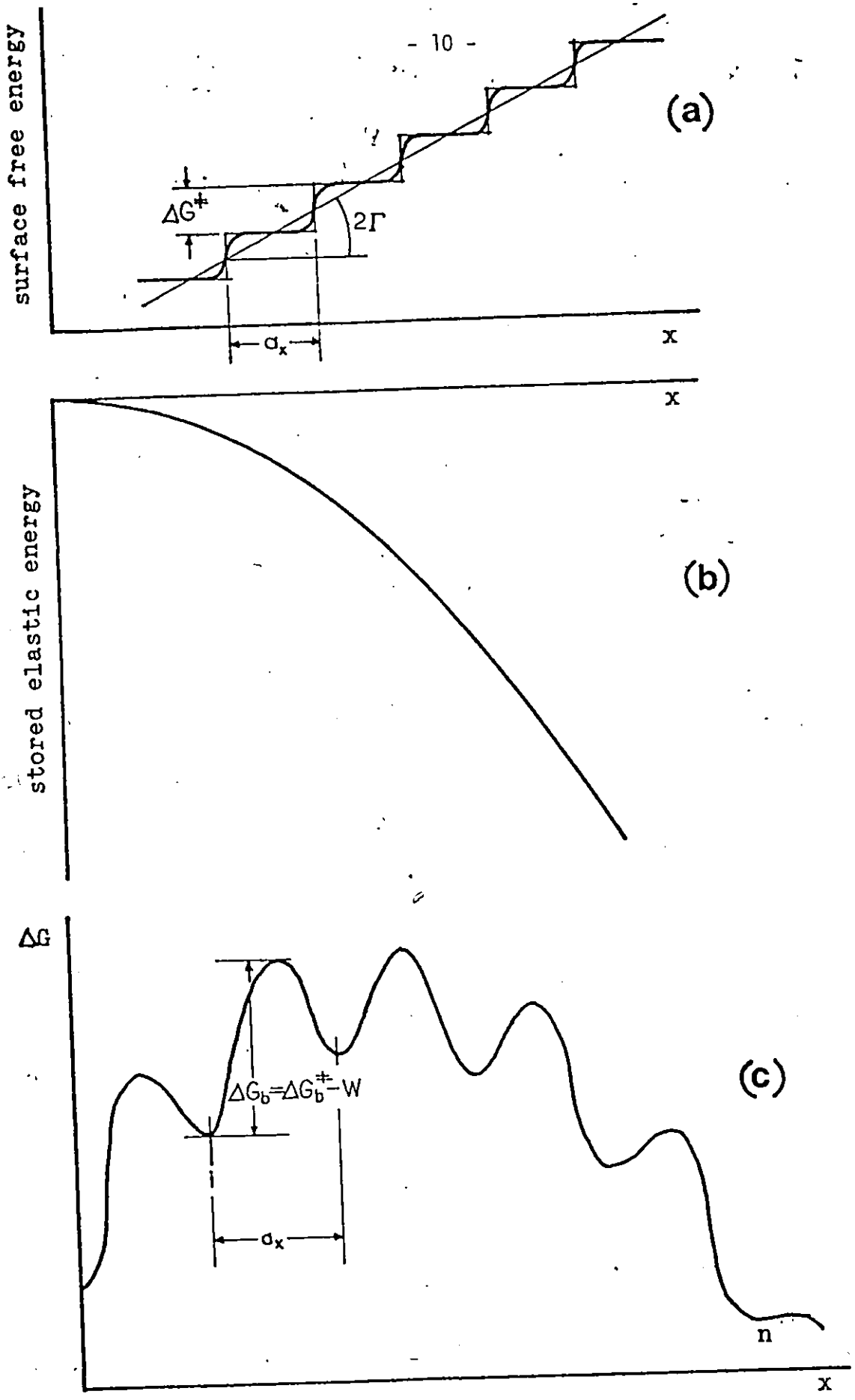

Figure 1.7 (a) The surface energy as a function of crack size (b) The stored elastic energy change as a function of crack size (c) The apparent free energy change ΔG_b during crack propagation.

Type of Bond	Typical examples
Covalent	Diamond, Chlorine molecule, Hydrogen molecule, etc.
Ionic	Ceasium chloride, Sodium chloride, Calcium fluoride, etc.
Metallic	Iron, Copper, Aluminum, Silver, etc.

Table 1.1 Typical Examples of atomic bonds.

change ΔG during crack propagation. The crack tip model clearly shows that the crack propagates through the material by consecutive bond breaking and, as will be shown later, occasional mending steps. The potential function for a pair of crack tip atoms takes the form shown in Fig. 1.8 (a). To break the bond the two atoms have to be separated from the equilibrium spacing a_o to infinity and the force transmitted to the crack tip by the applied load must exceed F_o (Fig. 1.8 (b) and (c)) and supply the dissociation energy E_o. However, it was pointed out earlier that brittle fracture takes place under low stress conditions. Consequently, the mechanical energy supplied by the force transmitted to the crack tip may be lower than the dissociation energy E_o. The additional energy required for bond breaking is supplied by the thermal energy [21]. Atoms vibrate randomly (Fig. 1.8 (a)) about their equilibrium lattice points with an amplitude dependent on the temperature of the material. Bonds break or heal as a consequence of the applied mechanical energy and the random thermal activations [22]. Because thermal energy has to be supplied for the bond to break or heal, the consecutive bonds can be represented by

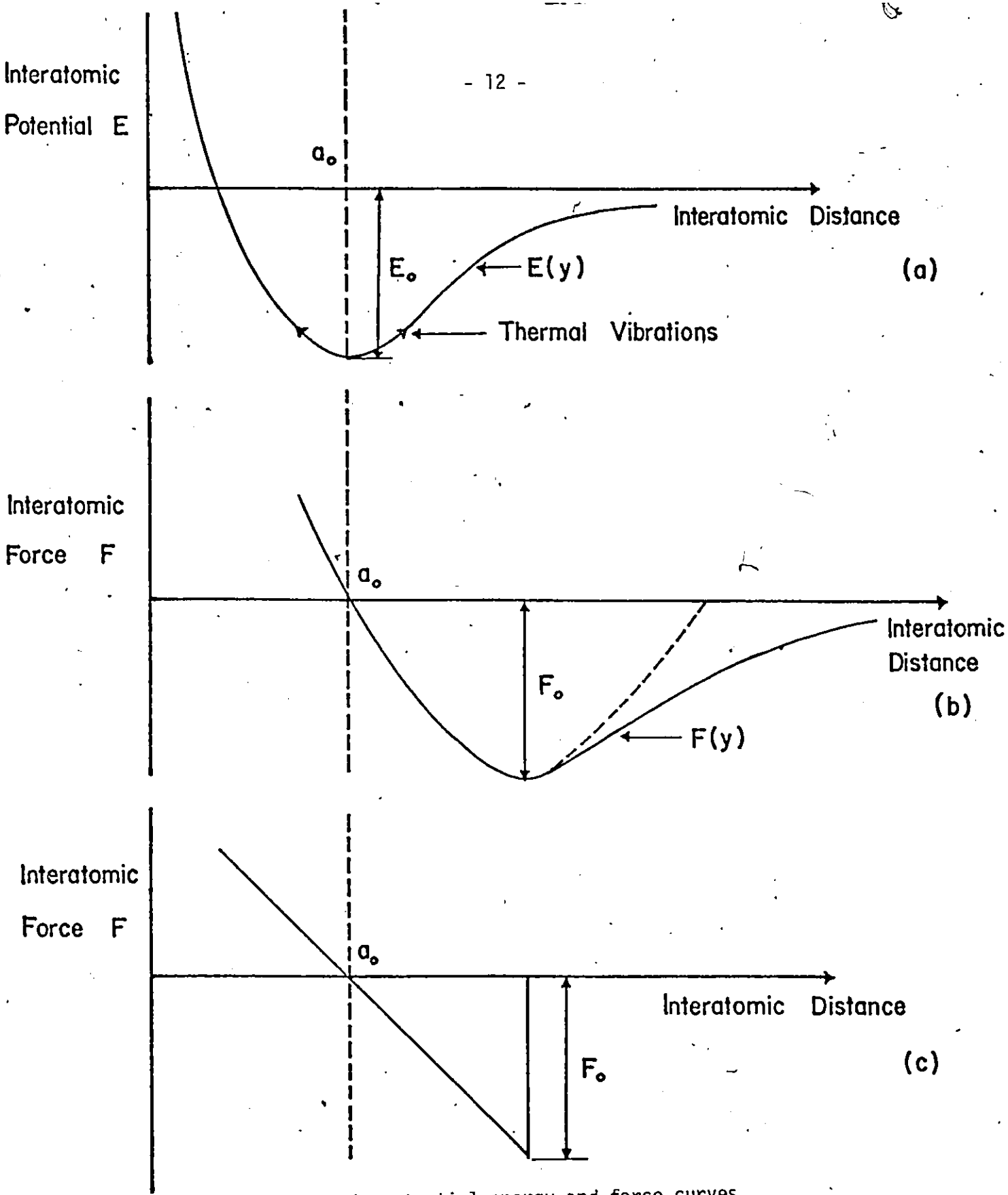

Figure 1.8 Interatomic potential energy and force curves
(a) Interatomic potential energy vs. interatomic distance
(b), (c) Interatomic force vs. interatomic distance -
(b) half sine approximation, dotted [4]
(c) linear approximation [20]

consecutive free energy barriers. At each of the equilibrium lattice points a_o, $2a_o$, $3a_o$ .... ja_o in Fig. 1.7 (c) the crack will momentarily stop until the random thermal activation enables the next bond to break or the previously broken bond to heal. The crack is mechanically trapped within a stable stress region that lies interjacent to two unstable regions; viz, one in which the crack heals spontaneously, and one in which catastrophic fracture occurs (Fig. 1.9). This is the so-called lattice trapping theory developed in analogy to the Peierls-Nabarro dislocation motion [23,63]. This effect of the lattice is in contradiction with the continuum prediction of Griffith that a crack will be stable at a single crack size, above which it propagates catastrophically and below which it heals.

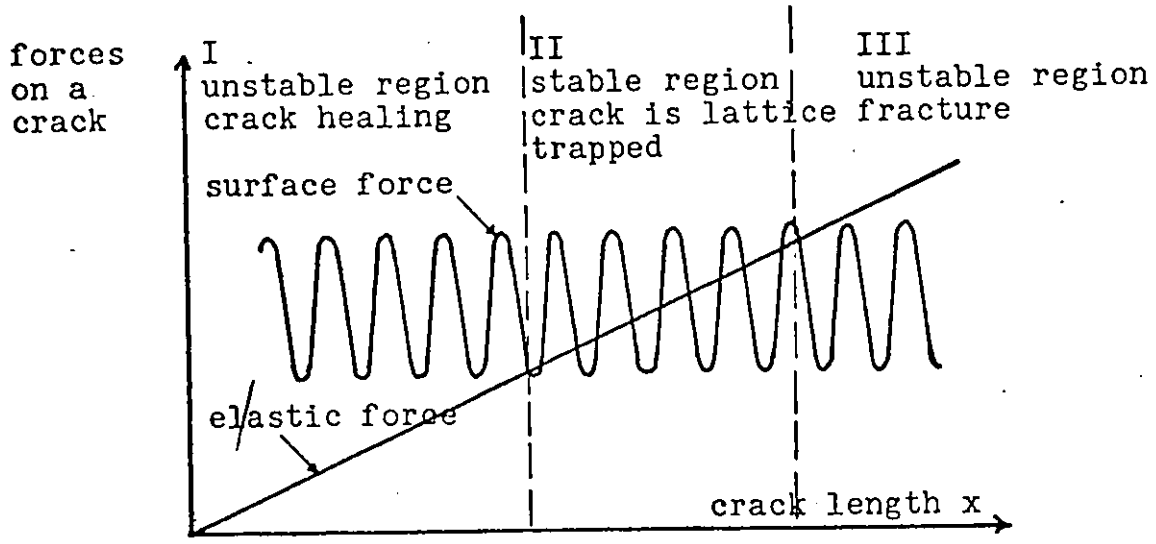

Figure 1.9 Schematic diagram of the surface and elastic forces on the crack. The elastic force is linear while the force on the crack due to the surface energy is the periodic function (after C. Hsieh and R. Thomson [20]).

With the introduction of the lattice trapping theory, therefore, it is advantageous to study the crack tip events in terms of the fundamental atomic bond breaking and healing processes.

That a crack propagates as a result of a series of time dependent, thermally activated atomic bond breaking and healing steps was established by Tobolsky and Eyring [24] in their classical theory of time dependent fracture. The process of bond breaking and bond healing while the composition of the specimen remains constant is identical to the dissociation process in chemical reactions where a molecule breaks into smaller molecules while the composition remains unchanged. Because of this identity the study of fracture can be considered as a special branch of chemical kinetics [21]. Hence the rates of bond breaking and mending processes are described by expressions that are identical to the corresponding processes in a chemical reaction. In general the process of bond breaking and mending is identical to an elementary first order reaction defined as [21]

$$k_b = \kappa_b \frac{Q^{\ddagger}}{Q_r} \frac{kT}{h} \exp\left(-\frac{\Delta E_b}{kT}\right) \tag{1.18}$$

for the forward reaction or bond breaking process and

$$k_h = \kappa_h \frac{Q^{\ddagger}}{Q_r} \frac{kT}{h} \exp\left(-\frac{\Delta E_h}{kT}\right) \tag{1.19}$$

for the reverse or bond healing process.

In this analogy the intact bond is in the reactant state while the broken bond is in the product state (Fig. 1.10). The change in the potential energy ΔE_b for the bond breaking and ΔE_h for the bond healing have to be supplied by the thermal energy of the material. The statistical thermodynamics definition of the Gibbs free energy ΔG leads to the expression [21]

$$\frac{Q^{\ddagger}}{Q_r} \exp\left(-\frac{\Delta E_b^{\ddagger}}{kT}\right) = \exp\left(-\frac{\Delta G_b^{\ddagger}}{kT}\right) \tag{1.20}$$

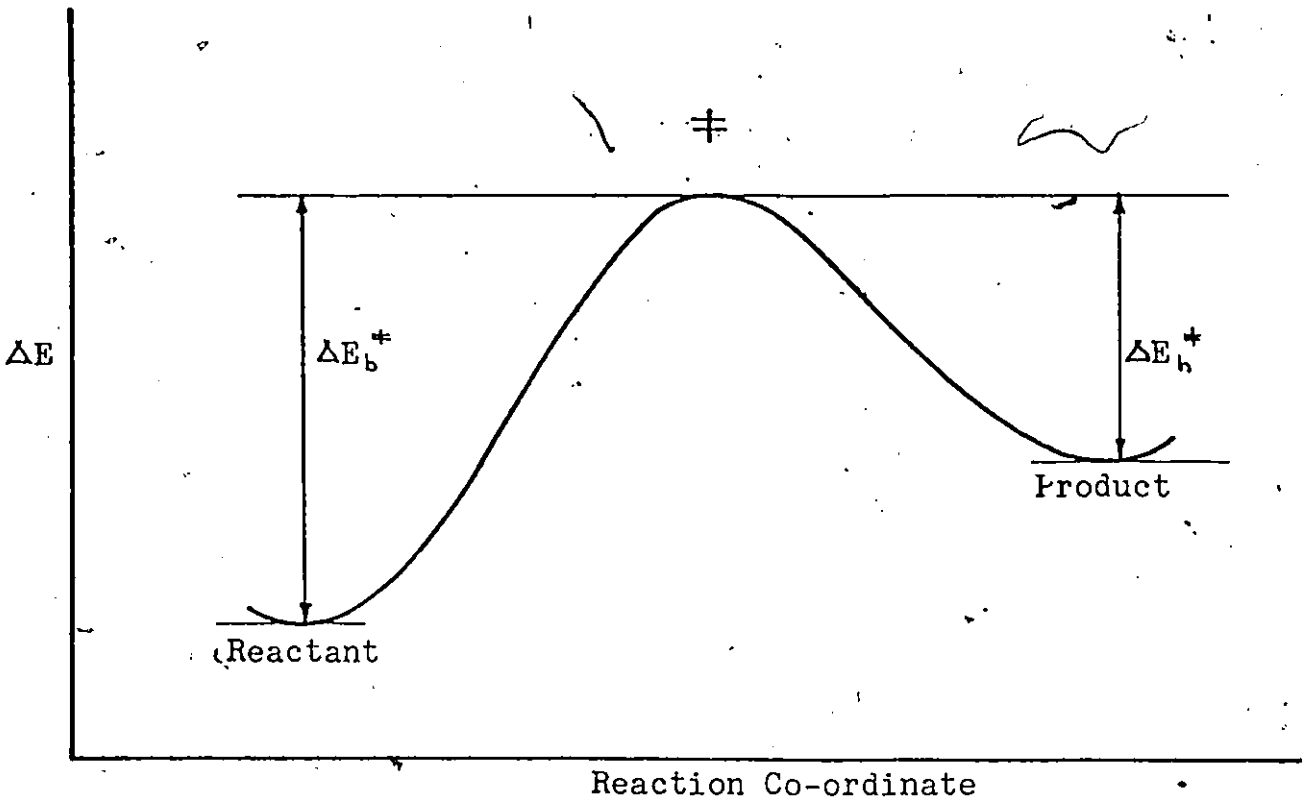

Figure 1.10 Schematic representation of the potential energy change along the reaction path.

The apparent free energy for the bond breaking process, ΔG_b, and ΔG_h for the bond healing process are functions of the mechanical energy and the intrinsic energy of the material (bond energy). They are defined as

$$\Delta G_b = \Delta G_b^{\ddagger} - W_b(\sigma)$$
$$\text{and} \qquad \Delta G_h = \Delta G_h^{\ddagger} + W_h(\sigma) \tag{1.21}$$

In Eqs. (1.21) the mechanical energy $W(\sigma)$ is indicated as being a function of the applied stress. However, in some problems it could also be a function of the crack length (as stress intensity actually is) and a function of time when the loading is time dependent. Finally, the rates of bond breaking and healing events in terms of the material property and the loading conditions are expressed as

$$k_b = \frac{kT}{h} \exp\left(-\frac{(\Delta G_b^{\ddagger} - W_b(\sigma))}{kT}\right)$$

$$k_h = \frac{kT}{h} \exp\left(-\frac{(\Delta G_h^{\ddagger} + W_h(\sigma))}{kT}\right) \qquad (1.22)$$

In Eqs. (1.22) κ_b and κ_h were considered to be unity. k_b and k_h are proportional to the probability of the bond breaking and the bond healing events respectively.

Inglis [2] showed that the stored elastic strain energy is proportional to the square of the applied stress so that the mechanical energy is expressed as

$$W(\sigma) \propto \sigma^2 \qquad (1.23)(a)$$

while Irwin [3] argued that the mechanical energy should be proportional to the applied stress, thus

$$W(\sigma) \propto \sigma \qquad (1.23)(b)$$

Equation (1.23 (b)) was found to be valid by Speidel [25,26], Brown [27] and also by H. M. Cekirge, W. R. Tyson, and A. S. Krausz [15] while Eq. (1.23 (a)) was found to be valid by Lawn [28,29] and also by W. R. Tyson, H. M. Cekirge and A. S. Krausz [30]. Both expressions are now generally accepted.

Tobolsky and Eyring used the expressions 1.22 to develop the fundamental concepts of the molecular theory of time dependent fracture. They showed that the net rate of individual bond breaking can be expressed as

$$\frac{d N_i}{dt} = N_i k_b - (N_o - N_i) k_h \qquad (1.24)$$

Hsiao [31] further refined this theory while Robinson [32] and Zhurkov [33] tested it experimentally. Zhurkov confirmed that the life time of a component under load is given by the expression

$$t_f = \tau_o \exp \frac{(\Delta G_b^{\ddagger} - W(\sigma))}{kT} \tag{1.25}$$

The conclusions derived from the experimental results were in good agreement with the theory for about 50 metals and polymers tested in creep and for a polymeric solid rocket propellant tested in a complex loading fracture regime.

Krausz [34] extended the Tobolsky-Eyring theory to describe fracture propagation at the molecular level. While the former theory determines the rate of individual bond breaking, that of Krausz determines the rate of cooperative bond breaking. The basis of the cooperative bond breaking theory is that during crack propagation, successive bond breaking takes place and that the crack moves over a periodic consecutive system of free energy barriers. At each barrier, forward and backward activations take place and the net number of activations will determine the crack propagation velocity. A simple quasi rigid crack front propagation (Fig. 1.11 (a)) with a constant stress field was assumed. The concentration of X sized cracks changes in unit time as

$$\frac{\partial \rho}{\partial t} = (k_h - k_b) \frac{\partial \rho}{\partial x} a_x + (k_h + k_b) \frac{a_x^2}{2} \frac{\partial^2 \rho}{\partial x^2} \tag{1.26}$$

Perhaps the most interesting remark about Equation (1.26) is that it is identical to the thermal conduction and diffusion equations-processes that are also controlled by consecutive atomic interaction changes in function of the interatomic energy-interatomic distance dependence [21]. The procedures for solving Equation (1.26) thus follow those used in diffusion and heat conduction problems and were outlined by Krausz [35]. The crack size distribution thus obtained is a function of time, temperature, the applied load and perhaps the concentration of the chemical environment.

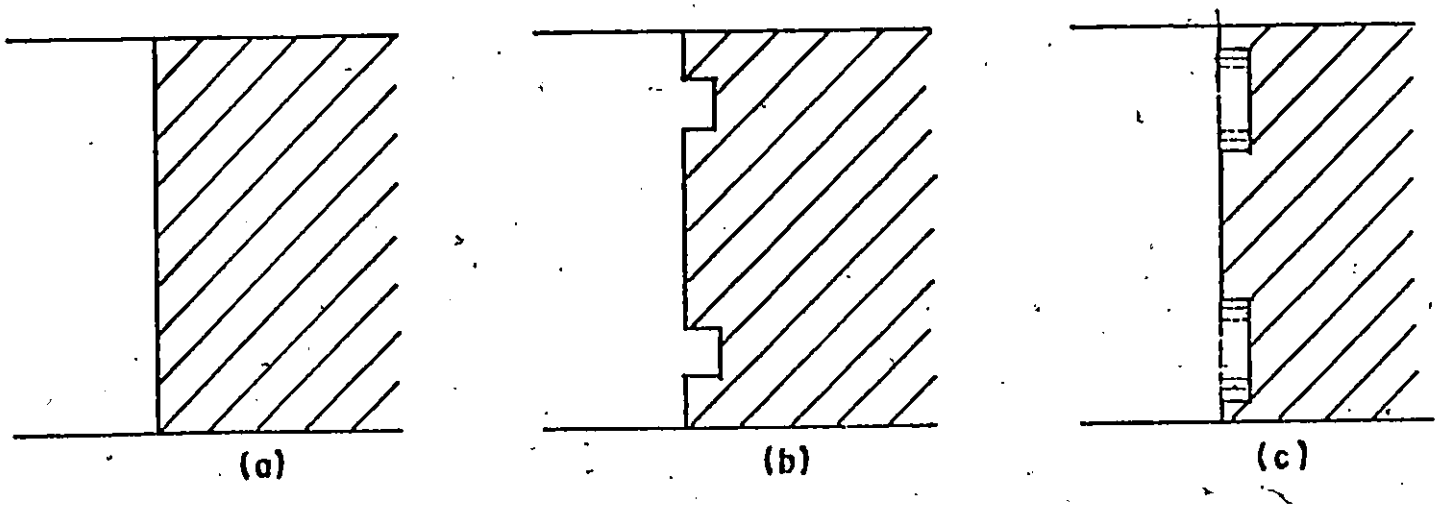

Figure 1.11 Crack front propagation modes
(a) quasi rigid crack front
(b) kinked crack front
(c) kink spreading sideways.

The study of the thermally activated, time dependent crack propagation is not complete without discussing the actual mechanisms of the crack nucleation and propagation. Kusenko et al. [36] observed experimentally by using small angle X-ray scattering, light scattering and electron microscopy methods that in polymers, ionic crystals and metallic solids, the fracture processes include a regular process of nucleation and development of submicro-cracks followed by a gradual accumulation of these incipient cracks, the accumulation rate being stress and temperature dependent. Because of the nature of most materials, the nucleation process will easily take place so that the rate of development and accumulation of the micro-cracks will determine the rate of crack growth. That this is indeed so, was shown experimentally by V. R. Regel and A. M. Leksovsky [37] who used polymer films to show that it is the kinetics of crack growth rather than the initiation that determines the lifetime of the materials under both

cyclic and static loading. Thompson et al. [19,20] argued that the rigid crack front propagation model is energetically unfavourable; instead they suggested that it is energetically more favourable for the crack propagation process to take place by kink nucleation followed by sideways spreading as shown in Figs. 1.11 (b) and 1.11 (c).

The double kinks nucleate along the crack front where vacancies or other defects have weakened the structure and offer a high probability location for the kink nucleation, requiring greatly less energy than the rigid crack front propagation does. Once a double kink has formed it can spread sideways in discrete steps of one or more atomic distances. This sequence is also a low energy process. A very large number of these events take place along the crack front, and when two adjacent kinks meet mutual annihilation takes place. As a result of these events crack front propagation is observed. Depending on the temperature and the stress level as well as the nature of the material, either the double kink nucleation or the spreading process can be rate controlling. Lawn [28,38] used this model to calculate the velocity of crack propagation. A steady state condition was considered whereby the kink pairs are nucleated thermally, and subsequently expand laterally to collide with and annihilate their neighbours. This takes place in the load range where a nucleated kink either heals back or propagates dynamically as shown in Fig. 1.12. When the nucleation rate equals the annihilation rate in steady state, the equilibrium kink concentration is

$$N_w^* = N_w \exp\left(-\frac{U_N^* - U_M^*}{2\,kT}\right) \qquad (1.27)$$

and the crack propagation velocity is

$$V_C = \frac{N_w}{N_A} \frac{kT}{h} \exp\left(-\frac{U_N^* + U_M^*}{2\,kT}\right) \tag{1.28}$$

It was noted that a theoretical basis for calculating the activation energy for the kink nucleation, U_N^*, and the activation energy for the kink motion, U_M^*, has not yet been established for cracks; and as an approximation, the activation energy for the kink motion may be determined from the Irwin-Orowan expression (1.13) as

$$\delta U_M^* \approx (-G + 2\Gamma)\, a_o\, \delta d \tag{1.29}$$

where $a_o\, \delta d$ is the surface area traced out by the moving kink.

Krausz [22] modified this theory by introducing statistical thermodynamics. He proposed that in a crack system where the nucleation and the spreading processes take place over the consecutive energy barrier system presented by the periodic energy field of the lattice, the same number of activations F_i occur over each of the consecutive barriers when steady state condition is attained. Accordingly, the flow equations are

$$\begin{aligned} F_{DKN} &= N_{DKN}\ {}_{DKN}k^{DKN} - N_1\ {}^{DKN}k_1 \\ F_1 &= N_1\ {}_1k^1 - N_2\ {}^1k_2 \\ F_i &= N_i\ {}_ik^i - N_{i+1}\ {}^ik_{i+1} \\ F_n &= N_n\ {}_nk^n \end{aligned} \tag{1.30}$$

where the symbol DKN was used for the double kink nucleation process. N_i is the number of specimens in front of the i-th barrier, ${}_ik^i$ is the rate constant for activation from the valley in front of the i-th barrier to the top of the barrier, and ${}^ik_{i+1}$ is the rate constant of the backward activation from the i+1-th valley to the top of the i-th barrier. $i=1,2\ldots n$ represents the spreading barriers. In steady state where

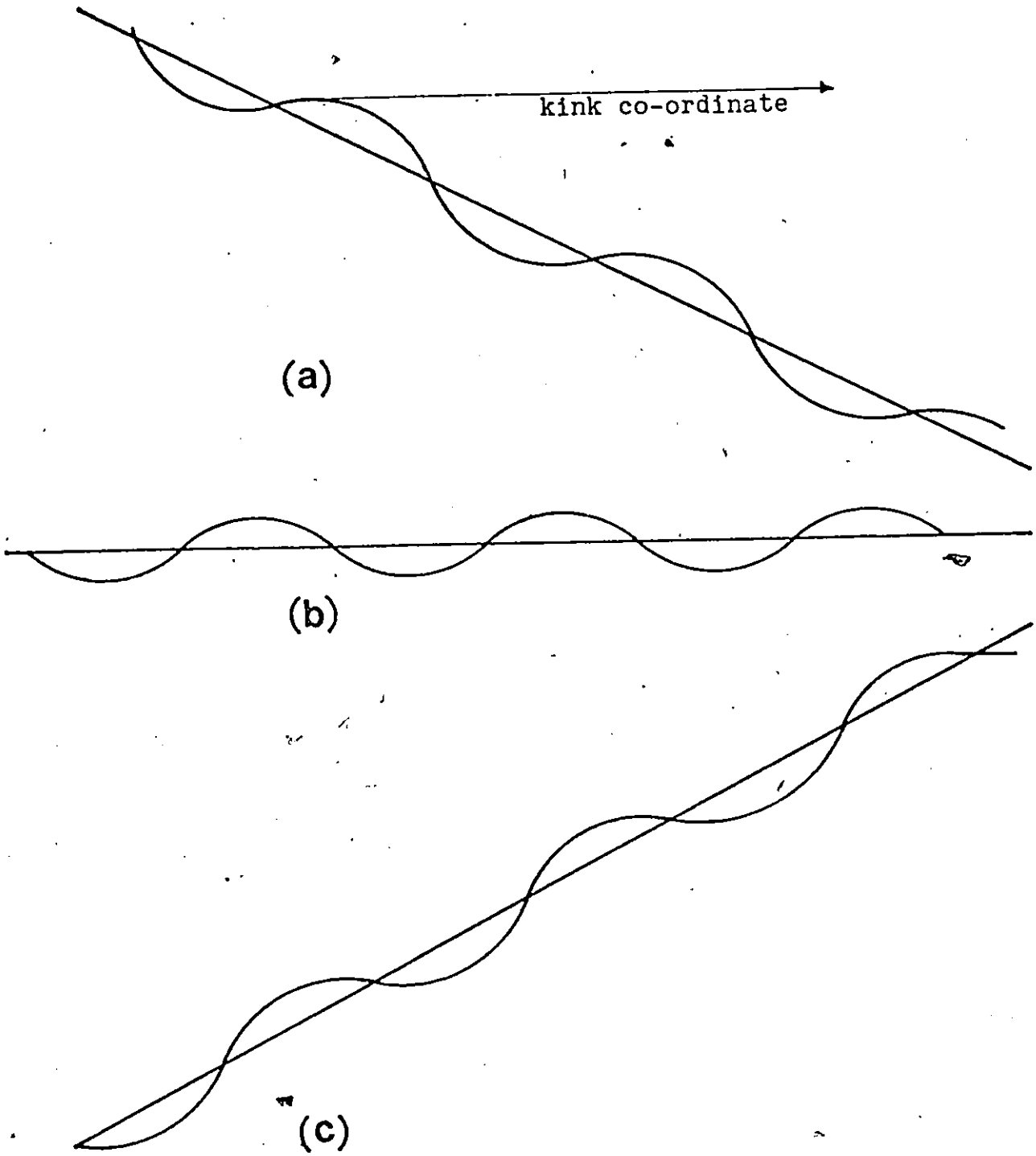

Figure 1.12 Potential energy diagrams for kink motion according to the lattice model. Activation barrier for discrete motion through an atomic spacing is indicated by heavy curved line. The corresponding continuum behaviour is indicated by full, straight line. (a) limiting state for the thermally activated kink spreading. (b) the Griffith equilibrium condition and (c) limiting state for crack healing.

$$F_{DKN} = F_1 = F_2 = \ldots F_i, \tag{1.31}$$

the flow of crack tips, F_i, is given by

$$F_i = N_{DKN} \left\{ \frac{h}{kT} \left[\exp\left(\frac{\Delta G^{\ddagger} - {}_iW^i}{kT} .b \right) + n \exp\left(\frac{2\,\Delta G^{\ddagger} - {}_iW^i - {}^iW_{i+1}}{kT} .b \right) \right. \right.$$
$$\left. \left. x \exp\left(\frac{\Delta G^{\ddagger} - {}_iW^i}{2\,kT} n\, a_y \right) \right] \right\}^{-1} \tag{1.32}$$

In Equation (1.31), b is the number of bonds that are broken in the nucleation step. The average crack propagation velocity was expressed as

$$\bar{V} = \left(\frac{1}{N_{DKN}} \right) a_x \sum_i F_i \tag{1.33}$$

Equations (1.32) and (1.33) are formally equivalent to the approximate relations derived by Lawn and Wilshaw [38] in Equations (1.27) and (1.28) for the equilibrium kink concentration and the crack propagation velocity respectively.

A further development of the kink nucleation and spreading theory by Lawn described the effect of the chemical environment on the crack growth. The theory of stress corrosion cracking (environmentally affected cracking) was developed by Charles [39] and Hillig [40] and was further modified by Wiederhorn [41]. In this theory, the generalized interaction between the crack tip bonds B and the environmental molecules of species A is expressed as

$$nA + B \rightarrow B^* \tag{1.34}$$

where the asterisk denotes passage over the activation barrier into the ruptured state. Thus, the interaction facilitates the lateral kink advance through one atomic distance while the reverse interaction conversely facilitates the crack retreat. The energy rate for the system i.e., the crack plus the environment is

$$\frac{dU}{dC} = - G + 2\Gamma' - n \mu_A N_A \tag{1.35}$$

while without the effect of the environmental molecules the energy rate is

$$\frac{dU}{dC} = - G + 2\Gamma \tag{1.36}$$

In Equation (1.35), the term $2\Gamma'$ is defined as

$$2\Gamma' = (\mu_{B*} - \mu_B) N_A$$

where μ_B and μ_{B*} are the chemical potentials for the crack tip bond before and after rupture respectively; and μ_A is the chemical potential for the environmental species. Thus, the effect of the chemical environment is to lower the free surface energy (bond energy) of the material. The kink concentration and the crack propagation velocity then changes accordingly. Good agreement was obtained between this theory and the stress corrosion cracking of sapphire in water vapour [38].

The concept of kink nucleation and spreading mode of the crack front propagation was further used by Brown [27] in his extensive study of stress corrosion cracking in ceramics. He approached stress corrosion cracking in terms of the multi-barrier kinetics (i.e., the network theory) suggesting that it consists of at least three consecutive and/or parallel rate processes. The resulting equation from his analysis for the crack propagation velocity as a function of the stress intensity is of the form

$$v = \Omega_o e^{\Omega_1 K_I} + \frac{\Omega_2 e^{\Omega_3 K_I} \left[1 - e^{-L (K_I - K_I^*)}\right]}{1 + \Omega_4 e^{\Omega_3 K_I}} \tag{1.37}$$

In Equation (1.37), Ω_o, Ω_1, Ω_2, Ω_3, Ω_4 and L are constants depending on the material and the environment. K_I^* is the threshold stress intensity. This theory was in good agreement with a wide variety of stress corrosion cracking data. While Lawn's analysis for the stress corrosion cracking was limited to Regions I and II of the stress corrosion cracking diagram

(Fig. 1.13), that of Brown can be used for Regions I, II and III.

Krausz [42,43] introduced a simpler system for studying stress corrosion cracking. He proposed that the crack propagation velocity in Regions I and II is controlled by a system of two consecutive energy barriers. Barrier I represents the (thermally activated) breaking of the (usually brittle) corroded material in front of the crack tip while barrier II represents the chemical reaction between the crack tip bonds and the environmental molecules (diffusion controlled process). The two consecutive energy barrier process is in parallel with a single barrier which accounts for the non-environmentally affected cracking in Region III. Although the mechanisms in Regions I and III were associated with single energy barriers, the actual mechanisms are double kink nucleation and sideways spreading |42|. The complete kinetics equation is of the form

$$v = \frac{n_c \, a \left[1 - \frac{kT}{h} \left({}_1k_1\right)^{-1}\right]}{\left[k(I)\right]^{-1} + \left[k(II)\right]^{-1}} + n_p \, a \, k(III) \qquad (1.38)$$

In Equation (1.38) $k(I)$, $k(II)$ and $k(III)$ are combined rate constants for Regions I, II and III respectively and are functions of the elementary rate constants k_b and k_h.

Experiments on stress corrosion cracking have shown that for some material-environment systems, there is a threshold stress intensity (K_{ISCC}) value below which stress corrosion cracking does not take place. Using Equation (1.37) of Brown or (1.38) of Krausz to fit the experimental data it is possible to calculate this parameter which has many applications in engineering design problems where stress corrosion cracking takes place.

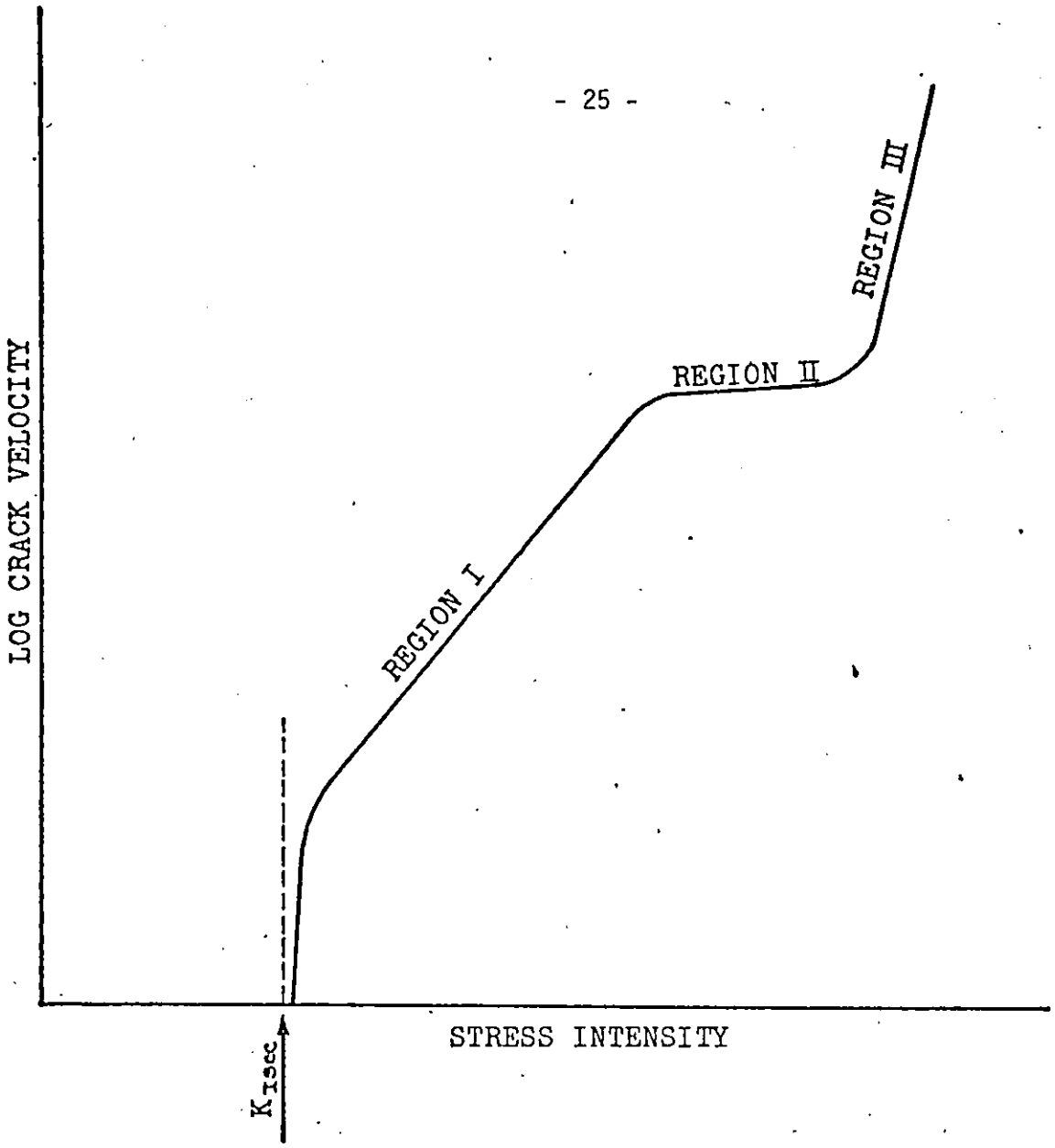

Figure 1.13 Schematic diagram of the typical stress corrosion crack propagation behavior of most metallic and non-metallic materials.

Considerable attempt has been made to study the crack tip events in terms of the fundamental bond breaking and bond mending processes and the effect of the chemical environment on such processes. This has lead to improved understanding of brittle fracture. The purpose of this thesis was to further develop the concepts of the crack tip events so far described and it is hoped that the conclusions that have been reached are helpful in controlling brittle fracture. The following will be discussed in this thesis.

First, using a quasi-rigid crack front that is double kink nucleation controlled (hereafter referred to as a rigid crack front model) model, a crack size distribution function was developed in continuation of Krausz's work on the non-steady state crack propagation. The effects of the applied stress, temperature and the material properties on the crack size distribution were investigated.

Secondly, an approximate mathematical expression for the kink concentration distribution function was developed and the results were compared with those from the discrete analysis. The effects of the applied stress, temperature and the defective nature of the material on the kink distribution and the crack propagation velocity will be discussed.

Finally, an introduction to the non-steady state fracture kinetics analysis is presented, with application to stress corrosion cracking.

Chapter 2

Crack Size Distribution in Homogeneous Solids

Crack propagation is the consequence of successive bond breaking and occasional bond mending steps during which the crack moves over a periodic consecutive system of free energy barriers [22,34,35,42,55,56]. The flow of crack tips over each of the consecutive energy barriers can be either a steady state or a non-steady state process. In this chapter, the crack size distribution function for a non-steady state process will be derived. The effect of the applied stress, temperature and the material properties on the crack size distribution will be discussed.

2.1 Kinetics Analysis

During a thermally activated crack propagation process bonds are successively broken under the combined effect of the available mechanical work and the thermal energy flowing into the crack tip region where vibrational interatomic distance changes occur. Because fracture and plastic flow have been identified to be a special branch of chemical kinetics, deformation kinetics concepts as well as chemical kinetics principles were used by Krausz and Eyring to develop the theory of consecutive bond breaking processes associated with steady state plastic flow [21] and by Krausz [34] to formulate the theory of the non-steady state fracture propagation rate.

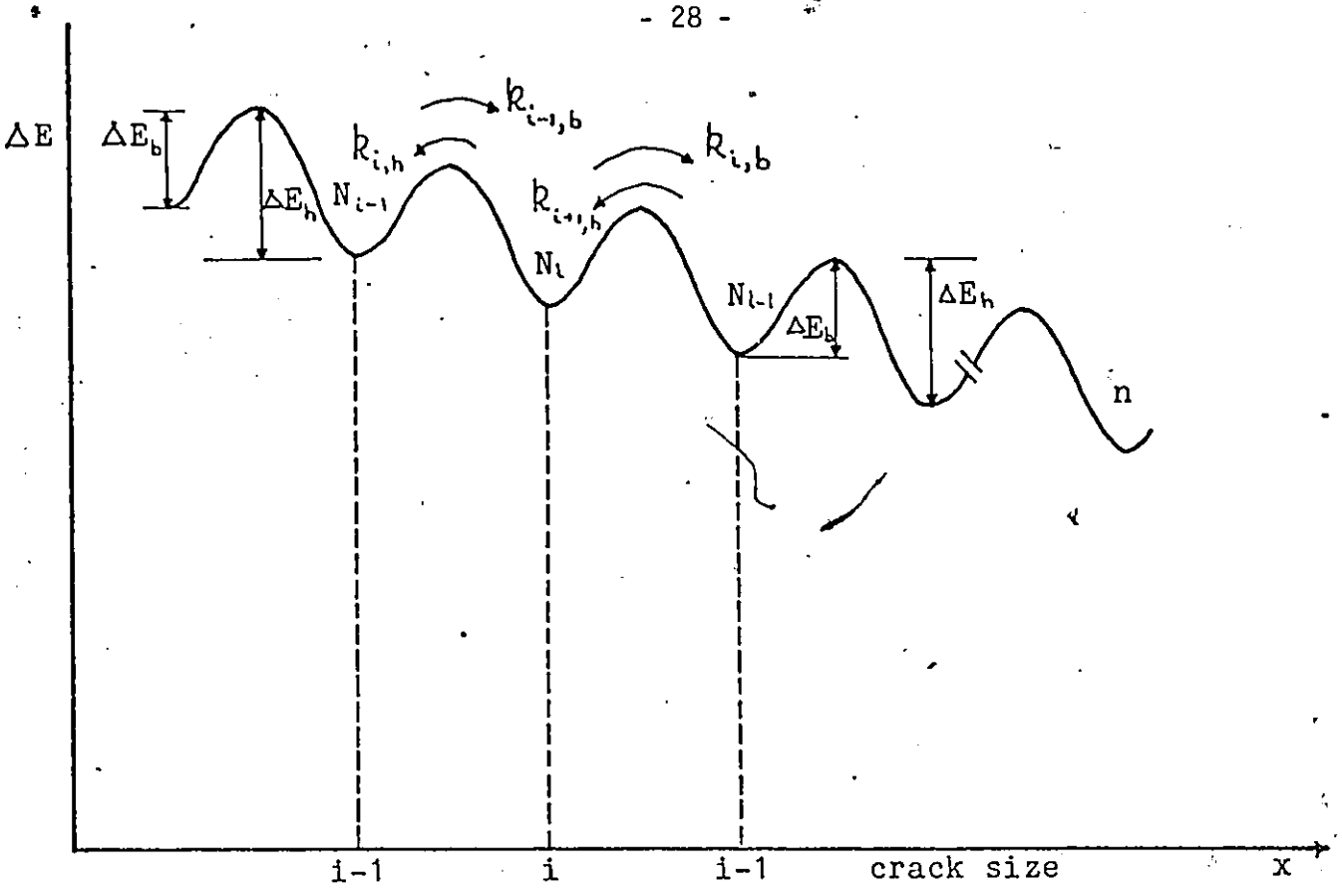

Figure 2.1 Apparent potential energy change ΔE when the crack size changes from the i-th bond to the i+1 or i-1 bond and the number of specimens N having the corresponding sizes.

In his theory, Krausz considered a statistically large number of specimens that are subjected to identical loading conditions. The total number of specimens is N_t. Another approach that may be used [71] is to consider a single loaded specimen in which simultaneous development of cracks may be energetically favourable at a large number of points, $N_t >> 1$.

The apparent potential energy given by

$$\Delta E = \Delta E^{\ddagger} \pm W(\sigma) \tag{2.1}$$

is shown in Fig. 2.1. Of the total N_t specimens, N_{i-1} specimens will have a crack of size i-1 atomic distances N_i will have a crack of size i atomic distances, etc. There are N_i specimens or cracks in which the crack size increases in consequence of bond breaking from X_i to X_{i+1} and decreases in consequence of bond healing from X_i to X_{i-1}. The rate of bond breaking $k_{i,b}$ and bond healing $k_{i,h}$ are defined for unit number of cracks per unit length of the crack of X_i size. The change in the number of cracks of X_i size is the net result of crack growth from the (i-1)-th valley across the activated state into the i-th valley and from the i-th valley into the i+1-th valley across the activated state following the i-th valley. The rate of flow across the activated state between the valleys i-1 and i is described by the kinetics equation as

$$R^{i}_{i-1} = k_{i-1,b} N_{i-1} - k_{i,h} N_i \tag{2.2}$$

The rate of flow across the activated state between X_i and X_{i+1} sized cracks is

$$R^{i+1}_{i} = k_{i,b} N_i - k_{i+1,h} N_{i+1} \tag{2.3}$$

The rate of change in X_i sized crack concentration X_i is then

$$\frac{\partial N_i}{\partial t} = R^{i}_{i-1} - R^{i+1}_{i} \tag{2.4}$$

In general, the change of the number of specimens with crack size X_i per unit time is given by the net number of specimens with cracks flowing into valley i minus the net number of specimens with cracks flowing out of valley i. In steady state, the net number of specimens with cracks flowing into valley i is equal to the net number of specimens with cracks

flowing out of the valley i. The crack tip concentrations N_{i+1} and N_{i-1} can be expressed with the truncated Taylor polynomial in terms of X_i sized crack concentration N_i as

$$N_{i+1} = N_i + a_x \frac{\partial N_i}{\partial X_i} + \frac{1}{2!} \frac{\partial^2 N_i}{\partial X_i^2} a_x^2 \tag{2.5}$$

$$N_{i-1} = N_i - \frac{a_x \partial N_i}{\partial X_i} + \frac{1}{2!} \frac{\partial^2 N_i}{\partial X_i^2} a_x^2$$

Substituting Eqs. (2.2) and (2.3) in Eq. (2.4) results in

$$\frac{\partial N_i}{\partial t} = k_{i-1,b} N_{i-1} - k_{i,h} N_i - k_{i,b} N_i + k_{i+1,h} N_{i+1} \tag{2.6}$$

and from Eq. (2.5), Eq. (2.6) becomes

$$\frac{\partial N_i}{\partial t} = k_{i-1,b} \left(N_i - a_x \frac{\partial N_i}{\partial X_i} + \frac{1}{2} a_x^2 \frac{\partial^2 N_i}{\partial X_i^2}\right) - k_{i,h} N_i$$

$$- k_{i,b} N_i + k_{i+1,h} \left(N_i + a_x \frac{\partial N_i}{\partial X_i} + \frac{1}{2} \frac{\partial^2 N_i}{\partial X_i^2} a_x^2\right) \tag{2.7}$$

In cases where the rate of bond breaking k_b and the rate of bond mending k_h are independent of the crack size and time, the propagation rate is

$$\frac{\partial N}{\partial t} = (k_h - k_b) \frac{\partial N}{\partial X} a_x + (k_b + k_h) \frac{a_x^2}{2} \frac{\partial^2 N}{\partial X^2} \tag{2.8}$$

Equation (2.8) is the one dimensional crack propagation differential equation; the solution of which gives the crack size distribution function.

2.2 Solution of the Differential Equation

Equation 2.8 can be rewritten as

$$\frac{\partial N}{\partial t} = K \frac{\partial^2 N}{\partial X^2} + C \frac{\partial N}{\partial X} \tag{2.9}$$

where $K = \frac{a_x^2}{2}(k_h + k_b)$ and

$$C = a_x(k_h - k_b)$$

In deriving Eq. (2.9), it was considered that crack propagation was taking place in sufficiently large specimens so that the stress field around the propagating crack remains unchanged. Under this condition, the specific rate constant k can be considered, in the first approximation, to be independent of the crack size. Consequently, K and C are constants.

It is of interest to note that the differential equation of crack propagation is identical to the heat transfer and diffusion equations. This, as Krausz pointed out, is a necessary consequence of the fact that all three are controlled by the same physical condition: the consecutive atomic interaction changes in function of the interatomic energy -- interatomic distance dependence [21]. Hence, the solution of Eq. (2.9) follows the mathematical methods that have been developed in heat transfer and diffusion. In particular, Eq. (2.9) is recognized as the description of a diffusion process in a convection field [44,45,46] where C is proportional to the acceleration caused by the external field and K is equivalent to the diffusion coefficient.

Consider the simplest initial condition when at t=0 only microcracks of indentical size X_o exist in semi-infinitely large specimens. Because cracks cannot heal back across the surface at X=0, the boundary condition is expressed as, (Fig. 2.2(b)).

$$k_b\, N(-\frac{a_x}{2}, t) - k_h\, N(\frac{a_x}{2}, t) = 0 \qquad (2.10)$$

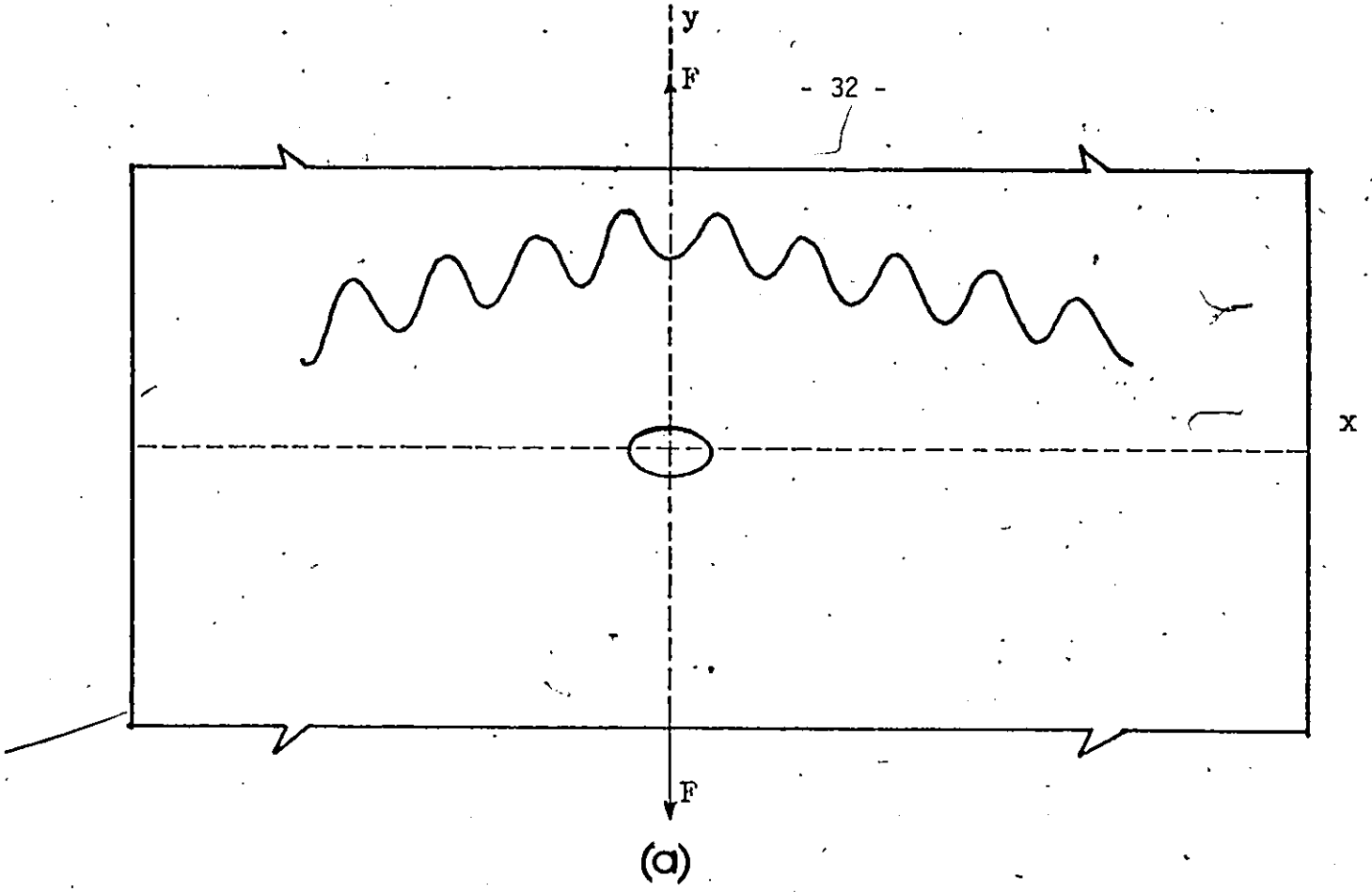

(a)

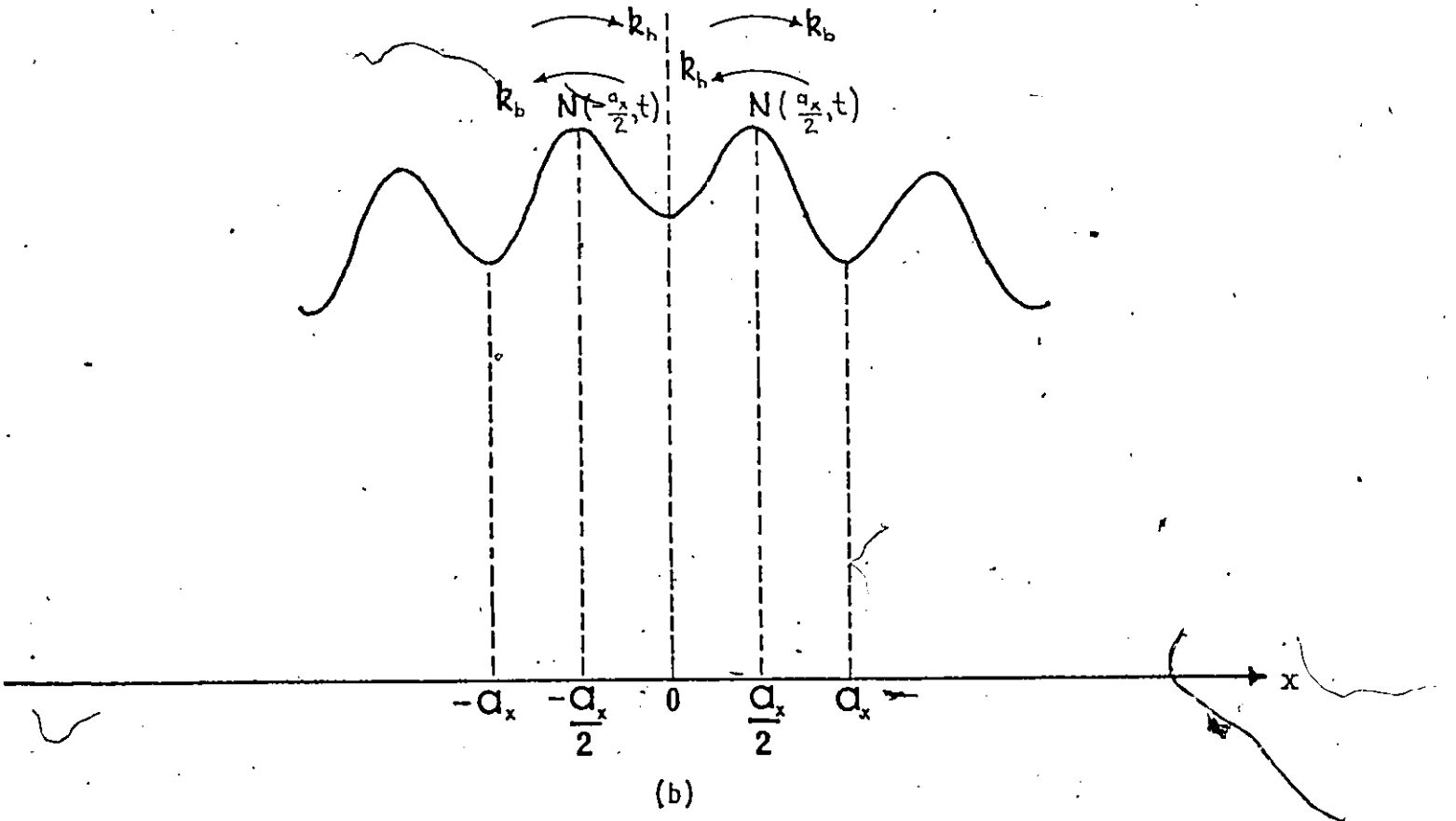

(b)

Figure 2.2 (a) An elliptical crack in a semi-infinite plate loaded in the Y-direction. Free energy barriers are indicated in the direction of crack propagation.
(b) A schematic drawing showing the free energy barriers at X=0.

that is, the net number of crack tips flowing to the free energy valley corresponding to X=0 must be equal to zero.

That macroscopic crack healing indeed takes place was shown experimentally by Orowan [47], as well as by Wiederhorn [48] in experiments with mica and glass respectively. However, this is only under very closely defined, limited conditions. The crack healing will only take place if there is no plastic deformation at the crack tip because such deformation causes geometrical mismatch of the broken bonds. Also, the crack healing will not occur if there is chemical contamination of the crack surface.

In analogy to Ficks 2nd law in diffusion or Fourier equation in heat transfer, the flow of crack tips in the X-direction per unit area, per unit time is expressed as

$$F = K \frac{\partial N}{\partial X} + CN \tag{2.11}$$

Thus, the boundary condition can be stated as

$$K \frac{\partial N}{\partial X} + CN = 0 \tag{2.12}$$

at X=0 for all $t \geq 0$

The solution of the differential equation (2.9) with the boundary condition (2.12) is obtained by first introducing the transformation [44,49] of the variables

$$N(X,t) = n(X,t) \exp \left[- \frac{C(X - X_o)}{2K} - \frac{C^2 t}{4K} \right] \tag{2.13}$$

Eq. (2.9) then reduces to the standard form

$$\frac{\partial n(X,t)}{\partial t} = K \frac{\partial^2 n(X,t)}{\partial x^2} \tag{2.14}$$

while the boundary condition (2.12) becomes

$$K \frac{\partial n(X,t)}{\partial X} + \frac{1}{2} C\, n(X,t) = 0 \qquad (2.15)$$

at $X=0$, $t \geq 0$

Eq. (2.14) with boundary condition (2.15) is a standard problem in the theory of heat transfer. The solution is [49,50]

$$\frac{n(X,t)}{n_t} = \frac{1}{2(\pi Kt)^{\frac{1}{2}}} \left\{ \exp\left[-\frac{(X - X_o)^2}{4Kt}\right] + \exp\left[-\frac{(X + X_o)^2}{4Kt}\right]\right\} + \frac{C}{2K(\pi Kt)^{\frac{1}{2}}} \int_{X_o}^{\infty} \left\{\exp\left[-\frac{(\alpha + X)^2}{4Kt} + \frac{C(\alpha - X_o)}{2K}\right]\right\} d\alpha \qquad (2.16)$$

After some transformations, (Appendix 1), Eq. (2.16) takes the form

$$\frac{n(X,t)}{n_t} = \frac{1}{2(\pi Kt)^{\frac{1}{2}}} \left\{\exp\left[-\frac{(X - X_o)^2}{4Kt}\right] + \exp\left[-\frac{(X + X_o)^2}{4Kt}\right]\right\} + \frac{C}{K\sqrt{\pi}} \exp\left[\frac{C^2 t}{4K} - \frac{C(X + X_o)}{2K}\right] \int_{\frac{X+X_o-Ct}{2(Kt)^{\frac{1}{2}}}}^{\infty} \exp(-y^2)\, dy \qquad (2.17)$$

Substituting Eq. (2.17) into Eq. (2.13) we obtain

$$\frac{N(X,t)}{N_t} = \frac{1}{2(\pi Kt)^{\frac{1}{2}}} \left\{\exp\left[-\frac{(X - X_o)^2}{4Kt}\right] + \exp\left[-\frac{(X + X_o)^2}{4Kt}\right]\right\} \exp\left[-\frac{C(X - X_o)}{2K} - \frac{C^2 t}{4K}\right] + \frac{C}{2K} \exp\left(-\frac{CX}{K}\right) \operatorname{erfc}\left(\frac{X + X_o - Ct}{2(Kt)^{\frac{1}{2}}}\right) \qquad (2.18)$$

Eq.(2.18)thus describes the crack size distribution. At time t, the equation gives the concentration (number of specimens per unit length of the crack) of the specimens in which the crack size is X.

The initial microcrack of size X_o, may, in most cases, be very small compared to the practical macrocrack sizes. In these cases, it can be assumed that $X_o \simeq 0$ and Eq.(2.18)reduces to

$$\frac{N(X,t)}{N_t} = \frac{1}{(\pi Kt)^{\frac{1}{2}}} \exp - \frac{(X + Ct)^2}{4Kt} +$$

$$\frac{C}{2K} \exp\left(\frac{-CX}{K}\right) \operatorname{erfc} \frac{(X - Ct)}{2(Kt)^{\frac{1}{2}}} \qquad (2.19)$$

Depending on the stress and temperature, the constant C will be greater than zero, less than zero or equal to zero; as shown in Figs. 2.3 a, b and c.

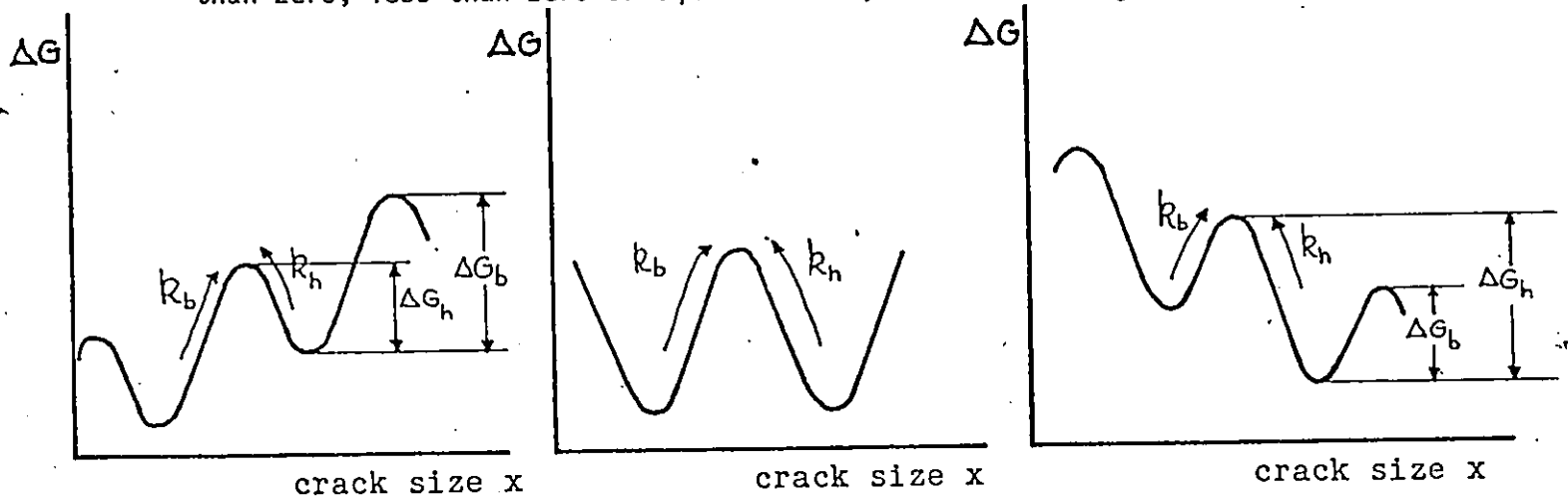

$\Delta G_b > \Delta G_h$ $\qquad$ $\Delta G_h = \Delta G_b$ $\qquad$ $\Delta G_b < \Delta G_h$

(a) $C > 0$ or $k_b < k_h$ $\qquad$ (b) $C = 0$ $k_b = k_h$ $\qquad$ (c) $C < 0$ $k_b > k_h$

Figure 2.3 Free energy change as a function of the crack size. (a) Crack healing condition when $k_b < k_h$. (b) The Griffith's critical condition, $k_b = k_h = k$, and (c) Crack propagation condition when $k_b > k_h$.

Consequently, Eq. (2.18) or (2.19) has three forms that describe the crack size distribution in the three conditions.

Case i: $k_b < k_h$

The crack size distribution when $k_b < k_h$ can be obtained from Eq. (2.18) when $X_o \neq 0$ and from Eq.(2.19)when $X_o = 0$. The former condition, however, is not of practical interest because, as discussed earlier, physical conditions will not allow the crack to heal back.

From Eq. (2.18) or (2.19), when $t \to \infty$ the crack size distribution is

$$\frac{N(X,\infty)}{N_t} = \frac{C}{K} \exp\left(- \frac{CX}{K} \right), \; C > 0 \qquad (2.20)$$

It is interesting to note that the stationary crack size distribution (Eq. 2.20), is independent of the initial microcrack size. Equation (2.20) could also be derived by considering the stationary state of Eq. (2.9), thus

$$K \frac{\partial^2 N}{\partial X^2} + C \frac{\partial N}{\partial X} = \frac{\partial N}{\partial t} = 0 \qquad (2.21)$$

On integration,

$$K \frac{\partial N}{\partial X} + CN = a_1$$

The solution of this differential equation is

$$N = \frac{a_1}{C} + a_2 \exp\left(- \frac{C}{K} X \right)$$

where a_1 and a_2 are integration constants. Because of the boundary condition (2.12), $a_1 = 0$. The total number of specimens N_t is defined as

$$N_t = \int_o^\infty N \, dx,$$

from which $a_2 = \frac{C}{K} N_t$

Thus, the crack size distribution is

$$\frac{N(X,t)}{N_t} = \frac{C}{K} \exp(-\frac{CX}{K}) \tag{2.22}$$

Defining the constants k^+ and k^- as

$$k^+ = (k_b + k_h)$$

$$k^- = (k_h - k_b),$$

Eq. (2.20) can be written in dimensionless form as

$$a_x \frac{N(X,t)}{N_t} = \frac{2k^-}{k^+} \exp\left[(-\frac{2k^-}{k^+})(\frac{X}{a_x})\right] \tag{2.23}$$

Case ii: $k_h = k_b = k$

The condition that $k_h = k_b = k$ corresponds to the Griffith's equilibrium condition where the crack can either heal back or propagate. From Eq. (2.18), when $C = 0$, the crack size distribution is

$$\frac{N(X,t)}{N_t} = \frac{1}{2(\pi Kt)^{\frac{1}{2}}} \{\exp - \frac{(X - X_o)^2}{4Kt} + \exp - \frac{(X + X_o)^2}{4Kt}\} \tag{2.24}$$

and when $X_o = 0$

$$\frac{N(X,t)}{N_t} = \frac{1}{(\pi Kt)^{\frac{1}{2}}} \exp(-\frac{X^2}{4Kt}) \tag{2.25}$$

The average crack size $\bar{X}$ is given by [45]

$$\bar{X} = \left[\frac{\int_o^\infty X^2 N(X,t)\, dx}{\int_o^\infty N(X,t)\, dx}\right]^{\frac{1}{2}} \tag{2.26}$$

and from Appendix 2, when $k_h = k_b = k$,

$$\bar{X} = a_x(2kt)^{\frac{1}{2}} \tag{2.27}$$

As before, Eq. (2.25) can be written in dimensionless form as

$$a_x \frac{N(X,t)}{N_t} = \frac{1}{(\pi k t)^{\frac{1}{2}}} \exp - \frac{\left(\frac{X}{a_x}\right)^2}{4kt} \tag{2.28}$$

Case (iii): $k_b > k_h$

When $k_b > k_h$ the crack size distribution can be obtained from Eq. (2.18) when $X_o \neq 0$ and from Eq. (2.19) when $X_o \doteq 0$. It can be shown that when t is large, Eq. (2.19) takes the form (Appendix 3).

$$\frac{N(X,t)}{N_t} = \frac{1}{2(\pi K t)^{\frac{1}{2}}} \exp - \frac{(X + Ct)^2}{4Kt} \tag{2.29}$$

The average crack size $\bar{X}$ is

$$\bar{X} = \left[\frac{\int_o^\infty X^2 \, N(X,t) \, dx}{\int_o^\infty N(X,t) \, dx} \right]^{\frac{1}{2}}$$

which leads to [79]

$$\bar{X} = - Ct \tag{2.30}$$

or $$\frac{\bar{X}}{a_x} = - k^- t$$

In dimensionless form, Eq. (2.29) is

$$\frac{a_x \, N(X,t)}{N_t} = \frac{1}{(2\pi k^+ t)^{\frac{1}{2}}} \exp \left[- \frac{\left(\frac{X}{a_x} + k^- t\right)^2}{2k^+ t} \right] \tag{2.31}$$

In summary, Eqs. (2.23), (2.28) and (2.31) describe the crack size distribution for the three conditions $k_b < k_h$, $k_b = k_h = k$ and $k_b > k_h$ respectively.

2.3 Discussion

(a) Crack Healing Condition, $k_b < k_h$

Figures 2.4, 2.5 and 2.6 show the crack size distribution when the rate of bond breaking is less than the rate of bond healing and the initial microcrack size is approximately zero. The curves were calculated from Eq. (2.19). The rate constants k_b and k_h were calculated from Eq. (1.22). The activation free energy associated with the bond breaking process was taken as 1.0 eV while the activation free energy associated with the bond healing process was considered to be approximately zero [20,28,22]. Typical values of the activation free energy for different materials are given in Appendix 4. The mechanical energy values were generally considered without assuming any mechanical energy-applied stress relationship. Both the Griffith and the Irwin conditions described in Eqs. (1.23) are incorporated.

The curves in Fig. (2.4) were calculated with the mechanical energy value of 0.49 eV. It is of interest to note that because the activation free energy associated with the bond healing process is zero, the forward rate constant k_b will be equal to the backward rate constant k_h when the mechanical energy is equal to half the activation free energy associated with the bond breaking process. Thus, for $W(\sigma) = 0.49$ eV, the rate of bond breaking is less than the rate of bond healing. Figures 2.4 and 2.5 illustrate the effect of the mechanical energy and temperature on the crack size distribution while the summary of the calculation results is shown in Table 2.1. For a mechanical energy of 0.49 eV and a

temperature of 200K (Fig. 2.4(a)), the time taken to reach steady state is 100 seconds while, if the temperature is increased to 300K (Fig. 2.4(a)), the time taken to reach steady state is only one hundredth of a second. The steady state crack size change in Table 2.1 was defined for a negligibly small value of the crack tip concentration (a_x $N/N_t \simeq 0.005$) relative to the concentration scale. The steady state crack size change is 0-6 atomic distances when the temperature is 200K and 0-9 atomic distances when the temperature is 300K, for a mechanical energy value of 0.49 eV.

Mechanical energy (eV)	Temperature K	Time needed to reach steady state (sec)	Steady state crack size change (atomic distances)
0.49	200	100	0 - 6
	300	0.01	0 - 9
0.499	200	10^4	0 - 30
	300	1	0 - 44

Table 2.1. The table shows the summary of the effect of the mechanical energy and temperature on the steady state crack size change and the time needed to reach steady state illustrated in Figs. 2.4 and 2.5.

When the mechanical energy is increased from 0.49 eV to 0.499 eV at 200K, the time to reach steady state increases from 100 sec. to 10,000 sec. (about 3 hrs) while the steady state crack size change increases from 0-6 atomic distances to 0-30 atomic distances. For the same increase in the mechanical energy but at a temperature of 300K, the steady state crack size change increases from 0-9 atomic distances to 0-44 atomic distances, while the time to reach steady state increases from 0.01 seconds to 1.0 second.

It follows that the steady state crack size change (distribution) increases while the time to reach steady state decreases with increasing temperature. On the other hand, both the steady state crack size distribution and the time needed to reach steady state increases as the mechanical energy increases. In general, the steady state crack size distribution increases with a decreasing ratio of k^-/k^+ as shown in Fig. 2.6. The curves in Fig. 2.6 were calculated by using Eq. (2.23). The steady state crack size distribution is, therefore, controlled by the magnitude of the ratio of k^-/k^+ which is determined by the mechanical energy, temperature and the activation free energy of the material.

When the rate of bond breaking is less than the rate of bond healing, incipient cracks develop in the specimen. That these incipient cracks are of the order of a few atomic distances in size and that they are different in size was shown experimentally by Zhurkov and his co-workers [53] as well as Kusenko et al. [36] in metals, polymers and ionic solids. The knowledge of the size and concentration of the incipient cracks is useful in the study of polymer and metal fracture where the main crack is formed by the accumulation of these microcracks [53].

The observations in this study are in contradiction with the Griffith theory which proposed that crack propagation takes place when $k_b > k_h$.

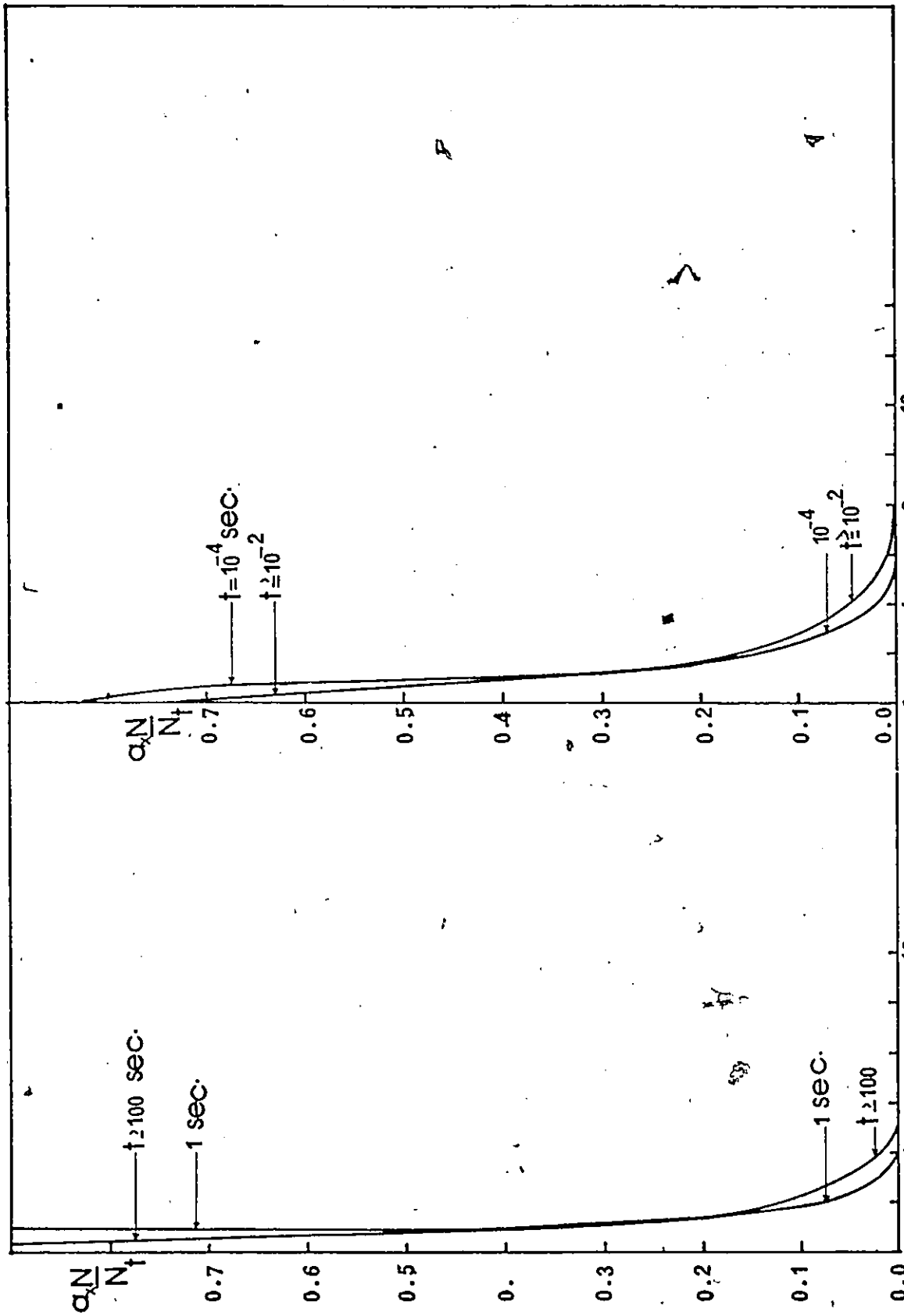

Figure 2.4(a)

Figure 2.4(b)

Figure 2.4 The figure shows the crack size distribution when the rate of forward activation is less than the rate of backward activation. The curves were calculated from Eq.(2.19). The numbers on each curve represent the time in seconds at which the crack size is described. The parameters are: $\Delta G^{\ddagger} = 1.0$ eV, $\Delta G^{\ddagger}_b = 0$, $W(\sigma) = 0.49$ eV. (a) Crack size distribution when the temperature is 200K. (b) Crack size distribution when the temperature is 300K.

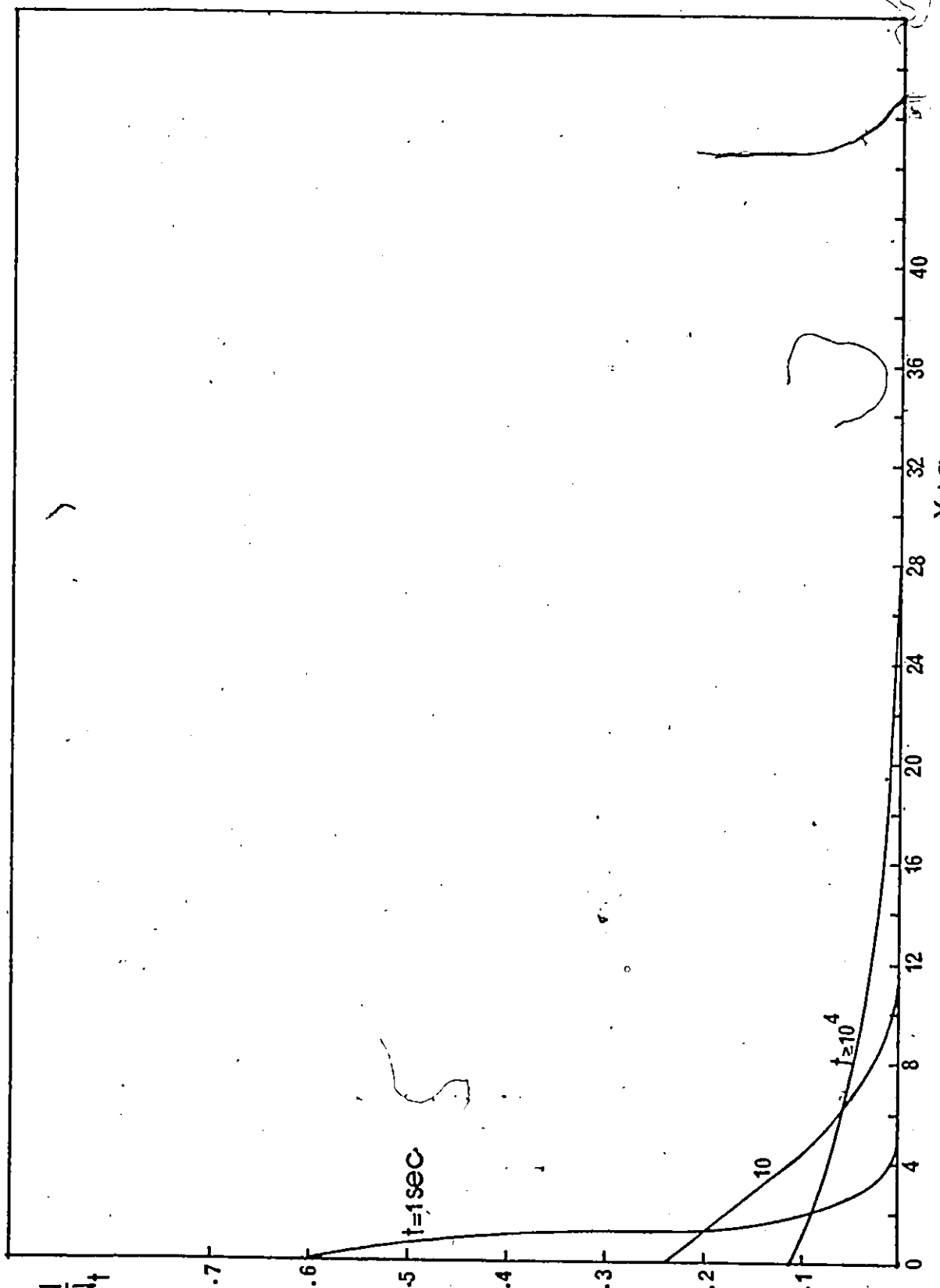
$\alpha_x N/N_t$
0.7
0.6
0.5
0.4
0.3
0.2
0.1
t=1 sec
10
$t \geq 10^4$
0
4
8
12
16
20
24
28
32
36
40
X/α_x

Figure 2.5(a)

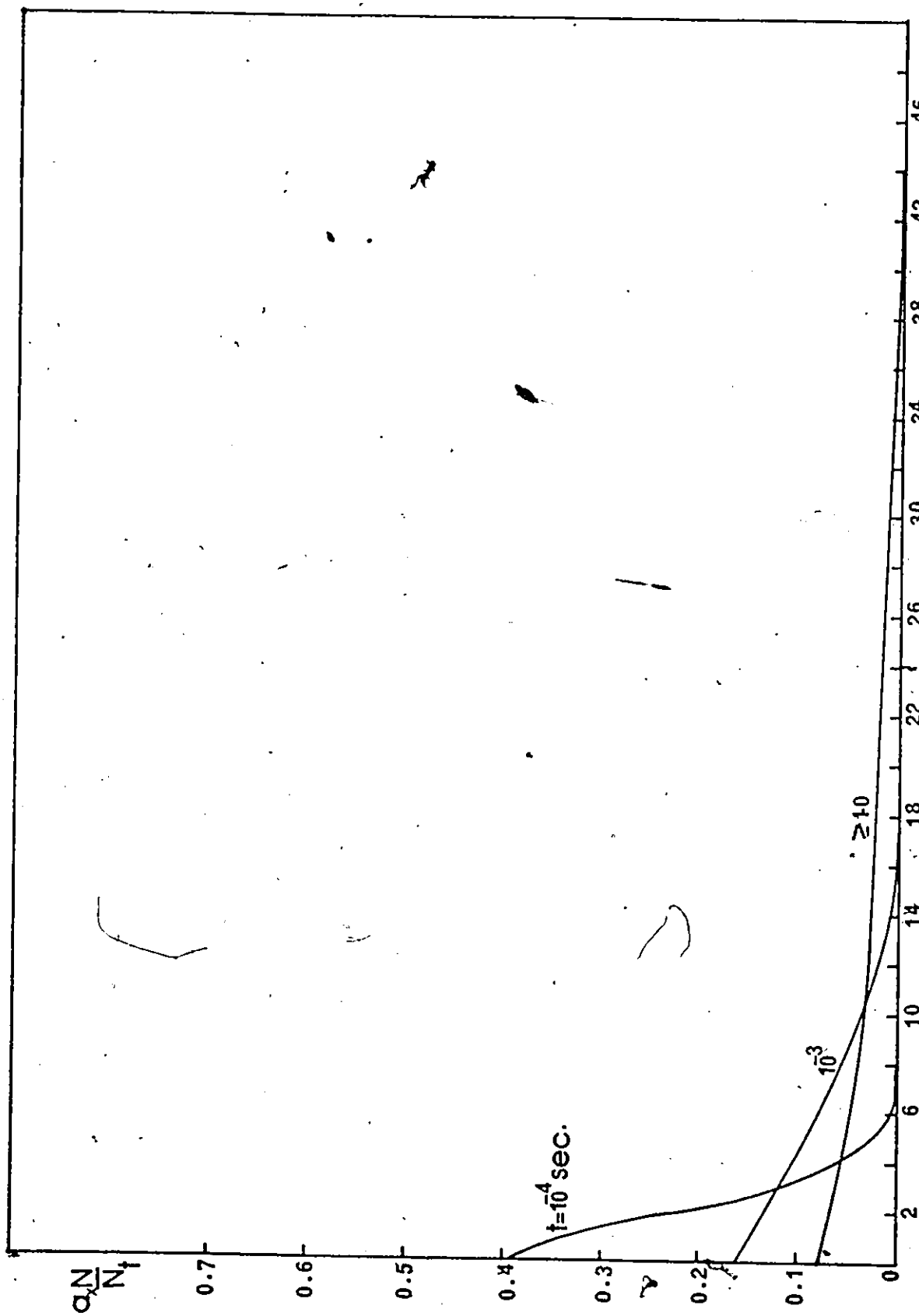

Figure 2.5(b)

Figure 2.5 The figure shows the crack size distribution for the same conditions as in Fig. 2.4, but with the mechanical energy increased to 0.499 eV.

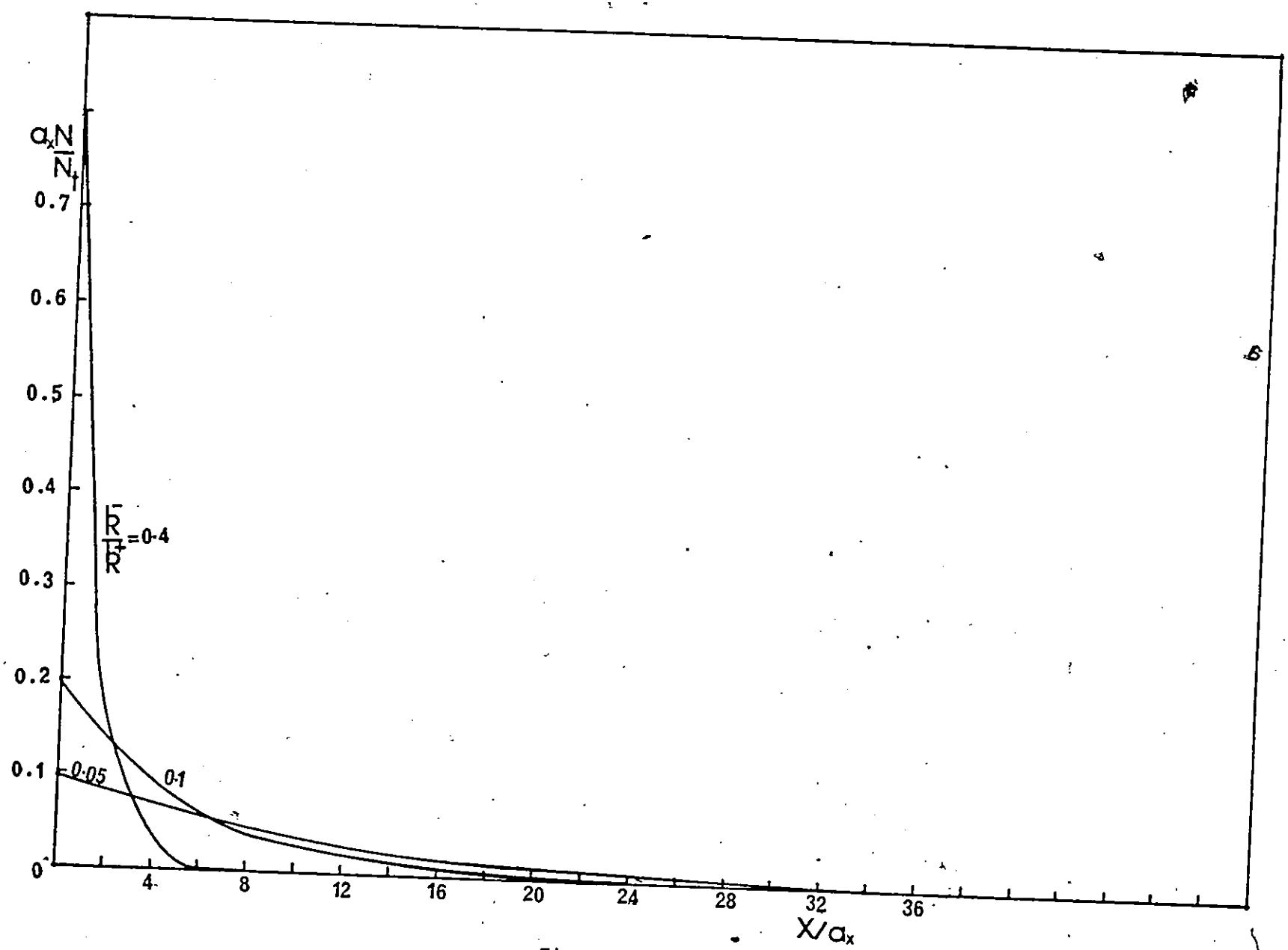

Figure 2.6

Figure 2.6 The figure shows the steady state crack size distribution as a function of the ratio of k^-/k^+ as indicated on each curve. The curves were calculated from Eq.(2.23).

(b) Crack Propagation, $k_b > k_h$

The existing submicrocracks in a specimen will propagate when the rate of bond breaking is greater than or equal to the rate of bond healing. It was, however, observed in the proceeding section that even when the rate of bond breaking is less than the rate of bond healing, microcracks are generated in the specimen. Because k_b and k_h are proportional to the probability of the bond breaking and healing events respectively, the size of the crack is not defined by an exact number, but as a range on the crack size scale. The probability and the crack size distribution are described by the distribution function. Equations (2.28) and (2.31) are the distribution functions when $k_b = k_h = k$ and $k_b > k_h$ respectively.

Figures 2.7, 2.8, 2.9 and 2.10 are typical probability curves calculated by using Eq. (2.31). The probability curves describe the crack size distribution as a function of the mechanical energy, temperature, time, and the activation free energy of the material. As in part (a) of the discussion, the activation free energy associated with the bond breaking process was taken to be 1.0 eV and the same procedure was used to calculate the rate constants. The effect of the applied stress and temperature on the crack size distribution is illustrated in Figs. 2.7, 2.8, 2.9 and 2.10 and summarized in Table 2.2. The crack size distribution was defined (as before), for a negligibly small value of the concentration ($a_x N/N_t \simeq 10^{-7}$). The curves in Figs. 2.7 and 2.8 were calculated with a mechanical energy of 0.501 eV. When the temperature is increased

from 300K to 350K (Figs. 2.7 and 2.8), the crack size distribution increases by about 230% while the average crack size increases by about 1500% when the time is 10^4 seconds.

Mechanical energy eV	Temperature ^oK	Time	Average crack size X 10^5 atomic distance	Crack size distribution 10^5 atomic distance	Figure
0.501	300	10^4	192.4	± 0.8	2.7 a
		2×10^4	384.8	± 1.0	2.7 b
		4×10^4	769.6	± 1.3	2.7 c
	350	10^4	3049.3	± 2.7	2.8 a
		2×10^4	6098.6	± 3.6	2.8 b
		4×10^4	12197.2	± 4.5	2.8 c
0.54	300	10^4	11153	± 1.1	2.9 a
		2×10^4	22306	± 1.4	2.9 b
		4×10^4	44612	± 2.0	2.9 c
	350	10^4	160990	± 3.5	2.10 a
		2×10^4	321980	± 5.0	2.10 b
		4×10^4	643960	± 6.5	2.10 c

Table 2.2 Summary of the effect of the mechanical energy and temperature on the crack size distribution illustrated in Figures 2.7, 2.8, 2.9 and 2.10.

Similar observations are made when the mechanical energy is 0.54 eV. The curves in Figs. 2.7 (a) and 2.9 (a) were calculated with the mechanical energy values of 0.501 and 0.54 eV respectively. Due to the increase in the mechanical energy (i.e. from 0.501 to 0.54 eV) the crack size distribution increases by about 40% and the average crack size increases by about 5600%.

The distribution or probability curves in Fig. 2.11 were calculated by using Eq. (2.31) with the value of $(k^{+}t)$ for curve 1 = 2.5 x 10^{8}, curve 2 = 10^{9}, curve 3 = 2 x 10^{9} and $|(k^{-}t)| = 2 \times 10^{7}$ = constant. The crack size distribution increases with the increasing value of $(k^{+}t)$. In Fig. 2.12, the distribution curves were calculated by using Eq. (2.31) with the values of $(k^{+}t)$ for curve 1 = 2.5 x 10^{8}, curve 2 = 5 x 10^{8}, curve 3 = 10^{9}, and the values of $k^{-}t$ for curve 1 = 2 x 10^{7}, curve 2 = 2.01 x 10^{7} and curve 3 = 2.02 x 10^{7}. It follows that the crack size distribution or the shape of the crack size distribution curves is controlled by the value of $(k^{+}t)$ while the average crack size or the location is controlled by the value of $(k^{-}t)$. However, when $k_b = k_h = k$, the average crack size is $a_x(2kt)^{\frac{1}{2}}$ and it is stationary. Similar results were obtained by Krausz [54] using random walk mathematics. It is not a coincidence that the two approaches give similar results. In the present analysis, the mathematical treatment of crack propagation leads to a differential equation that is formally equivalent to the differential equation of diffusion which is a typical random walk process.

The crack size distribution is actually the scatter of experimental readings in the crack propagation measurements. However, the results above predict a scattering of experimental readings in the order of one tenth of a millimeter (10^{6} Å) while in actual experiments the scatter is larger. The reason for this discrepancy may be due to the fact that most materials are not homogeneous as assumed in the analysis. Consequently, the rate constants will not remain constant during crack

propagation, but will vary according to the local potential energy of the material. Due to the structural inhomogeneities each of the N_t cracks in the ensemble (for a given specimen with an ensemble of N_t cracks) has its own characteristic potential surface [71]. Also, scatter in the applied load, temperature and the geometry of the crack lead to the observed crack size scatter in the crack propagation measurements.

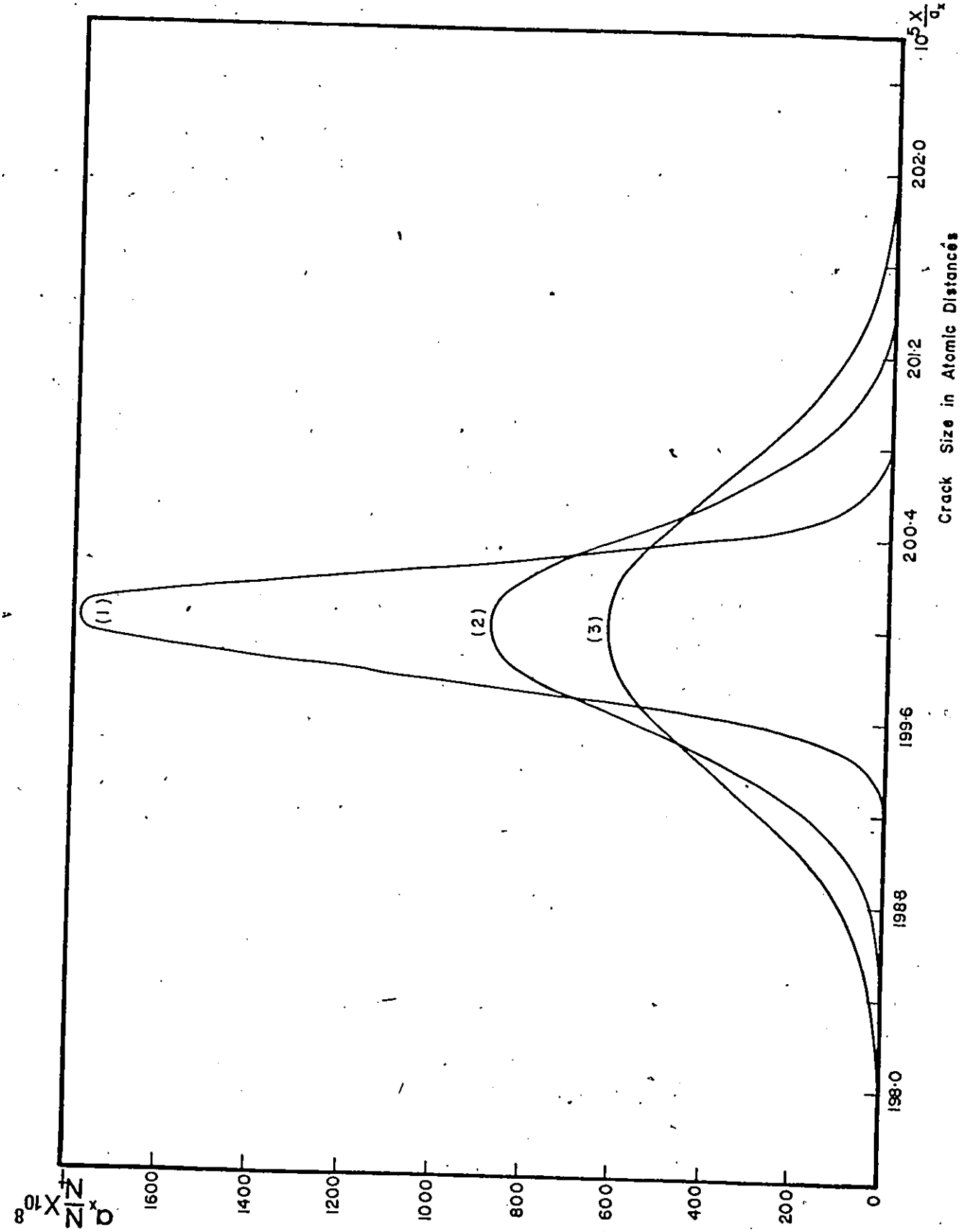

Figure 2.11

Figure 2.11 The figure shows the crack size distribution when the value of $(k-t)$ is constant and the value of $(k+t)$ is varying. The parameters are $(k-t) = 200 \times 10^5$ = constant curve 1 -$(k+t) = 2.5 \times 10^8$, curve 2 - $(k+t) = 10^9$, curve 3 - $(k+t) = 2 \times 10^9$. Curves 1, 2 and 3 were calculated from Eq. (2.31).

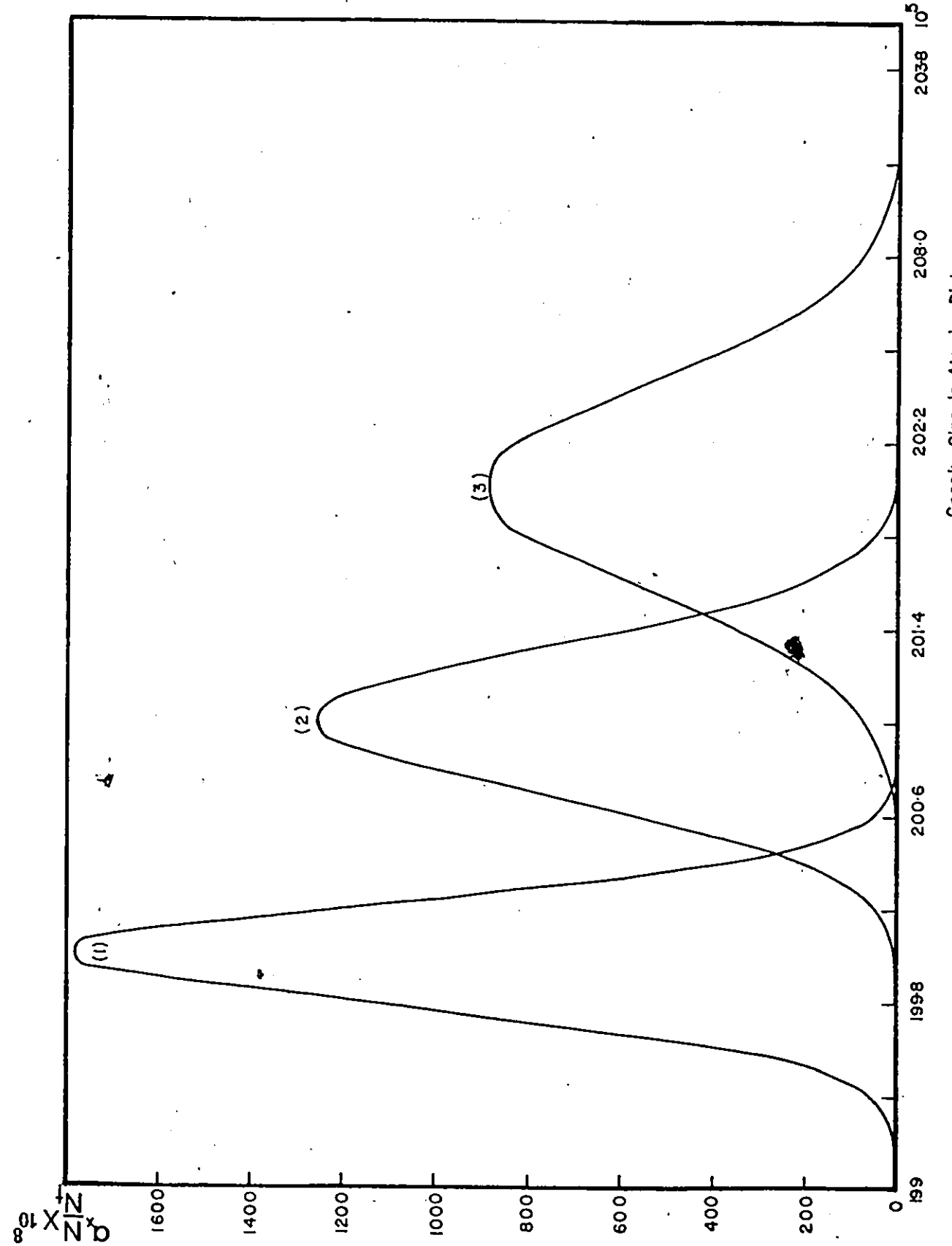

Figure 2.12

Figure 2.12 The figure shows the crack size distribution when both $(k+t)$ and $(k-t)$ are varying. The curves were calculated by using Eq. (2.31). The parameters are: $(k+t)_1 = 2.5\times10^8$, $(k-t) = 2\times10^7$; $(k+t)_2 = 5\times10^8$, $(k-t)_2 = 2.01\times10^7$; $(k+t)_3 = 10^9$, $(k-t)_3 = 2.02\times10^7$. Subscripts 1, 2 and 3 represent curves 1, 2 and 3 respectively.

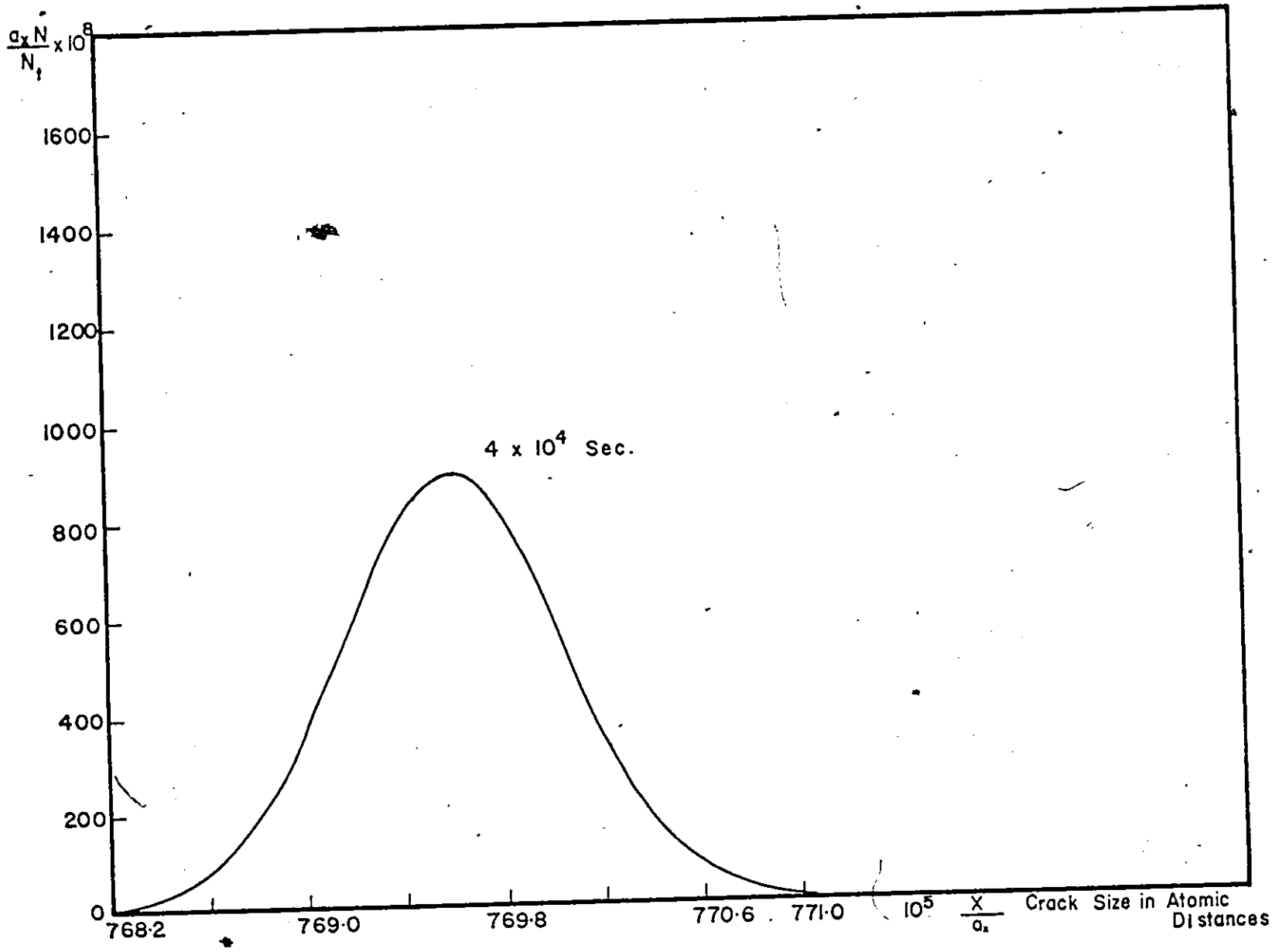

Figure 2.7(c)

Figure 2.7 The figure shows the crack size distribution in a material with a bond energy of 1.0 eV when $k_b > k_h$. The curves were calculated from Eq. (2.31). The parameters are $\Delta G^{\ddagger} = 1.0$ eV, W = 0.501 eV, T = 300K. (a) Crack size distribution after 10^4 seconds. (b) Crack size distribution after 2×10^4 seconds. (c) crack size distribution after 4×10^4 seconds.

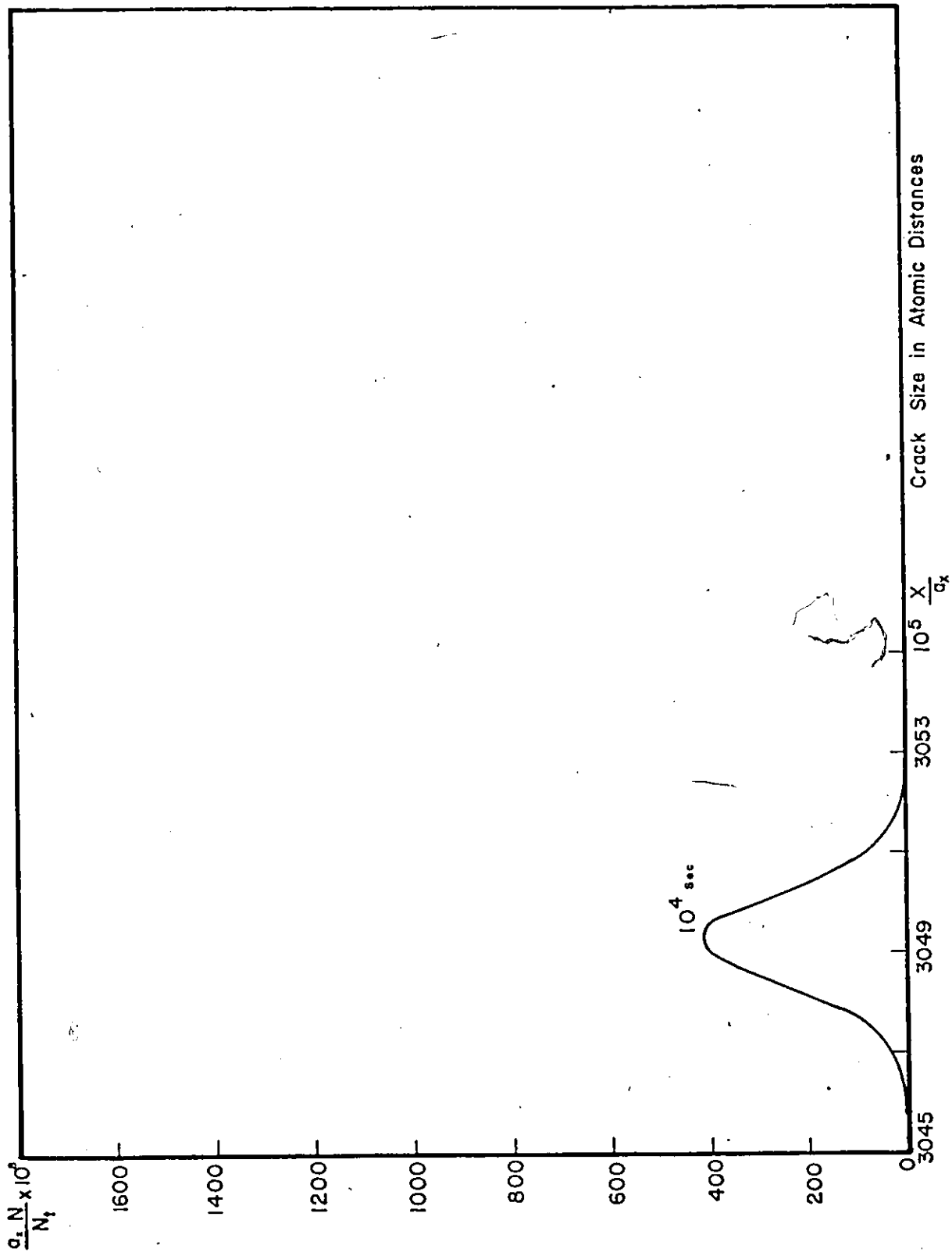
$\frac{a_x}{N_t} N \times 10^6$
1600
1400
1200
1000
800
600
400
200
0
3045
3049
3053
$10^5 \frac{X}{a_x}$
Crack Size in Atomic Distances
10^4 sec

Figure 2.8(a)

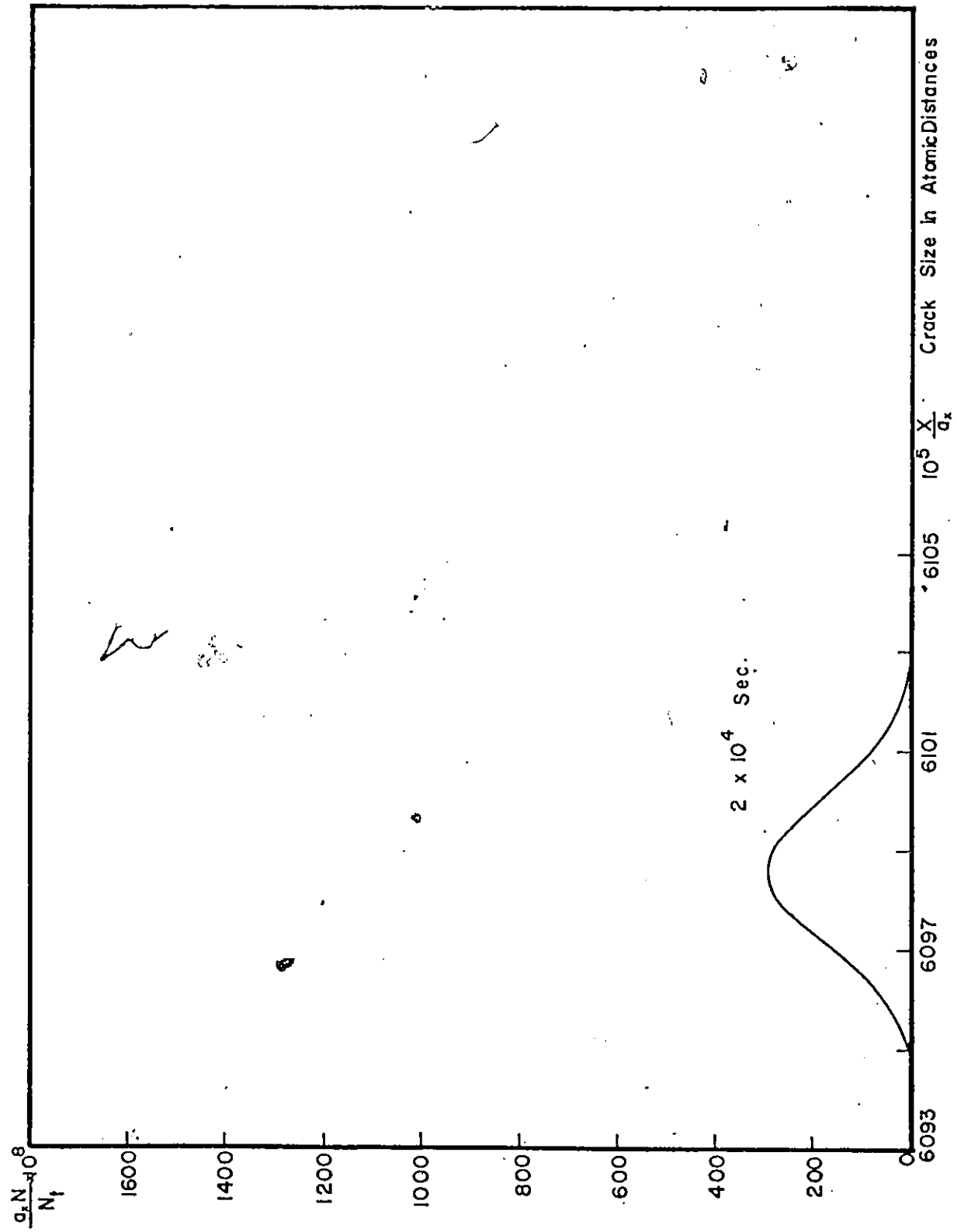
$\frac{a_x N_f 10^8}{N_f}$
1600
1400
1200
1000
800
600
400
200
0
6093
6097
6101
6105
$10^5 \frac{X}{a_x}$ Crack Size in Atomic Distances
2×10^4 Sec.

Figure 2.8(b)

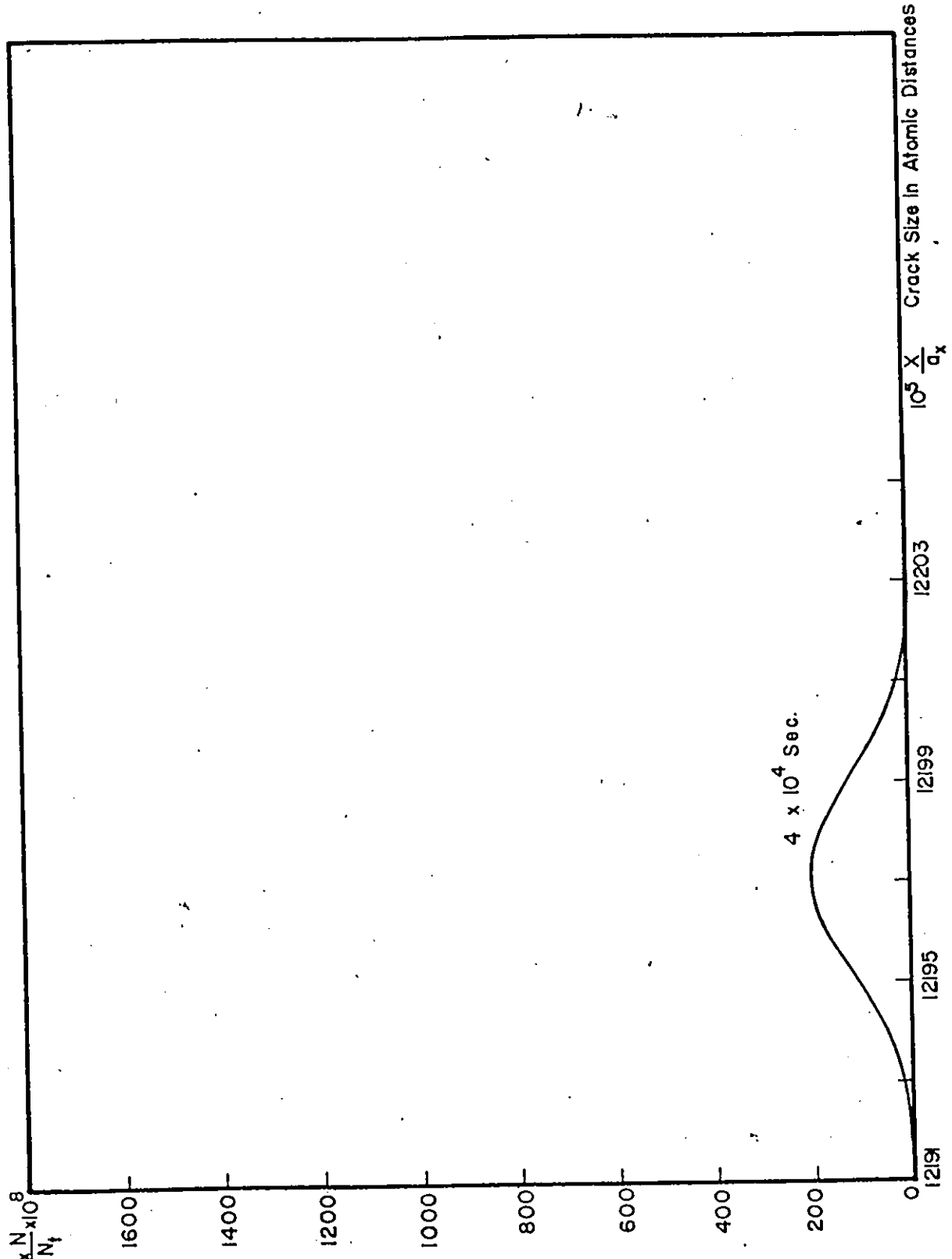

Figure 2.8(c)

Figure 2.8 The figure shows the crack size distribution for the same conditions as in Fig. 2.7 but at a temperature of 350K.

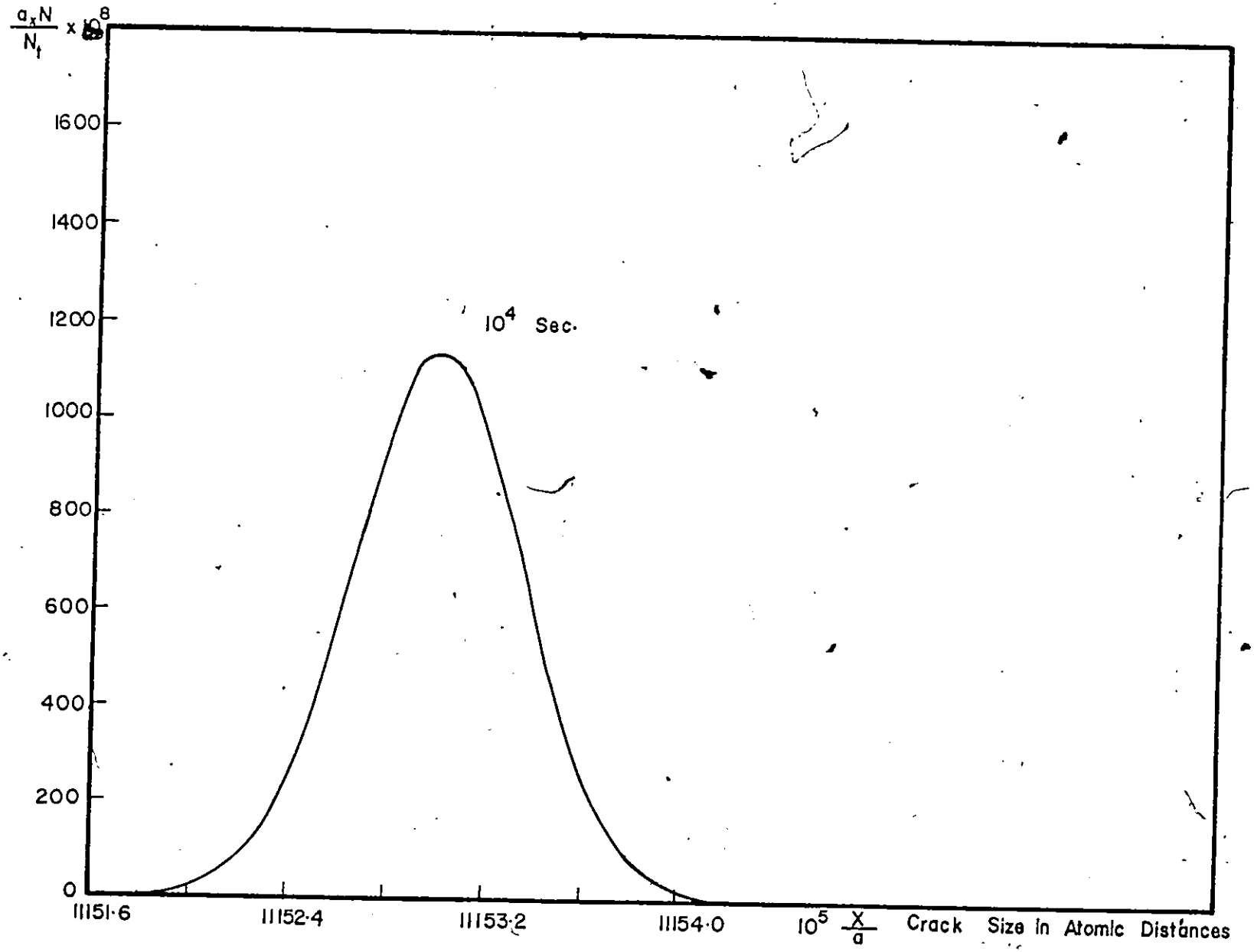
$\frac{a_x N}{N_f} \times 10^8$
1600
1400
1200
1000
800
600
400
200
0
10^4 Sec.
11151·6
11152·4
11153·2
11154·0
$10^5 \frac{X}{a}$ Crack Size in Atomic Distances

Figure 2.9(a)

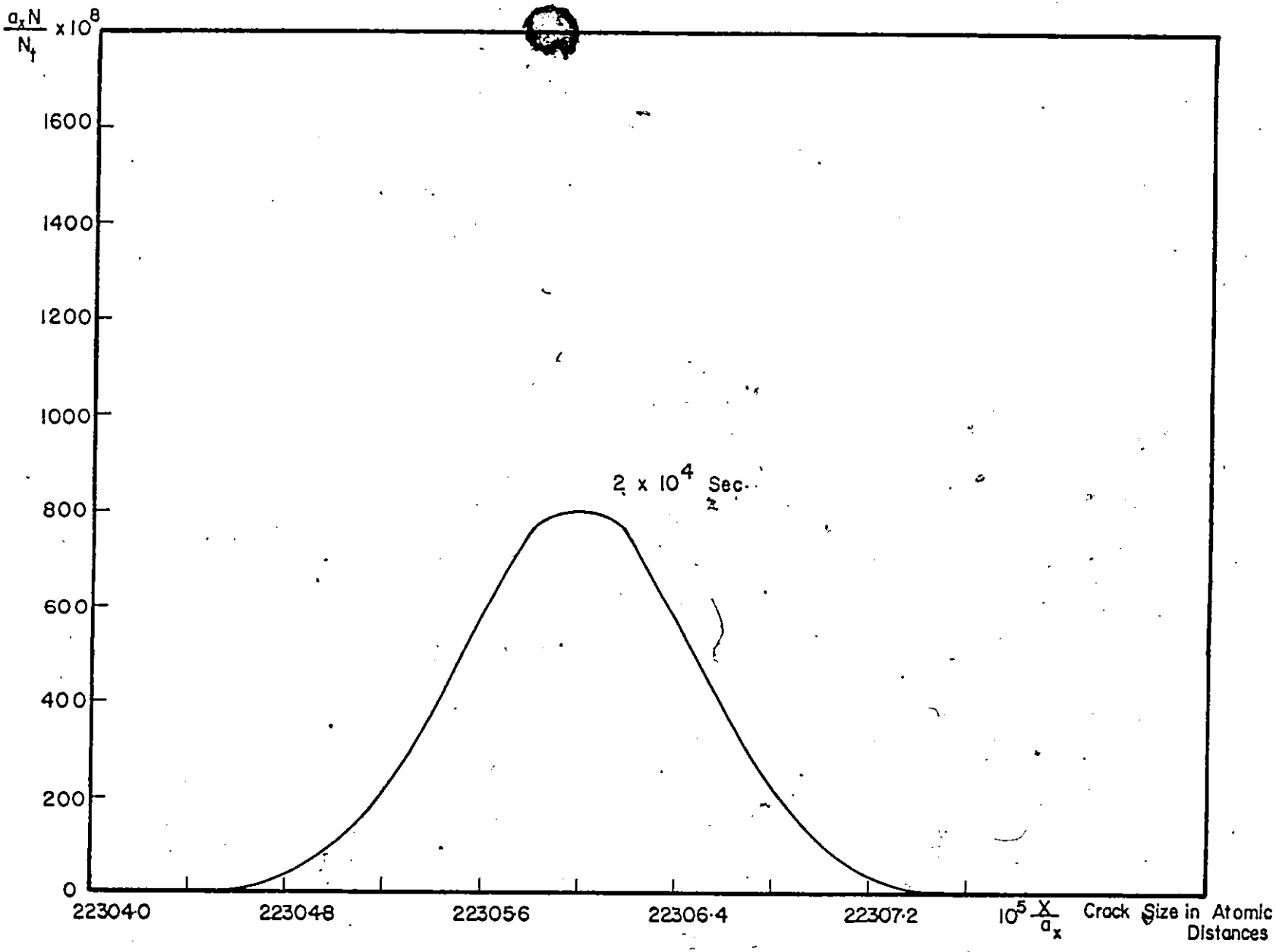
$\frac{a_x N}{N_f} \times 10^8$
1600
1400
1200
1000
800
600
400
200
0
2×10^4 Sec.
223040
223048
223056
22306·4
22307·2
$10^5 \frac{X}{a_x}$ Crack Size in Atomic Distances

Figure 2.9(b)

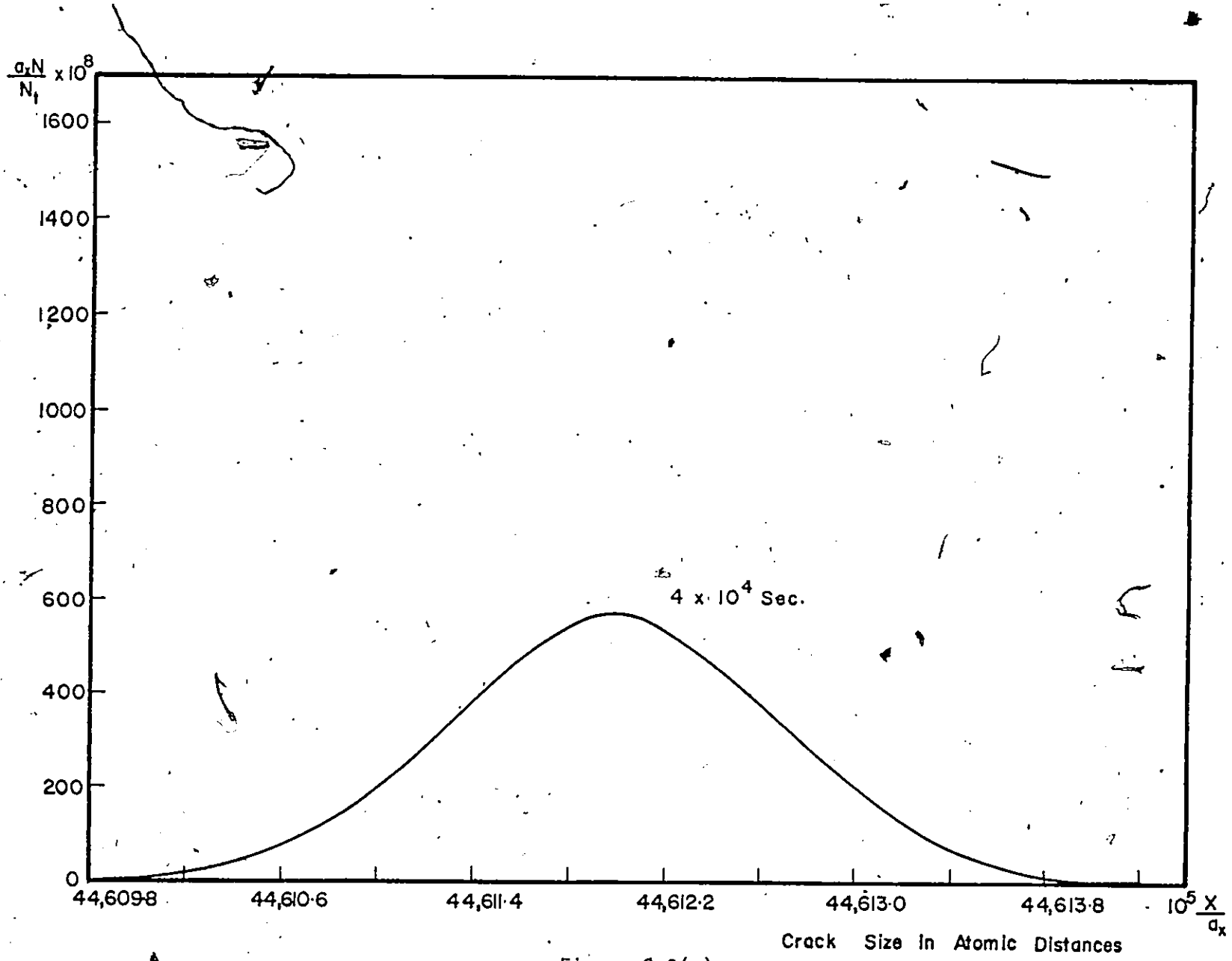

Figure 2.9(c)

Figure 2.9 The figure shows the crack size distribution for same conditions as in Fig. 2.7 but with a mechanical energy value of 0.54 eV.

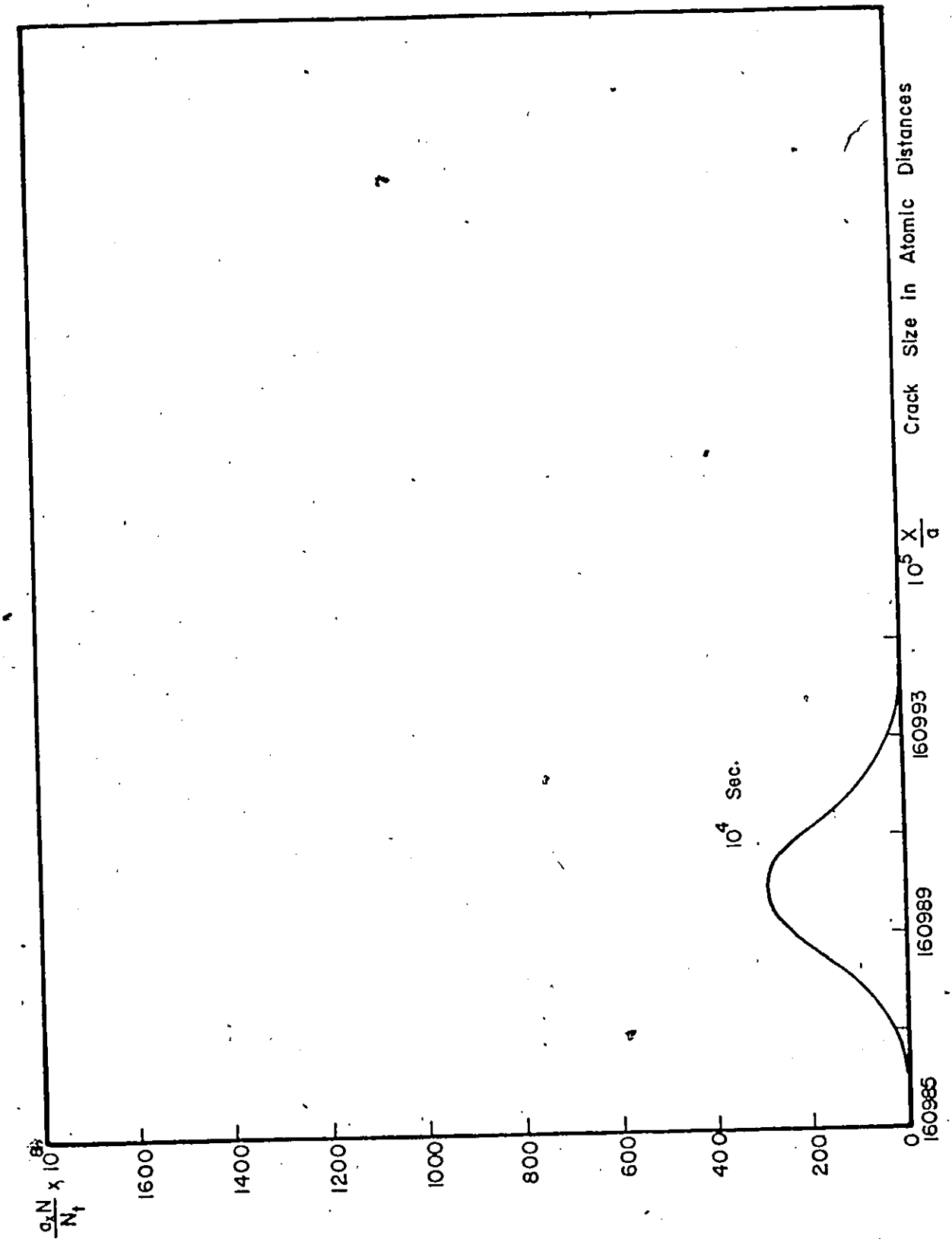
$\frac{\sigma_x N}{N_f} \times 10^{8}$
1600
1400
1200
1000
800
600
400
200
0
160985
160989
160993
10^4 Sec.
$10^5 \frac{X}{a}$
Crack Size In Atomic Distances

Figure 2.10(a)

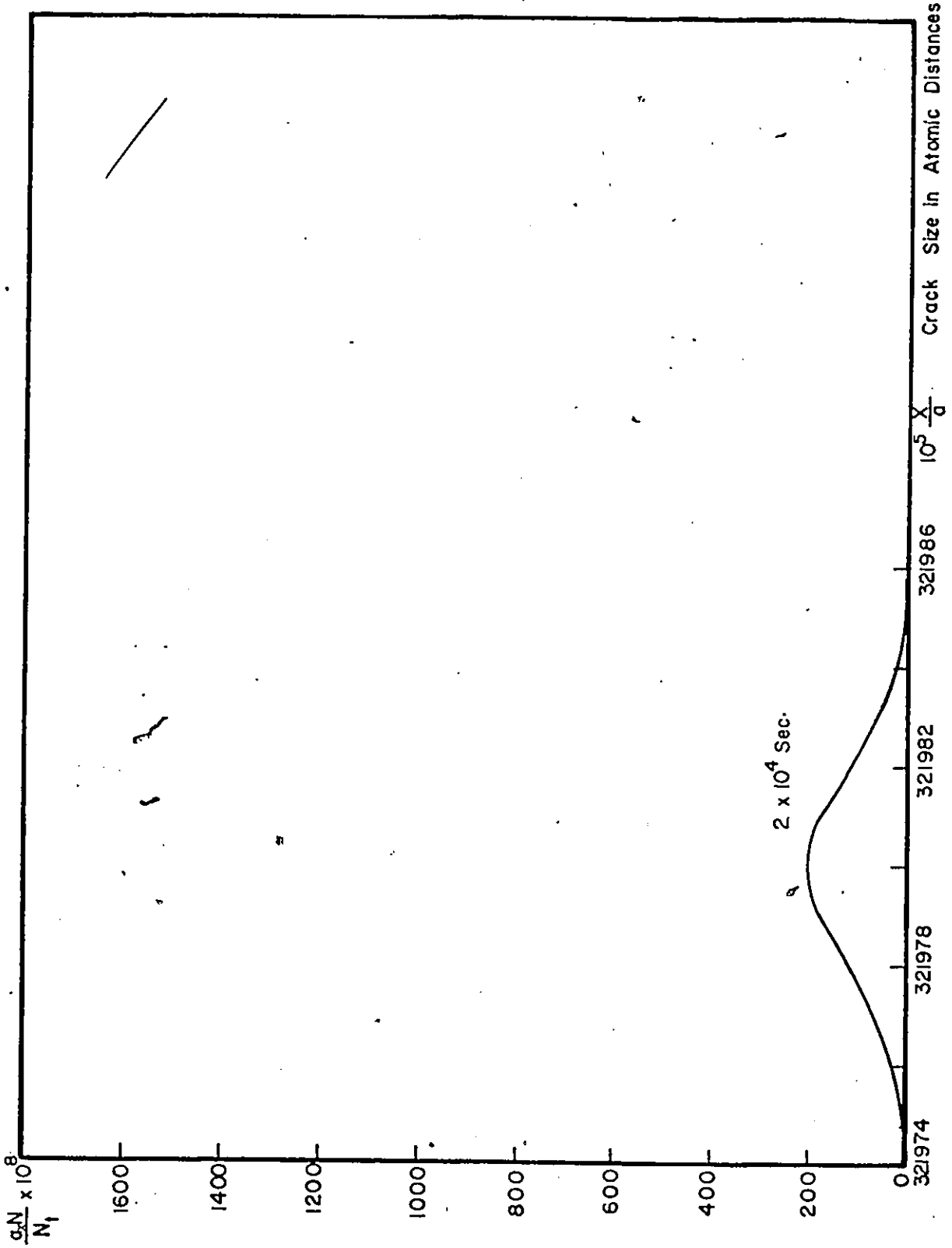
$\frac{\sigma_2 N}{N_1} \times 10^8$
1600
1400
1200
1000
800
600
400
200
0
321974
321978
321982
321986
$10^5 \frac{X}{a}$
Crack Size in Atomic Distances
2×10^4 Sec.

Figure 2.10(b)

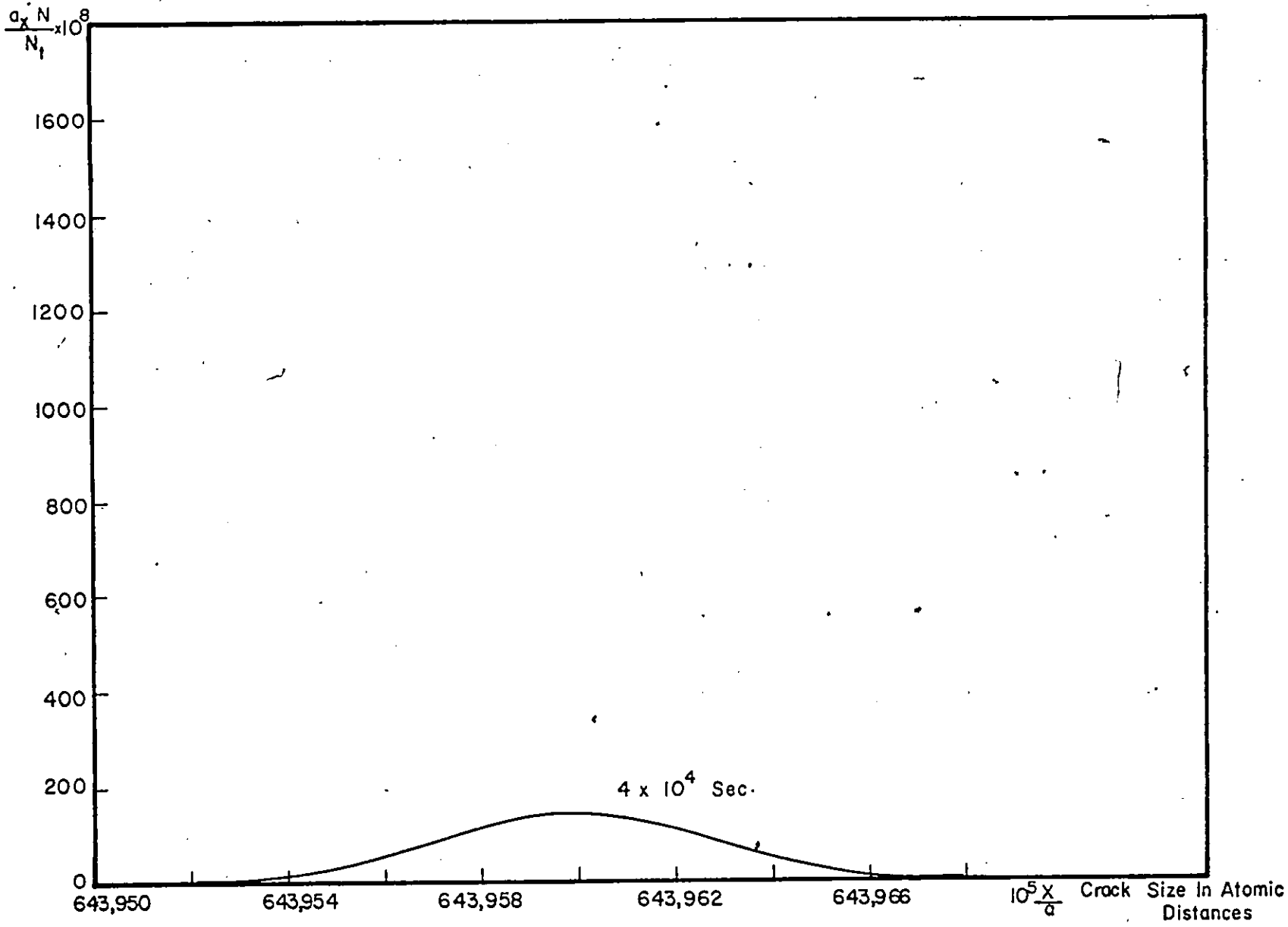

Figure 2.10(c)

Figure 2.10 The figure shows the crack size distribution for the same conditions as in Fig. 2.8 but with a mechanical energy equal to 0.54 eV.

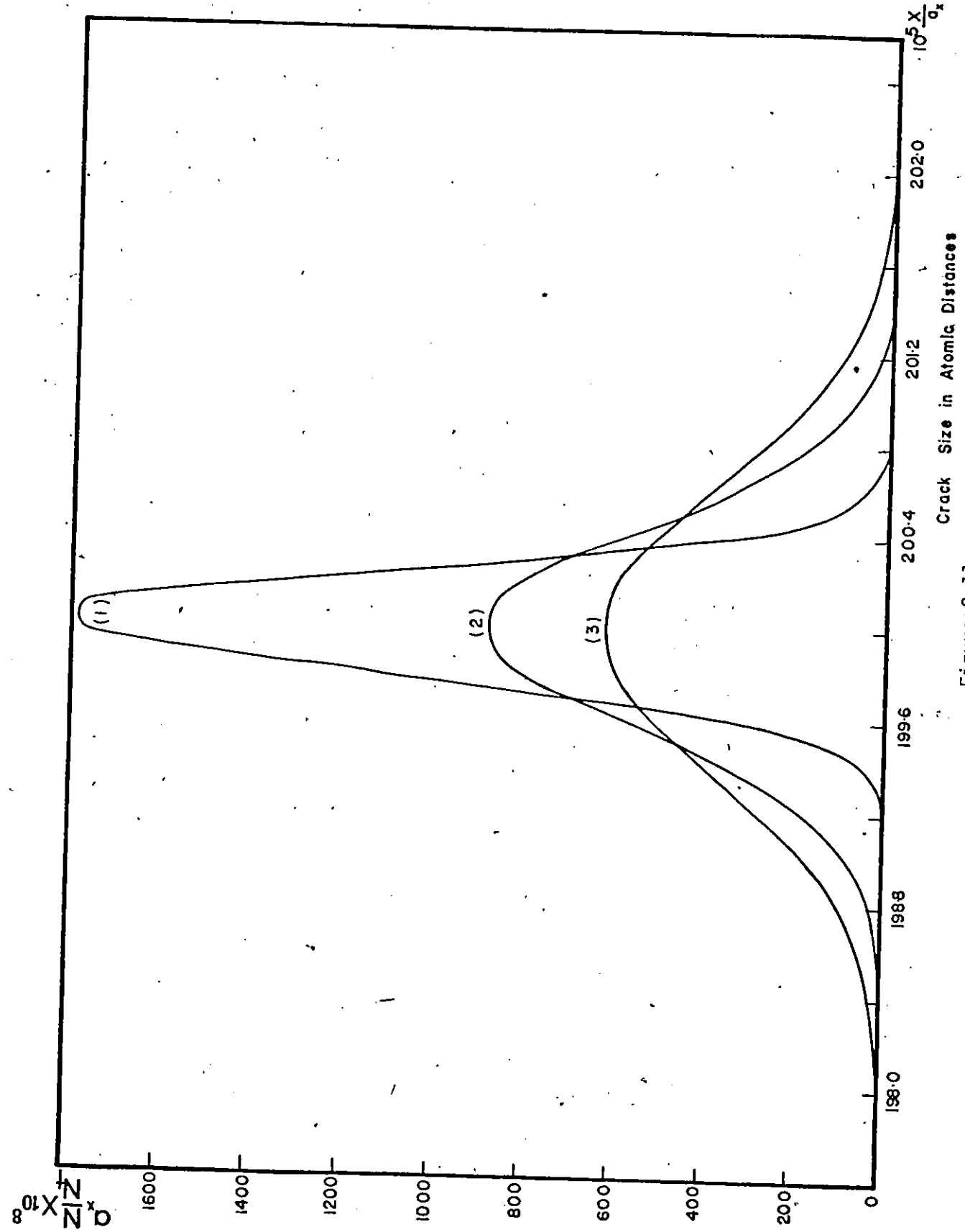

Figure 2.11 The figure shows the crack size distribution when the value of $(k\text{-}t)$ is constant and the value of $(k+t)$ is varying. The parameters are $(k\text{-}t) = 200\times10^5$ = constant curve 1 -$(k+t) = 2.5\times10^8$, curve 2 - $(k+t) = 10^9$, curve 3 - $(k+t) = 2\times10^9$. Curves 1, 2 and 3 were calculated from Eq. (2.31).

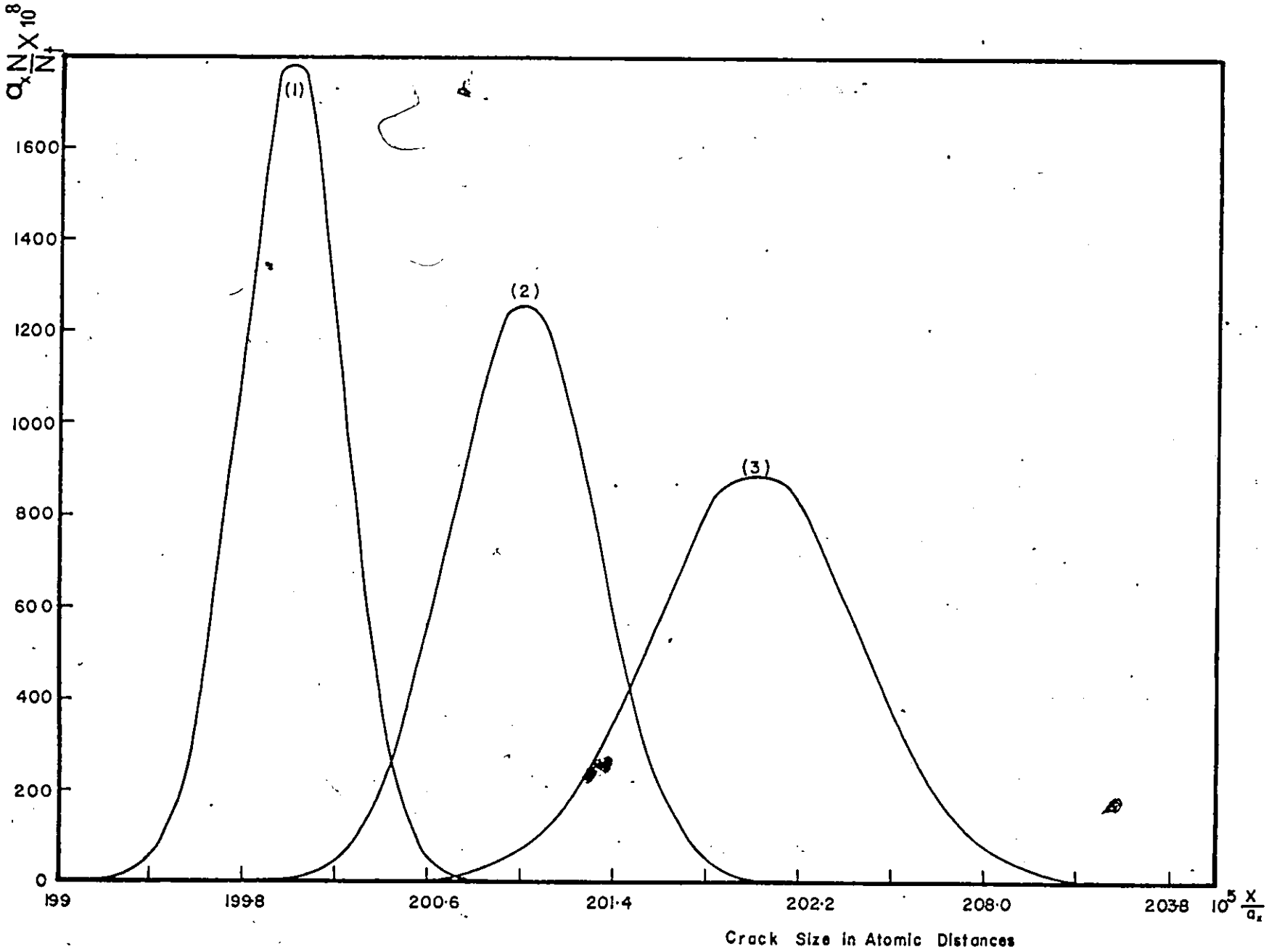

Figure 2.12

Figure 2.12 The figure shows the crack size distribution when both $(k+t)$ and $(k-t)$ are varying. The curves were calculated by using Eq. (2.31). The parameters are: $(k+t)_1 = 2.5\times10^8$, $(k-t) = 2\times10^7$; $(k+t)_2 = 5\times10^8$, $(k-t)_2 = 2.01\times10^7$; $(k+t)_3 = 10^9$, $(k-t)_3 = 2.02\times10^7$. Subscripts 1, 2 and 3 represent curves 1, 2 and 3 respectively.

Chapter 3

The Steady State Fracture Kinetics of Crack Propagation

In Chapter 2, the crack size distribution was analyzed for the non-steady state flow of crack tips over a periodic consecutive system of free energy barriers in which rigid crack front propagation was assumed and a continuous function for the crack size distribution was used. Thomson et al. [19,20], Lawn [28] and Krausz [42] have proposed that the crack propagation process is controlled by double kink nucleation and subsequent spreading over a consecutive free energy barrier system in analogy to the Peierls-Nabarro mechanism of dislocation movement. This, they argued, is an energetically more favourable process than the rigid crack front propagation. The continuous function description for the crack size distribution that was used in the previous Chapter is an approximation of the actual discrete description. The actual crack size distribution function should, therefore, be discrete and also incorporate the concepts of the double kink nucleation and spreading processes of the crack front propagation.

In this Chapter, the steady state fracture kinetics of the crack-front spreading will be discussed. First, the discrete analysis of the steady state double kink spreading will be carried out to derive the kink concentration distribution and the crack propagation velocity expressions. Secondly, an approximate, continuous mathematical description will be introduced and the kink concentration distribution and the crack propagation velocity expressions will be derived. In both cases, the kink distribution and the crack propagation velocity will be determined in a generally valid form when the plastic flow in front of the crack tip is negligible. The effect

of the applied stress and temperature on the kink distribution and the crack propagation velocity will be discussed.

3.1 Kinetics Analysis

The crack front propagation by double kink nucleation and sideways spreading appears to be an energetically more favourable and important mechanism than the rigid crack front propagation mechanism. Figure 3.1 illustrates the process that takes place. Both the double kink nucleation and spreading processes involve breaking and occasional healing of the atomic bonds. These are low energy processes compared to the rigid crack front propagation mode. The nucleation process is expected to occur at the weak segments of the material such as at the conglomerations of point defects, dangling bonds, dislocations, inclusions, etc. Because the activation free energy at these segments is relatively low, it was shown experimentally [37] that the nucleation process will be instantaneous. The spreading process needs a higher activation energy and consequently it controls the rate of crack propagation. There is not yet a theoretical basis for calculating the kink nucleation energy but the energy associated with the spreading process may, as an approximation [38] be determined from the Irwin-Orowan expression 1.29.

a) Discrete Analysis

Consider n consecutive spreading step process. The net flow of crack tips, F, over each barrier is described as

$$F_i = N_i \, {}_i k^i - N_{i+1} \, {}^{i+1}_{i+1} k \tag{3.1}$$

where ${}_i k^i$ is the bond breaking rate constant over the i-th barrier, i.e., the number of thermal activations per unit time that acts on the N_i number

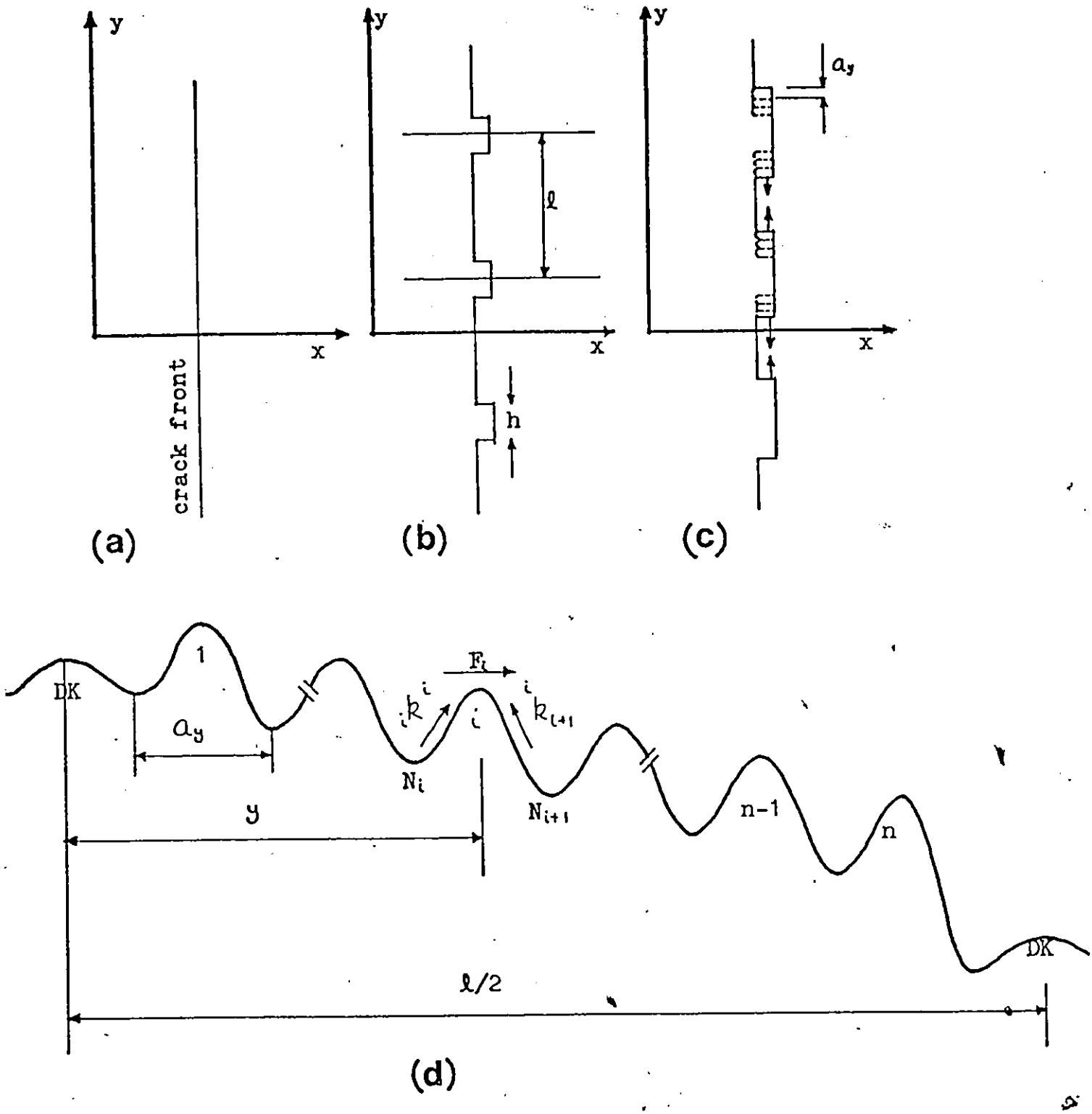

Figure 3.1 Diagrams (a) to (c) illustrate the crack front movement in the x direction as the result of nucleation and spreading of kinks in the y direction over consecutive free energy barriers illustrated by dashed lines. Diagram (d) is the energy barrier system associated with the n spreading step process illustrated in (c). DK identifies the energy barrier associated with nucleation of the double kink.

of kinks that are in the valley in front of the i-th barrier. The activation moves the kink from the valley to the activated state at the top of the barrier. The rate constant ${}^{i}k_{i+1}$ represents the reverse process - the bond healing rate that acts on the N_{i+1} kinks in front of the i+1-th barrier, causing the backward flow. The superscripts and subscripts show the graphics of the two activation types. The net flow of kinks over the i-th barrier is given by Eq. (3.1). The breaking and healing rate constants are defined in Eqs. (1.21), respectively as

$$ {}_{i}k^{i} = \frac{kT}{h} \exp\left[-\frac{{}^{i}\Delta G^{\ddagger i} - {}_{i}W^{i}(\sigma, i, t)}{kT}\right] \qquad (3.2(a)) $$

$$ {}^{i}k_{i+1} = \frac{kT}{h} \exp\left[-\frac{{}^{i}\Delta G^{\ddagger}_{i+1} + {}^{i}W_{i+1}(\sigma, i, t)}{kT}\right] \qquad (3.2(b)) $$

Because all spreading barriers are equal, when the crack front is much longer than the distance ℓ between the double kinks the work is independent of the location i of the kink. If static loading condition is assumed, then the mechanical energy is independent of time. Hence Eqs. (3.2(a)) and (3.2(b)) can be expressed as

$$ {}_{i}k^{i} = k_b = \frac{kT}{h} \exp\left[-\frac{\Delta G_b^{\ddagger} - W_b(\sigma)}{kT}\right] \qquad (3.3(a)) $$

$$ {}^{i}k_{i+1} = k_h = \frac{kT}{h} \exp\left[-\frac{\Delta G_h^{\ddagger} + W_h(\sigma)}{kT}\right] \qquad (3.3(b)) $$

Because the double kink pattern repeats itself, and because the spreading process is symmetrical about $y = \frac{\ell}{2}$, it is sufficient to analyze the kinetics over a distance $\ell/2$ only. The number of spreading barriers is $(\ell/2a_y - 1)$ or n. Due to annihilation at the n+1-th barrier, the concentration at the n+1-th valley is zero and the flow over the n-th barrier is

$$ F_n = N_n \, {}_{n}k^{n} \qquad (3.4) $$

Writing the net flow of kinks over each barrier, starting from the n-th barrier results in

$$
\begin{aligned}
F_n &= N_n\, {}_n k^n && && (1)\\
F_{n-1} &= N_{n-1}\, {}_{n-1}k^{n-1} && - N_n\, {}^{n-1}k_n && (2)\\
F_{n-2} &= N_{n-2}\, {}_{n-2}k^{n-2} && - N_{n-1}\, {}^{n-2}k_{n-1} && (3)\\
&\vdots && \vdots && (3.5)\\
F_i &= N_i\, {}_i k^i && - N_{i+1}\, {}^i k_{i+1} && (i)\\
F_1 &= N_1\, {}_1 k^1 && - N_2\, {}^1 k_2 && (n)\\
F_{dk} &= N_{dk}\, {}_{dk}k^{dk} && - N_1\, {}^{dk}k_1 && (n+1)
\end{aligned}
$$

In steady state, $F_1 = F_2 = \ldots = F_i = \ldots F_n = F_{ss}$. Equations (3.5) then contain (n+1) unknowns, N_{dk}, N_1, N_2 ... N_n and n+1 algebraic equations.

Solution of the Algebraic Equations.

From the first expression of Eqs. (3.5), we have

$$N_n = \frac{F_{ss}}{{}_n k^n}$$

Multiplication of the second equation by ${}_n k^n / {}^{n-1}k_n$ and adding the first two equations leads to

$$F\left(1 + \frac{{}_n k^n}{{}_{n-1}k_n}\right) = \frac{N_{n-1}\, {}_{n-1}k^{n-1}\; {}_n k^n}{{}_{n-1}k_n} \qquad (3.6)$$

hence

$$N_{n-1} = F_{ss}\left[\frac{{}_{n-1}k_n}{{}_n k^n\; {}_{n-1}k^{n-1}} + \frac{1}{{}_{n-1}k^{n-1}}\right] \qquad (3.7)$$

Multiplying the third equation by

$$\frac{{}_n k^n\; {}_{n-1}k^{n-1}}{{}_{n-1}k_n\; {}^{n-2}k_{n-1}}$$

and adding to Eq. (3.6) results in

$$F_{ss}\left(1+\frac{{}^{n}k^{n}}{{}^{n-1}k_{n}}+\frac{{}^{n}k^{n}\ {}^{n-1}k^{n-1}}{{}^{n-1}k_{n}\ {}^{n-2}k_{n-1}}\right)=\frac{N_{n-2}\ {}^{n}k^{n}\ {}^{n-1}k^{n-1}\ {}^{n-2}k^{n-2}}{{}^{n-1}k_{n}\ {}^{n-2}k_{n-1}}$$

and

$$N_{n-2}=F_{ss}\left[\frac{{}^{n-1}k_{n}\ {}^{n-2}k_{n-1}}{{}^{n}k^{n}\ {}^{n-1}k^{n-1}\ {}^{n-2}k^{n-2}}+\frac{{}^{n-2}k_{n-1}}{{}^{n-1}k^{n-1}\ {}^{n-2}k^{n-2}}+\frac{1}{{}^{n-2}k^{n-2}}\right] \tag{3.8}$$

From the pattern established now the general term is

$$N_{i}=F_{ss}\left[\frac{{}^{n-1}k_{n}\ {}^{n-2}k_{n-1}\ \cdots\ {}^{i}k_{i+1}}{{}^{n}k^{n}\ {}^{n-1}k^{n-1}\ \cdots\ {}^{i}k^{i}}+\frac{{}^{n-2}k_{n-1}\ {}^{n-3}k_{n-2}\ \cdots\ {}^{i}k_{i+1}}{{}^{n-1}k^{n-1}\ {}^{n-2}k^{n-2}\ \cdots\ {}^{i}k^{i}}+\cdots\ \frac{1}{{}^{i}k^{i}}\right] \tag{3.9}$$

The first term of Equation (3.9) expresses the activation from the i-th valley to the top of the n-th barrier, while the second term expresses the activation from the i-th valley to the top of the (n-1)-th barrier, etc. The last term expresses the activation from the i-th valley to the top of the i-th barrier. As an illustration, consider the number of kinks in front of the first barrier.

$$N_{1}=F_{ss}\left(\frac{1}{{}^{1}k^{1}}+\frac{{}^{1}k_{2}}{{}^{1}k^{1}\ {}^{2}k^{2}}+\frac{{}^{1}k_{2}\ {}^{2}k_{3}}{{}^{1}k^{1}\ {}^{2}k^{2}\ {}^{3}k^{3}}+\cdots+\frac{{}^{1}k_{2}\ {}^{2}k_{3}\ \cdots\ {}^{i-1}k_{i}}{{}^{1}k^{1}\ {}^{2}k^{2}\ \cdots\ {}^{i}k^{i}}\right.$$

$$\left.+\frac{{}^{1}k_{2}\ {}^{2}k_{3}\ {}^{i-1}k_{i}\ \cdots\ {}^{n-1}k_{n}}{{}^{1}k^{1}\ {}^{2}k^{2}\ \cdots\ {}^{i}k^{i}\ \cdots\ {}^{n}k^{n}}\right) \tag{3.10}$$

It can be shown that (Appendix 5) a term, for instance of the type

$$\frac{{}^{1}k_{2}}{{}^{1}k^{1}\ {}^{2}k^{2}}$$

is expressed as

$$\frac{{}_1k_2}{{}_1k^1\ {}_2k^2} = \frac{h}{kT} \exp \frac{{}_1\Delta G^2}{kT} = \frac{1}{{}_1k^2} .$$

Similarly, the term

$$\frac{{}_1k_2\ {}_2k_3}{{}_1k^1\ {}_2k^2\ {}_3k^3}$$

is expressed as

$$\frac{{}_1k_2\ {}_2k_3}{{}_1k^1\ {}_2k^2\ {}_3k^3} = \frac{1}{{}_1k^3}$$

The terms N_i in Equation (3.5) can now be written in short hand notation as

$$N_i = F_{ss} \left[\frac{1}{{}_ik^i} + \frac{1}{{}_ik^{i+1}} + \frac{1}{{}_ik^{i+1}} + \ldots + \frac{1}{{}_ik^n} \right]$$

or

$$N_i = F_{ss} \sum_{j=0}^{j=n-i} \frac{1}{{}_ik^{i+j}} \qquad (3.11)$$

From Appendix 6,

$$\frac{1}{{}_ik^{i+j}} = \left(\frac{k_h}{k_b}\right)^j \frac{1}{k_b}$$

Thus

$$N_i = F_{ss} \sum_{j=0}^{j=n-i} \left(\frac{k_h}{k_b}\right)^j \frac{1}{k_b}$$

$$= \frac{F_{ss}}{k_b} \sum_{j=0}^{j=n-i} U^j, \text{ where } U = \frac{k_h}{k_b}$$

$$= \frac{F_{ss}}{k_b} \left(\frac{1 - U^{n+1-i}}{1 - U}\right)$$

$$= \frac{F_{ss}}{k^-} \left[1 - \left(\frac{k_h}{k_b}\right)^{n+1-i} \right]$$

Expressing the number of kinks in valley i in terms of concentration i.e., the number of crack tips per unit length of the crack front, the above expression becomes,

$$N = \frac{F_{ss}}{a_y k^-} \left[1 - \left(\frac{k_h}{k_b}\right)^{n+1-i} \right] \tag{3.12}$$

where $k^- = k_b - k_h$

Determination of F_{ss}.

The steady state flux is determined from the total number of kinks, N_t, from the relation

$$N_t = N_{dk} + \sum_{i=1}^{n} N_i \tag{3.13}$$

where N_{dk} is the number of kink nucleation sites waiting for the double kink nucleation process, defined by

$$N_{dk} = F_{ss} \left(\frac{1}{dk^{dk}} + \frac{dk_{k_1}}{dk^{dk}} \sum_{j=0}^{j=n-1} \frac{1}{1^{k^{1+j}}} \right) \tag{3.14}$$

In Equation (3.13),

$$\sum_{i=1}^{n} N_i = \frac{F_{ss}}{k^-} \sum_{i=1}^{i=n} \left[1 - \left(\frac{k_h}{k_b}\right)^{n+1-i} \right]$$

and hence

$$\sum_{i=1}^{n} N_i = \frac{F_{ss}}{k^-} \left[n - \sum_{i=1}^{n} U^{n+1-i} \right]$$

where, as before, $U = \frac{k_h}{k_b}$

$$= \frac{F_{ss}}{k^-} \left[n - \frac{k_h}{k_b} \sum_{i=1}^{n} U^{n-i} \right]$$

$$= \frac{F_{ss}}{\bar{k}} \left[n - \frac{k_h}{k_b} \cdot \frac{1 - (\frac{k_h}{k_b})^n}{1 - \frac{k_h}{k_b}} \right]$$

also because $\frac{1}{1^{k^{1+j}}} = (\frac{k_h}{k_b})^j \frac{1}{k_b}$

then

$$N_{dk} = F_{ss} \left[\frac{1}{dk^{k^{dk}}} + \frac{dk_{k_1}}{dk^{k^{dk}}} \sum_{j=0}^{j=n-1} \frac{U^j}{k_b} \right]$$

$$= F_{ss} \left[\frac{1}{dk^{k^{dk}}} + \frac{dk_{k_1}}{dk^{k^{dk}}} \cdot \frac{1}{k_b} \cdot \frac{1 - (\frac{k_h}{k_b})^n}{1 - \frac{k_h}{k_b}} \right]$$

Since, as explained before, the activation free energy associated with the kink nucleation process is low, the rate constant associated with the double kink nucleation can be approximated as

$$dk^{k^{dk}} = \frac{kT}{h} \exp - \frac{dk^{\Delta G^{\ddagger dk}} - dk^{W^{dk}}}{kT} \simeq \frac{kT}{h}, \quad dk^{\Delta G^{\ddagger dk}} - dk^{W^{dk}} \simeq 0$$

$$dk_{k_1} = \frac{kT}{h} \exp - \frac{dk_{W_1}}{kT} \simeq \frac{kT}{h} \exp - \frac{W}{kT}$$

Thus

$$N_{dk} = \frac{F_{ss}}{\bar{k}} \left[\frac{h}{kT} \bar{k} + \frac{h}{kT} \bar{k} \frac{k_h}{k_b} \cdot \frac{1 - (\frac{k_h}{k_b})^n}{1 - \frac{k_h}{k_b}} \right]$$

Hence from Equation (3.13), the total number of kinks is

$$N_t = \frac{F_{ss}}{\bar{k}} \left[\frac{k_h}{k_b} \left\{ \frac{(\frac{k_h}{k_b})^n - 1}{\frac{k_h}{k_b} - 1} \right\} \left\{ \frac{h\bar{k}}{kT} - 1 \right\} + n + \frac{h\bar{k}}{kT} \right]$$

The steady state flow of kinks, F_{ss}, is then determined from the expression

$$F_{ss} = N_t \, k^- \left[\frac{k_h}{k_b} \left\{ \frac{\left(\frac{k_h}{k_b}\right)^n - 1}{\frac{k_h}{k_b} - 1} \right\} \left\{ \frac{h k^-}{kT} - 1 \right\} + n + \frac{h k^-}{kT} \right]^{-1} \qquad (3.15)$$

Equation (3.15) describes the steady state flow of kinks in terms of the rate constants, the total number of specimens (kinks) and the number of spreading barriers. It is assumed that there is a steady state, uniformly distributed number of the active double kink sites per unit length of the crack front. The number of the spreading barriers, n, therefore, is constant and it is the same for all the double kink patterns.

The concentration of the kinks in valley i can now be written as

$$N = \frac{N_t}{a_y} \left[\frac{1 - \left(\frac{k_h}{k_b}\right)^{n+1-i}}{\frac{k_h}{k_b} \left\{ \frac{\left(\frac{k_h}{k_b}\right)^n - 1}{\left(\frac{k_h}{k_b}\right) - 1} \right\} \left\{ \frac{h k^-}{kT} - 1 \right\} + n + \frac{h k^-}{kT}} \right] \qquad (3.16)(a)$$

Hence it follows that

$$\frac{a_y N}{N_t} = \frac{1 - \left(\frac{k_h}{k_b}\right)^{n+1-i}}{\frac{k_h}{k_b} \left\{ \frac{\left(\frac{k_h}{k_b}\right)^n - 1}{\frac{k_h}{k_b} - 1} \right\} \left\{ \frac{h k^-}{kT} - 1 \right\} + n + \frac{h k^-}{kT}} \qquad (3.16)(b)$$

When W is large so that

$$\frac{h}{kT} k^- = \exp\left(-\frac{\Delta G^{\ddagger} - W}{kT}\right) - \exp\left(\frac{-W}{kT}\right) \ll 1,$$

Equation (3.16) (b) becomes

$$\frac{a_y N}{N_t} = \frac{1 - \left(\frac{k_h}{k_b}\right)^{n+1-i}}{n - \frac{k_h}{k_b}\,\frac{1 - \left(\frac{k_h}{k_b}\right)^{n}}{1 - \frac{k_h}{k_b}}} \tag{3.17}$$

The concentration of the active kink sites waiting for a double kink nucleation step is

$$N_{dk} = \frac{\frac{k^- h}{kT}\,\frac{N_t}{a_y}\left[1 + \frac{k_h}{k_b}\,\frac{1 - \left(\frac{k_h}{k_b}\right)^{n}}{1 - k_h/k_b}\right]}{\frac{hk^-}{kT} + n + \left\{1 - \frac{hk^-}{kT}\right\}\left[\frac{k_h}{k_b}\,\frac{\left(\frac{k_h}{k_b}\right)^{n} - 1}{\frac{k_h}{k_b} - 1}\right]} \tag{3.18}$$

The condition that $k_b = k_h = k$ is a special case. From Appendix 7, the asymptotic expression of Equation (3.16) in this case is

$$N = \frac{2\,N_t}{a_y h}\left(1 - \frac{i}{n+1}\right) \tag{3.19}$$

Thus the concentration of kinks in any valley (1 to n) can be determined from Eqs. (3.16) and (3.17) while the concentration of the kink nucleation sites waiting for the double kink nucleation step can be determined from Equation (3.18) for a given applied stress and temperature. When $k_b = k_h = k$ Equation (3.19) is used to calculate the kink concentration.

b) Differential Equation Approach.

To facilitate the mathematical development, the kink distribution is described by a continuous function as an approximation of the discrete quantities of Equation (3.1) or (3.5). The number of kinks at the kink locations corresponding to N_i and N_{i+1} is defined as a function of the kink concentration N (y) (number of kinks over a unit length of the crack front in the y direction). The number of kinks in front of the i-th barrier, N_i, and the number of kinks in front of the i+1-th barrier, N_{i+1} can be expressed with the Taylor expansion respectively, as

$$N_i \doteq a_y \left[N(y) - \frac{dN(y)}{dy} \frac{a_y}{2} + \ldots \right] \qquad (3.20)(a)$$

and

$$N_{i+1} \doteq a_y \left[N(y) + \frac{dN(y)}{dy} \frac{a_y}{2} + \ldots \right] \qquad (3.20)(b)$$

Expressing the terms in Equation (3.1) from Eqs. (3.3) and (3.20) results in

$$F = a_y \left(N - \frac{a_y}{2} \frac{dN}{dy} \right) k_b - a_y \left(N + \frac{a_y}{2} \frac{dN}{dy} \right) k_h$$

or

$$F = \frac{-a_y^2}{2} (k_b + k_h) \frac{dN}{dy} + a_y (k_b - k_h) N \qquad (3.21)$$

In writing Equation (3.21) it was assumed that

$$_1k^1 = {}_2k^2 = \ldots = {}_ik^i = {}_nk^n = k_b$$

and

$$^1k_2 = {}^2k_3 = \ldots = {}^ik_{i+1} = {}^{n-1}k_n = k_n.$$

In steady state, the flux F is constant and the kink concentration defined by Equation (3.21) is

$$N = \frac{F_{ss}}{a_y k^-} + C \exp\left[\left(\frac{2k^-}{k^+}\right)\frac{y}{a_y}\right] \tag{3.22}$$

where $k^- = k_b - k_h$

$k^+ = k_h + k_b$

and C is an integration constant. The double kinks are nucleated at distances ℓ apart, and, therefore, a kink propagates over a distance $\ell/2$ (Fig. 3.1 (d)). When the two kinks meet, annihilation occurs and the concentration N at $y = \ell/2$ is zero. Accordingly, at the boundary, Equation (3.22) is

$$0 = \frac{F_{ss}}{a_y k^-} + C \exp\left[\frac{k^-}{k^+}\left(\frac{\ell}{a_y}\right)\right]$$

so that $$C = \frac{F}{a_y k^-} \exp\left(-\frac{k^-}{k^+}\frac{\ell}{a_y}\right) \tag{3.23}$$

Substituting (3.23) in (3.22), we get

$$N = \frac{F_{ss}}{a_y k^-}\left[1 - \exp\left\{\frac{2k^-}{k^+}\left(\frac{y}{a_y} - \frac{\ell}{2a_y}\right)\right\}\right] \tag{3.24}$$

Determination of F_{ss}.

The steady state flow of kinks, F_{ss}, is determined from the total number of kinks (specimens) N_t from the relation

$$N_t = \int_0^{\ell/2} N(y)\, dy$$

$$= \frac{F_{ss}}{k^-}\frac{\ell}{2a_y}\left[1 - \frac{a_y}{\ell}\frac{k^+}{k^-}\left(1 - \exp - \frac{\ell}{a_y}\frac{k^-}{k^+}\right)\right]$$

Hence it follows that

$$F_{ss} = \frac{2a_y}{\ell} k^- N_t \left[1 - \frac{a_y}{\ell}\frac{k^+}{k^-}\left\{1 - \exp - \frac{\ell}{a_y}\frac{k^-}{k^+}\right\}\right]^{-1} \tag{3.25}$$

Equation (3.24) can now be written as

$$N = \frac{2N_t}{\ell}\frac{1 - \exp\left\{\frac{2k^-}{k^+}\left(\frac{y}{a_y} - \frac{\ell}{2a_y}\right)\right\}}{1 - \frac{a_y}{\ell}\frac{k^+}{k^-}\left[1 - \exp - \frac{\ell}{a_y}\frac{k^-}{k^+}\right]} \tag{3.26}$$

Hence it follows that

$$\frac{a_y N}{N_t} = \frac{1 - \exp\{\frac{2k^-}{kt}\ (\frac{y}{a_y} - \frac{\ell}{2a_y})\}}{\frac{\ell}{2a_y}\left[1 - \frac{a_y}{\ell}\frac{k^+}{k^-}\{1 - \exp - \frac{\ell}{a_y}\frac{k^-}{k^+}\}\right]} \qquad (3.26)(b)$$

The condition that $k_n = k_h = k$ is a special case. The flux Equation (3.21) is

$$F_{ss} = - \frac{a_y^2\ k^+}{2}\frac{dN}{dy} = - a_y^2\ k \frac{dN}{dy} \qquad (3.27)$$

and the concentration of the kinks is

$$N = - \frac{F_{ss}\ y}{a^2\ k} + C \qquad (3.28)$$

Because, again, the concentration at $\ell/2$ is zero, the boundary condition leads to

$$C = \frac{F_{ss}}{a_y^2 k}\ \frac{\ell}{2}$$

and hence

$$N = - \frac{F_{ss}}{a_y k}\ (\frac{y}{a_y} - \frac{\ell}{2a_y}) \qquad (3.29)$$

The steady state flux, F_{ss}, can be determined as before from

$$N_t = \int_0^{\ell/2} N(y)\ dy = \frac{F_{ss}}{k}\ \frac{\ell^2}{8a_y^2}$$

Thus

$$F_{ss} = N_t\ k\ \frac{8a_y^2}{\ell^2} \qquad (3.30)$$

and the crack tip concentration is

$$N = \frac{2N_t}{\ell}\ (1 - \frac{2y}{\ell}) \qquad (3.31)$$

Equations (3.26) and (3.31) are the approximate expressions for the crack tip concentration derived from the continuous function description of the kink distribution. When $k_b = k_h = k$, Equation (3.31) should be used to calculate the kink concentration.

3.2 Crack Propagation Velocity.

Once a double kink has formed it can spread sideways in discrete steps of one or more atomic distances. A very large number of these events take place along the crack front, and when two adjacent kinks meet mutual annihilation takes place. When kink annihilation occurs the crack front moves forward in the x-direction by one atomic distance (or an integral multiple of it). There are N_t number of segments each containing one double kink. The number of times that each annihilation occurs for each segment is, (from Equation (3.15))

$$\frac{F_{ss}}{N_t} = \frac{\bar{k}}{\frac{k_h}{k_b}\left[\frac{(\frac{k_h}{k_b})^n - 1}{\frac{k_h}{k_b} - 1}\right]\left[\frac{h\bar{k}}{kT} - 1\right] + n + \frac{h\bar{k}}{kT}} \tag{3.32}$$

The frequency of annihilation is F_{ss}/N_t and it is the frequency of the crack front movement by one atomic distance a_x (or an integral multiple of it) in the x-direction. It will be assumed here that |27| there is a steady state number of the active kink nucleation sites so that the kink spreading distance (n+1 atomic distances) will remain constant. Thus, the crack propagation velocity is

$$V_x = a_x\bar{k}\left\{\frac{k_h}{k_b}\left[\frac{(\frac{k_h}{k_b})^n - 1}{\frac{k_h}{k_b} - 1}\right]\left[\frac{h\bar{k}}{kT} - 1\right] + n + \frac{h\bar{k}}{kT}\right\}^{-1} \tag{3.33}$$

The crack propagation velocity Equation (3.33) was derived from the discrete analysis approach. When the continuous function is used to describe the kink concentration distribution, the frequency of annihilation becomes (from Equation (3.25))

$$\frac{F_{ss}}{N_t} = \left(\frac{2a_y}{\ell}\right) k^- \left\{1 - \frac{a_y}{\ell}\frac{k^+}{k^-}\left[1 - \exp\left(-\frac{\ell}{a_y}\frac{k^-}{k^+}\right)\right]\right\}^{-1} \tag{3.34}$$

and the crack propagation velocity is

$$V_x = \frac{2a_y}{\ell} a_x k^- \left\{1 - \frac{a_y}{\ell}\frac{k^+}{k^-}\left[1 - \exp\left(-\frac{\ell}{a_y}\frac{k^-}{k^+}\right)\right]\right\}^{-1} \tag{3.35}$$

The condition that $k_b = k_h = k$ is a special case. The crack propagation velocity is derived from the asymptotic expression of Equation (3.33) for this condition, thus (Appendix 8)

$$V_x = \frac{2a_x}{n^2} k \tag{3.36}$$

Also when $k_b = k_h = k$, the continuous function description of the kink concentration leads to the frequency of annihilation expression

$$\frac{F_{ss}}{N_t} = 2\left(\frac{2a_y}{\ell}\right)^2 k$$

The crack propagation velocity is then expressed as

$$V_x = 2\, a_x \left(\frac{2a_y}{\ell}\right)^2 k \tag{3.37}$$

Because $\left(\frac{\ell}{2a_y}\right)^2 \simeq n^2$, Eqs. (3.36) and (3.37) are identical.

When the discrete analysis is used to calculate the kink distribution the crack propagation velocity is given by Equation (3.33) and by Equation (3.36) when $k_b = k_h = k$ while if the continuous function is used to describe the kink concentration, the crack propagation velocity is calculated from Equation (3.35) and from Equation (3.37) when $k_b = k_h = k$.

3.3 Discussion

a) The Kink Concentration Distribution.

Figures 3.2, 3.3, 3.4 and 3.5 show the kink concentration distribution along the kink spreading distance. The distribution curves were calculated by using Eqs.(3.16) and (3.19) that were derived from the discrete analysis approach and Eqs. (3.26) and (3.31) derived from the continuous function description of the kink concentration. The procedure for calculating the rate constants is the same as that outlined in Section 2.3 (a). Again, for illustration the activation free energy associated with the bond breaking process was taken to be 1.0 eV.

The kink distribution curves in Fig. 3.2 were calculated for a crack front with a steady state, uniformly distributed number of active kink nucleation sites per unit length such that the distance between two adjacent kink sites is 100 atomic distances. The kink spreading distance then is 50 atomic distances. When the mechanical energy is 0.49 eV ($k_b < k_h$) i.e., the kink is in the "uphill" condition, the slope of the concentration curve is very steep at the kink nucleation site ($y=0$) and it decreases to almost zero at the kink absorbing boundary ($y=\ell/2$). Further increase in the mechanical energy leads to a decrease in the slope of the concentration curve and in the concentration at $y=0$. The slope of the concentration curve at the absorbing boundary ($y=\ell/2$) increases with the increase in the mechanical work. It is of interest to note that when $k_b = k_h = k$, the kink concentration distribution is linear. When the mechanical energy is greater than half the activation free energy ($k_b > k_h$) the curvature of the concentration distribution curve changes from concave to convex.

However, when the mechanical energy is high ($k_b >> k_h$), the kink concentration is almost constant except for the last few barriers where it decreases sharply to zero at $y=\ell/2$. This behaviour of the kink concentration is indeed expected from Eqs. (3.26) and (3.16) which reduces to

$$N \simeq \frac{2N_t}{\ell}\left\{1 - \exp\left[2\left(\frac{y}{a_y} - \frac{\ell}{2a_y}\right)\right]\right\}$$

and

$$N \simeq \frac{N_t}{a_y n}\left[1 - \left(\frac{k_h}{k_b}\right)^{n+1-i}\right]$$

respectively when $k_b >> k_h$ and $k^-/k^+ \simeq 1.0$. Thus, an increase in the mechanical energy will, in general, lead to a decrease in the slope, dN/dy, and the concentration at the kink nucleation site ($y=0$) while at the kink absorbing boundary, $y=\ell/2$, the slope of the distribution curve will increase with the increase in the mechanical work. Because the steady state flow of kinks, F_{ss}, is directly proportional to the slope at the absorbing boundary (Equation (3.21)), the increase in the mechanical energy, as expected, will lead to an increase in the steady state flow of kinks and hence the crack propagation velocity.

The curves in Fig. 3.2 (b) show the kink concentration distribution for the same conditions as in Fig. 3.2 (a) but at a temperature of 500K. In the "uphill" range of the mechanical energy ($k_b < k_h$), the effect of the temperature increase on the kink concentration distribution is the same as that produced by increasing the mechanical energy, i.e., increase in the slope, dN/dy, at $y=\ell/2$ while at $y=0$, the slope and the concentration decreases. This behaviour is illustrated more clearly in Fig. 3.4 (a) where the mechanical energy is kept constant (0.499 eV) and only the temperature is varying. When $k_b = k_h = k$, the kink concentration

distribution is independent of temperature. In the "downhill" range of the mechanical energy ($k_b > k_h$), the effect of the temperature increase is the same as that of decreasing the mechanical energy, i.e., decrease in the slope at $y=\ell/2$ while the slope and the kink concentration at $y=0$ increases. Figure 3.4 (b) illustrates this behaviour. The curves were calculated by using Equation (3.26) with the value of the mechanical energy kept constant (0.501 eV) and only the temperature is varying.

It is of interest to note that in the "uphill" range of the mechanical energy, the effect of the temperature increase on the kink concentration distribution is the same as that of increasing the mechanical energy. In the "downhill" range, however, the effect of the temperature increase on the kink concentration distribution is the same as that of decreasing the mechanical energy. An increase in the mechanical energy leads to an increase in the rate of bond breaking, k_b, while the rate of bond healing, k_h, decreases with the increase in the mechanical energy. Both k_b and k_h will increase with an increase in temperature. It appears that the effect of the temperature increase on the kink concentration is analogous to decreasing the height of the apparent free energy barrier. For example,

$$\Delta G_1/kT_1 = \Delta G_2/kT_2$$

If $\Delta G_1 = 1.0$ eV and $T_2/T_1 = 2$, then $\Delta G_2 = 0.5$ eV. Consequently, a change in the height of the free energy barrier, whether it is due to the temperature or the mechanical energy change, will have a definite effect on the kink concentration distribution. Hence, in general, the kink concentration distribution will be determined by the ratio of k_h/k_b or k^-/k^+. Figure 3.5 (a) shows the general kink distribution as a function

of k_h/k_b. The curves were calculated from Equation (3.17) that was derived from the discrete analysis. For the same values of k_h/k_b, Equation (3.26) that was derived from the continuous function description of the kink concentration was used to calculate the kink concentration distribution curves in Fig. 3.5 (b). The numbers on each curve in Fig. 3.5 (b) represents the ratio of k^-/k^+ that was calculated from the corresponding ratio of k_h/k_b.

Apart from the temperature and the mechanical energy, the kink concentration distribution is affected by the defective nature of the material, that is, the number of the active kink nucleation sites available at the crack front. The greater the number of the kink nucleation sites, the smaller is the kink spreading distance ($\ell/2$). In Figs. 3.3 (a) and 3.3 (b) the curves were calculated with the same temperature and mechanical energy as in Figs. 3.2 (a) and 3.2 (b) respectively, but with a kink spreading distance of 100 atomic distances. The increase in the kink spreading distance from 50 (in Fig. 3.2) to 100 atomic distances (in Fig. 3.3) results in a decrease of both the kink concentration, N, and the slope, dN/dy, along the kink spreading distance for the same mechanical energy and temperature. Because the steady state flow of kinks is proportional to the slope dN/dy and the kink concentration N (Equation (3.21)), an increase in the kink spreading distance leads to a decrease in the steady state flow of the kinks, F_{ss}, and hence fewer kinks annihilate per second. Consequently, the crack propagation velocity, which is directly proportional to the steady state flow of crack tips (kinks) is inversely proportional to the kink spreading distance.

The agreement between the results from the continuous function description of the kink concentration and those from the discrete analysis is interesting. The kink concentration distribution curves in Fig. 3.2 (c) were calculated by using Equation (3.16) that was derived from the discrete analysis for the same conditions as those in Fig. 3.2 (a). The curves in Fig. 3.2 (a) were calculated from Equation (3.26) that was derived from the continuous function description of the kink concentration. There is a negligibly small difference (Appendix 10) between the results from the two approaches when the mechanical energy is 0.501, 0.505 and 0.54 eV; that is, when $k_b > k_h$. When $k_b = k_h = k$, however, the two approaches lead to the same kink concentration results. In general (Appendix 10), the difference between the results from the two approaches decreases as the mechanical energy increases. This behaviour is expected from Eqs. (3.12) and (3.24) derived from the discrete analysis and the continuous function respectively. These equations are

$$N = \frac{F_{ss}}{a_{yk^-}} \left[1 - \left(\frac{k_h}{k_b}\right)^{n+1-i}\right] \qquad A$$

for the discrete analysis and

$$N = \frac{F_{ss}}{a_{yk^-}} \left[1 - (\exp - \frac{k-}{k+}) \frac{k-2y}{a_y}\right] \qquad B$$

for the continuous function description. When $k_b > k_h$ the exponential terms in the RHS of both expressions are much less than unity, hence the smaller is the difference between the results from the two approaches. However, when $k_b < k_h$, the exponential term in Equation A becomes greater than that in Equation B. The greater the difference in the two exponential terms, the greater is the difference in the kink concentration

calculated from the two approaches. In the derivation of Equation B, the kink distribution was described as a continuous function. The number of kinks in front of the i-th barrier, N_i, and the number of kinks in front of the i+1-th barrier, N_{i+1}, were expressed with the Taylor expansion in which the higher order terms were neglected (Eqs. (3.20) (a) and (b)). It appears that the residue of the Taylor series is high in the "uphill" range ($k_b < k_h$). Hence the first order term approximation in the Taylor series is less satisfactory. To improve the results, therefore, higher order terms should be included in the Taylor expansion. This extension, however, is not necessary for the description of the kink distribution in the "downhill" range ($k_b > k_h$).

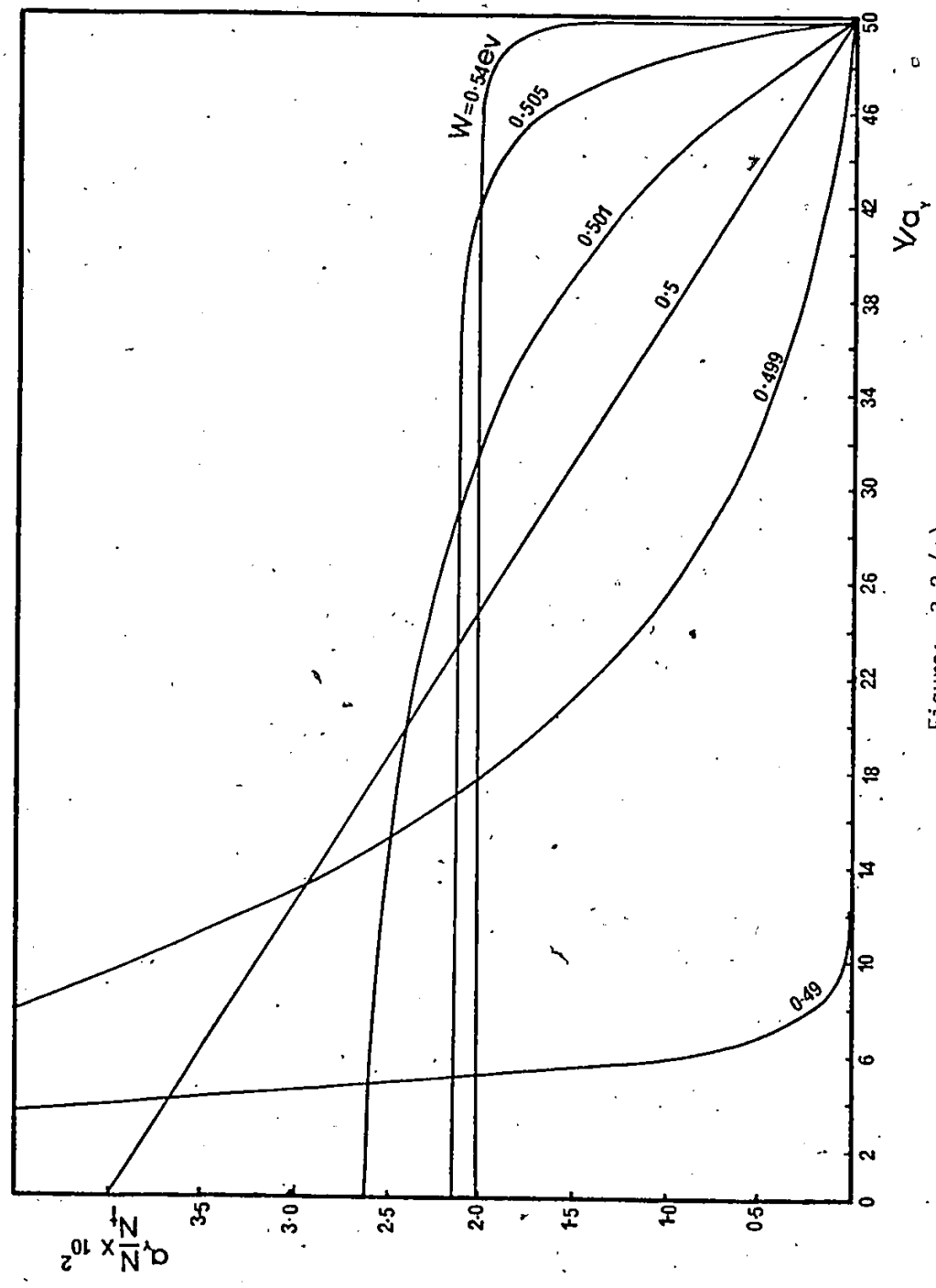
W=0·54ev
0·505
0·501
0·5
0·499
0·49
V/a
$q_1 \frac{N}{N_1} \times 10^2$
0
2
6
10
14
18
22
26
30
34
38
42
46
50
0·5
1·0
1·5
2·0
2·5
3·0
3·5

Figure: 3.2 (a)

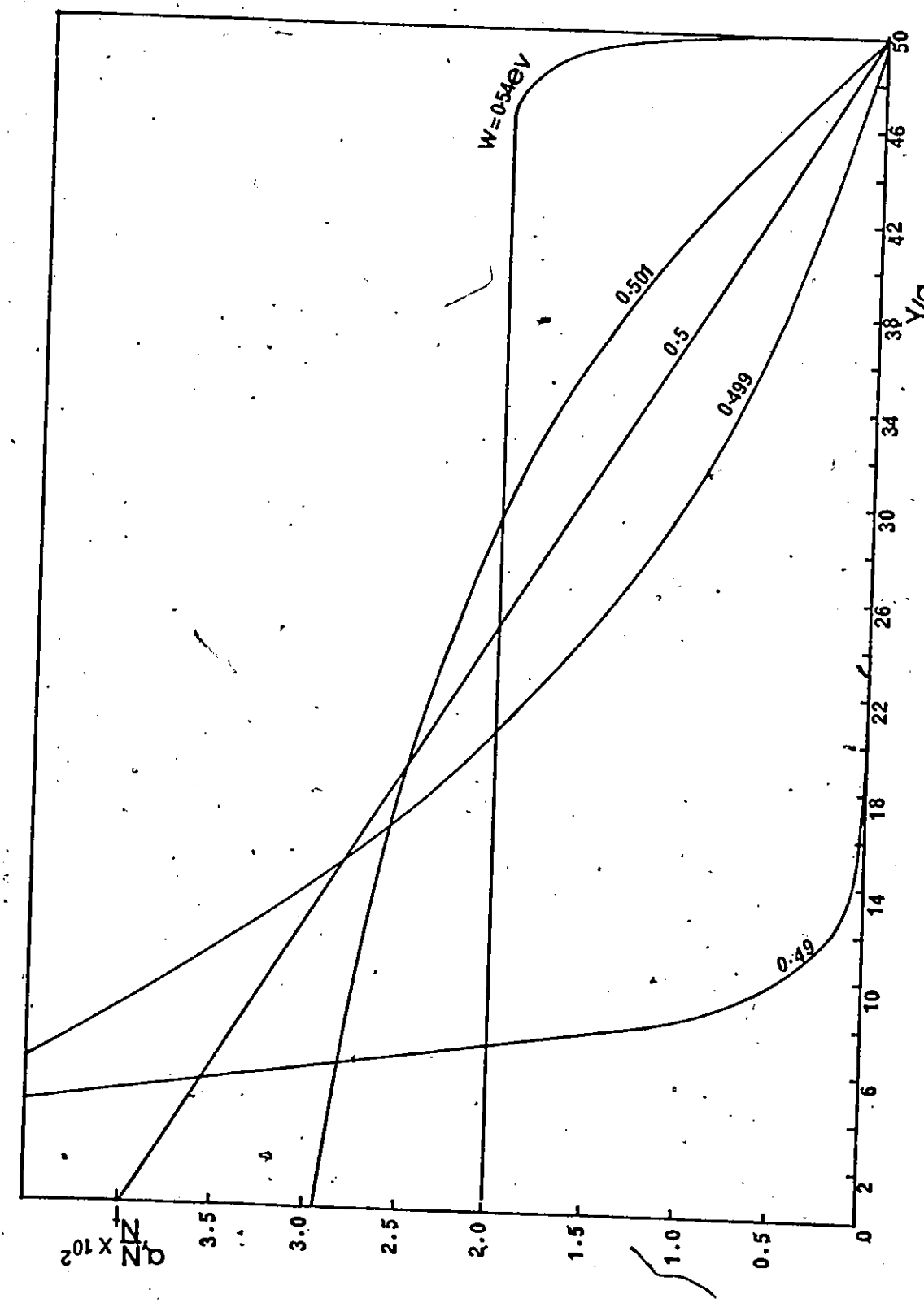
W=0.54eV
0.501
0.5
0.499
0.49
Y/α_Y
Q_N/N_1 x 10^2
0
2
6
10
14
18
22
26
30
34
38
42
46
50
0.5
1.0
1.5
2.0
2.5
3.0
3.5

Figure: 3.2 (b)

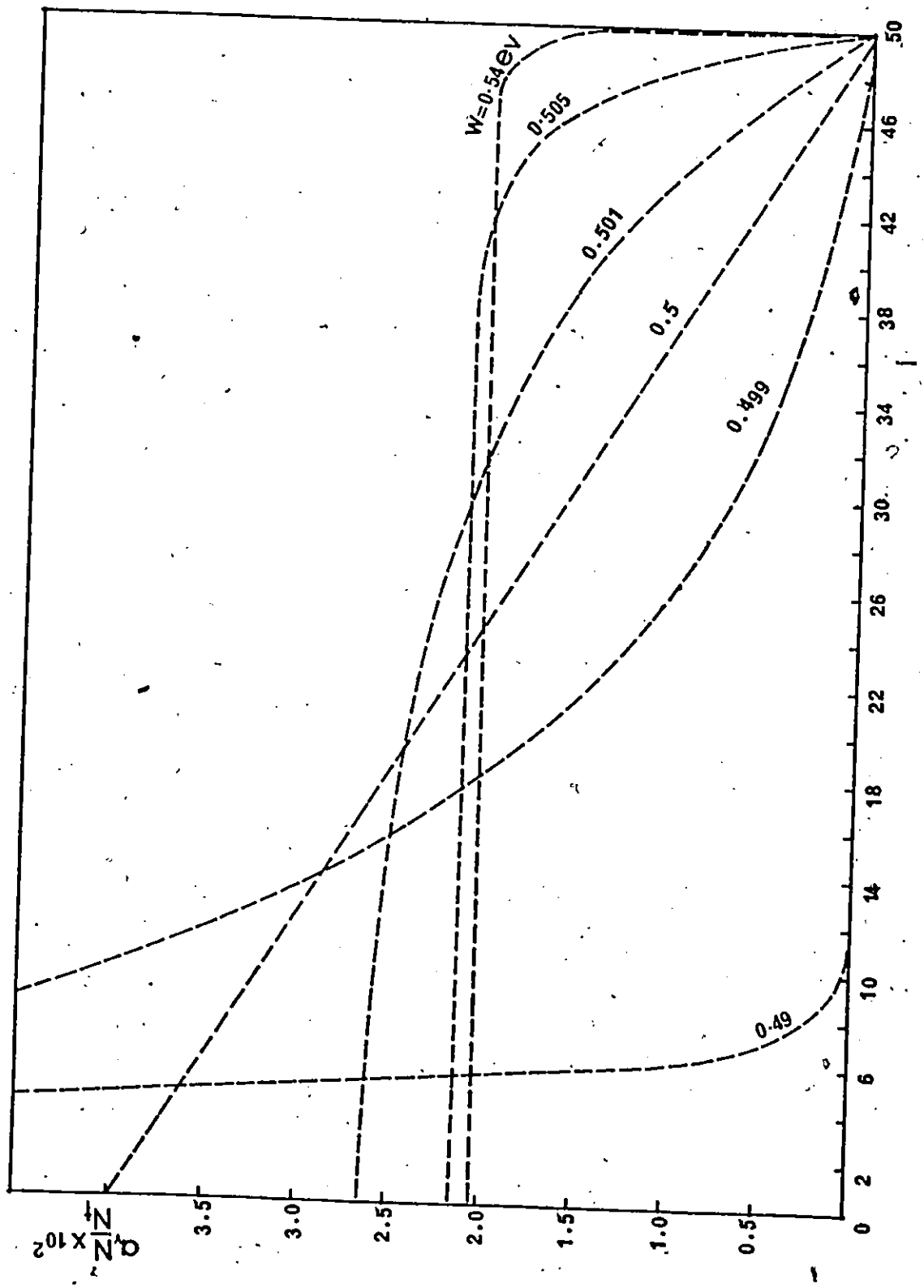

Figure: 3.2 (c)

Figure 3.2: The figure shows the kink distribution for a material with bond energy of 1 eV and a kink spreading distance of 50 atomic distances. The numbers indicated on each kink distribution curve represent the mechanical energy. The curves in Fig. 3.2 (a) and 3.2 (b) were calculated from Equation (3.26). (a) The kink distribution when the temperature is 300K. (b) The kink distribution when the temperature is 500K. (c) Same as Fig. 3.2 (a) but the curves were calculated by using the discrete analysis.

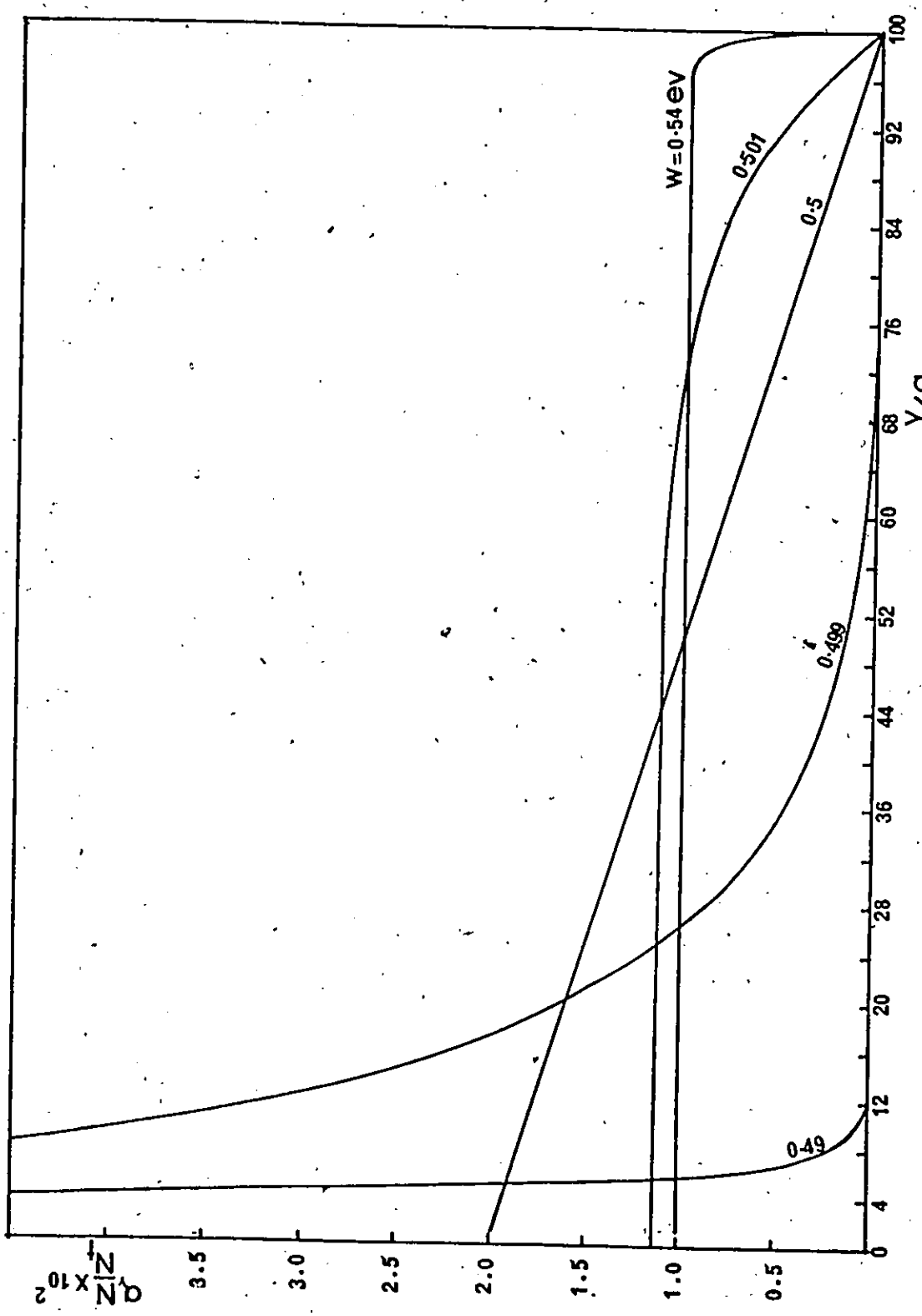
W=0·54 ev
0·501
0·5
0·499
0·49
Y/a_r
Q_i/N_i x 10^2
0
4
12
20
28
36
44
52
60
68
76
84
92
100
0.5
1.0
1.5
2.0
2.5
3.0
3.5

Figure: 3.3 (a)

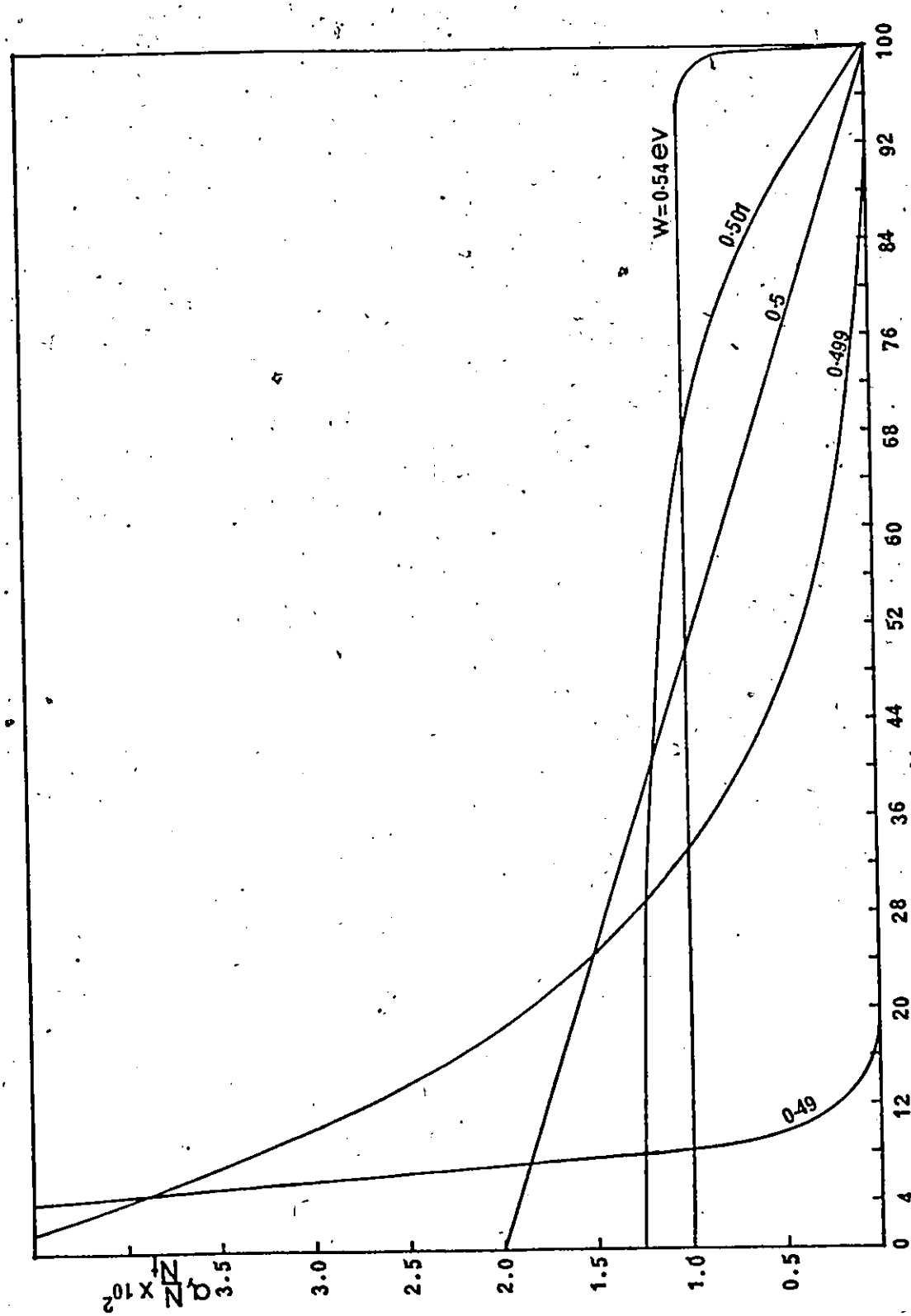
W=0.54eV
0.501
0.5
0.499
0.49
$\frac{Q_{ZZ}}{N} \times 10^2$
3.5
3.0
2.5
2.0
1.5
1.0
0.5
0
4
12
20
28
36
44
52
60
68
76
84
92
100
Y/a_r

Figure: 3.3 (b)

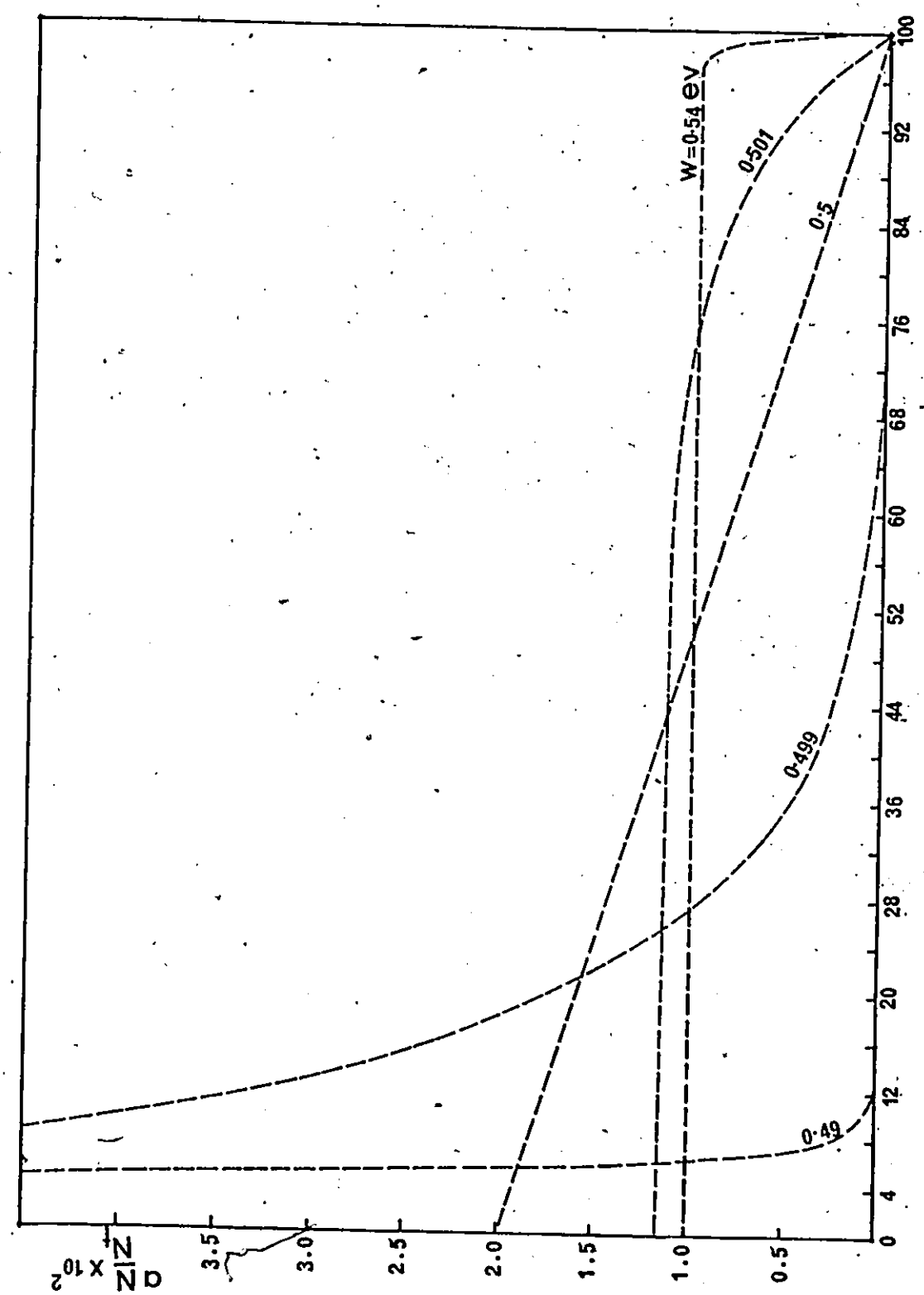

Figure: 3.3 (c)

Figure 3.3 The figure shows that kink distribution for a material with bond energy of 1 eV and a kink spreading distance of 100 atomic distances. The numbers indicated on each kink distribution curve represent the mechanical energy. (a) Kink distribution when the temperature is 300K. (b) Kink distribution when the temperature is 500K. (c) Same conditions as in Fig. 3.3 (a) but discrete analysis approach was used in calculating the kink distribution.

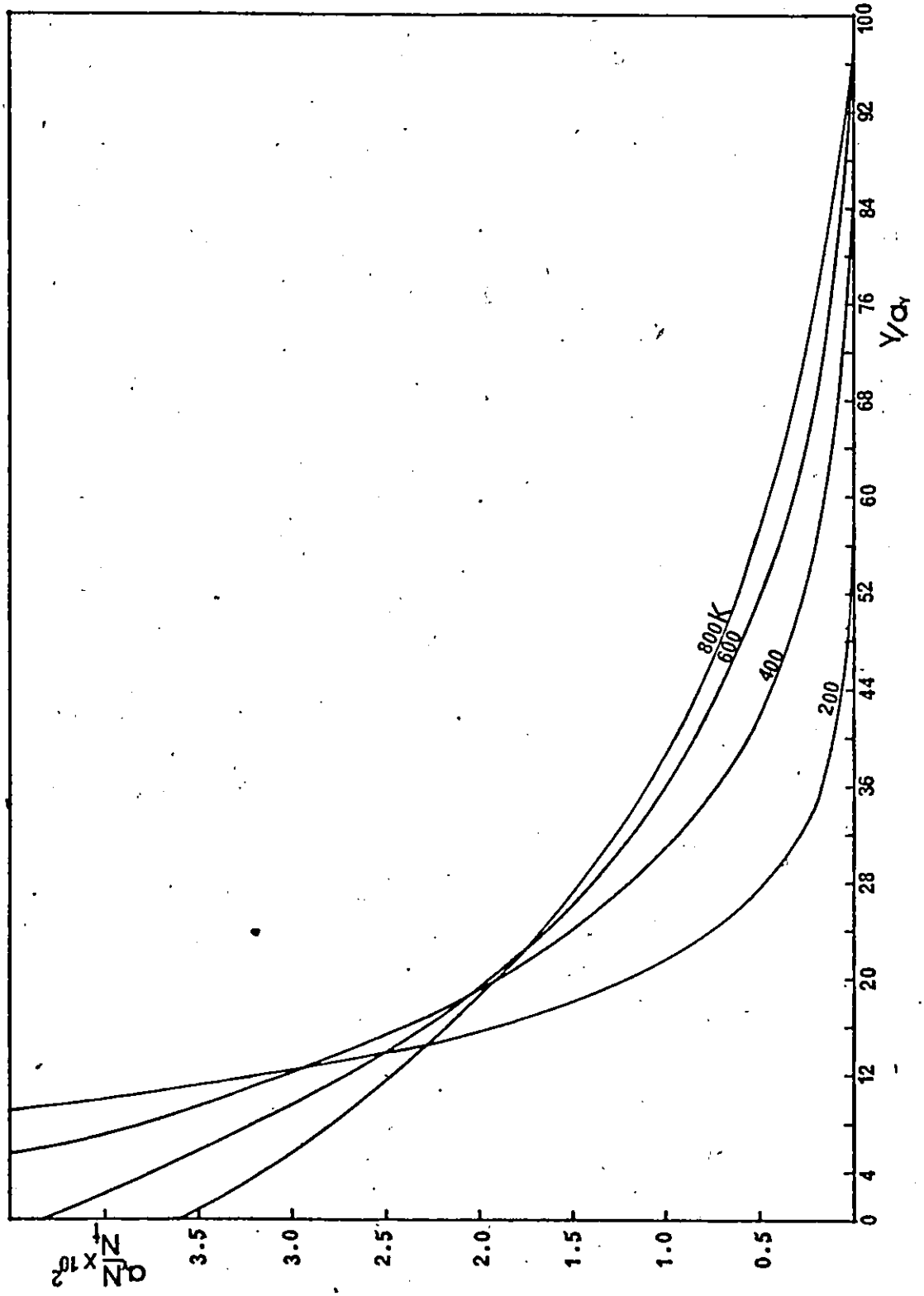
800K
600
400
200
Y/σy
0
4
12
20
28
36
44
52
60
68
76
84
92
100
0.5
1.0
1.5
2.0
2.5
3.0
3.5

Figure: 3.4 (a)

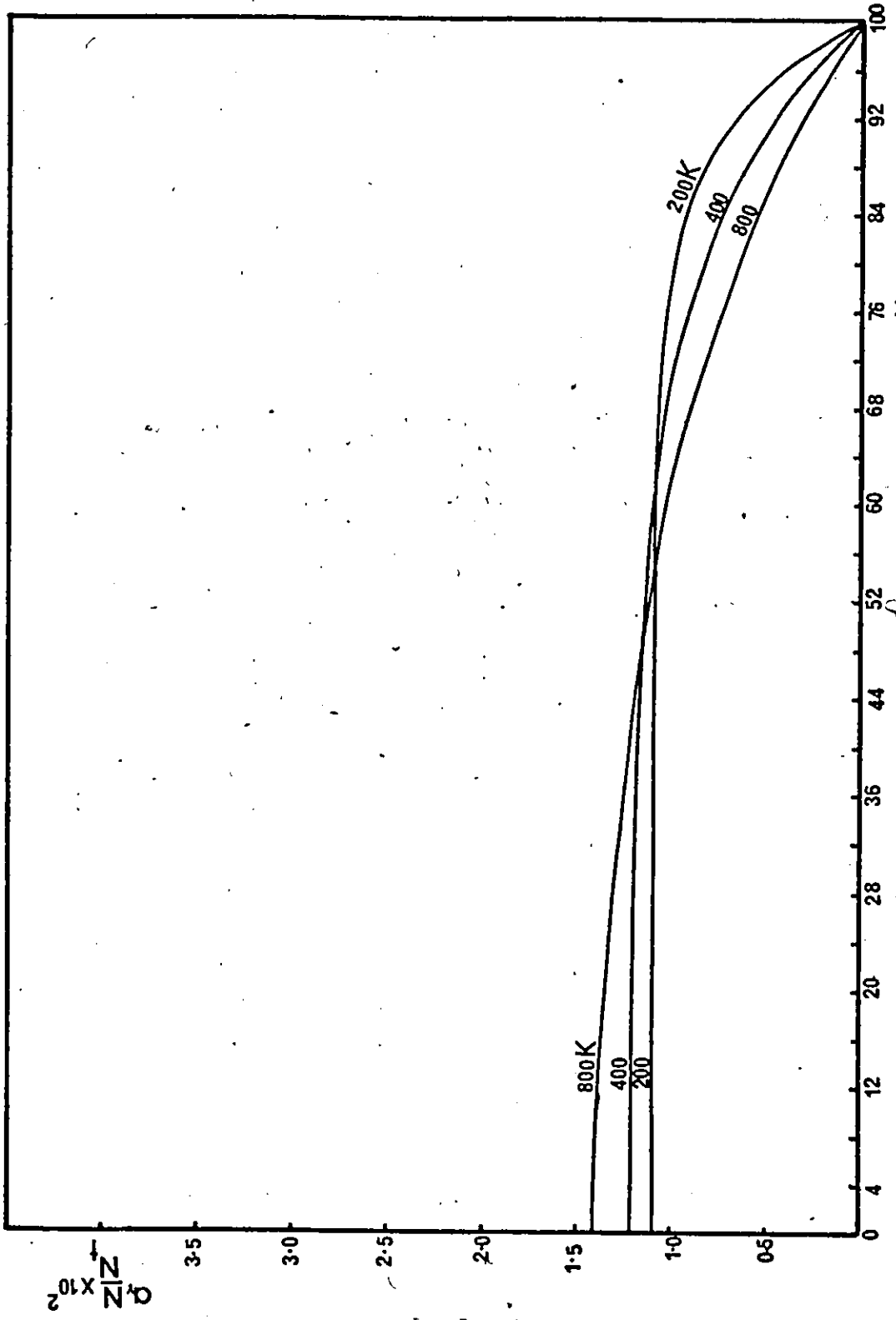

Figure: 3.4 (b)

Figure 3.4: The curves show the variation of the kink distribution with temperature for the "uphill" and "downhill" conditions of the kink spreading process. The parameters are $\Delta G^+ = 1.0$ eV, $\ell/2a_y = 100$. The numbers indicated on each kink distribution curve represents the temperature. (a) "Uphill" condition on the kink spreading, $k_b < k_h$, $W(\sigma) = 0.499$ eV. (b) "Downhill" condition of the kink spreading $k_b > k_h$, $W(\sigma) = 0.501$ eV.

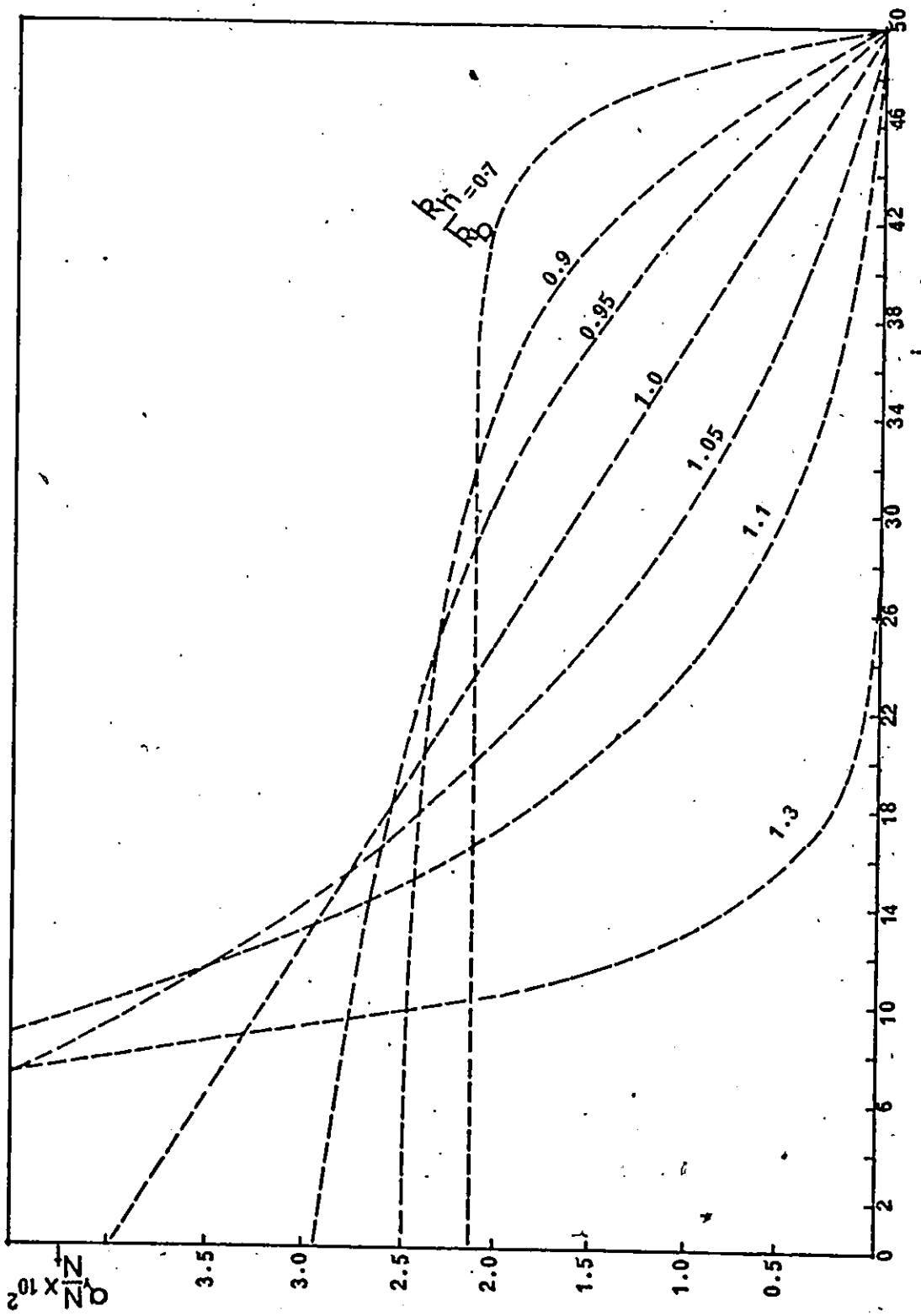
$\frac{R_H}{R_D}$=0.7
0.9
0.95
1.0
1.05
1.1
1.3
$\frac{Q_{in}}{N_i} \times 10^2$
3.5
3.0
2.5
2.0
1.5
1.0
0.5
i
0
2
6
10
14
18
22
26
30
34
38
42
46
50

Figure: 3.5 (a)

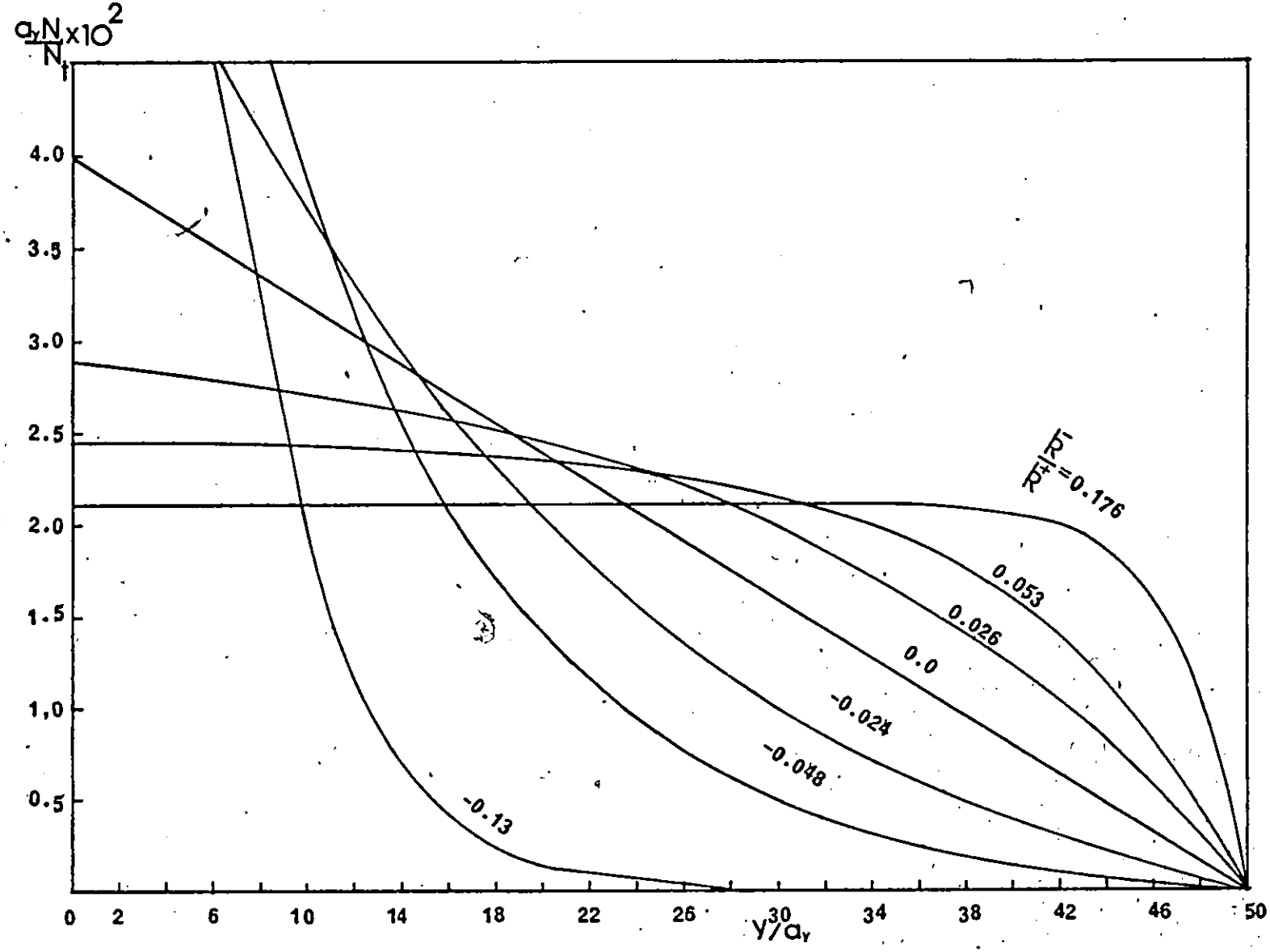

Figure: 3.5 (b)

Figure 3.5: The curves show the variation of the kink distribution with the ratio k_h/k_b for a given kink spreading distance. In Figure 3.5 (a) and 3.5 (b), the kink spreading distance is 50 atomic distances. (a) The kink distribution curves were calculated from discrete analysis approach. The numbers on each curve represent the ratio of k_h/k_b. (b) For the k_h/k_b values used in Fig. 3.5 (a), the kink distribution curves were calculated using continuous, approximate mathematical expression. The numbers on each curve represent the ratio k^-/k^+ calculated from the respective ratio k_h/k_b.

b) Crack Propagation Velocity.

Figures 3.6, 3.7, 3.8 and 3.9 show the variation of the crack propagation velocity with the mechanical energy, temperature and the kink spreading distance for activation free energy values of 1.0, 2.0, 3.0 and 4.0 eV respectively. The curves were calculated from Equation (3.33) that was derived from the discrete analysis. The solid lines indicate the slow crack growth region ranging from 10^{-10} to 10^{-3} m/s. The lower limit for this region was arbitrarily set to represent the lowest experimentarily measurable crack propagation velocity. It has been assumed in the absolute theory of rate processes that the complexes in the stable configuration are in equilibrium with the activated complexes [21], (Fig. 1.10). Zwolinski and Eyring [76] and others [77] showed that the error introduced by this assumption is negligible (5%) when

$$\frac{\Delta E^{\pm}}{kT} > 10 \qquad C$$

Because crack propagation is one of the rate processes, expression C was used to determine the upper limit for the slow crack growth region.

The results show that in the slow crack growth region as well as in the dynamic fracture range of the crack propagation velocity, both the continuous function description approach and the discrete analysis lead to the same results of the crack propagation velocity. Similar conclusions were arrived at in the case of the kink distribution.

In Figs. 3.6 to 3.9 the logarithm of the crack propagation velocity is plotted against the mechanical energy for different temperatures with constant kink spreading distance. The curves in Figs. 3.6(a), 3.7(a), 3.8(a) and 3.9 (a) were calculated for a kink spreading distance of 50 atomic distances

while the curves in Figs. 3.6 (b), 3.7 (b), 3.8 (b) and 3.9 (b) were calculated for a kink spreading distance of 100 atomic distances. The results show that the crack propagation velocity drop sharply to negligible values when the mechanical energy is less than half the activation free energy. The lower the kink spreading distance the less steep is the drop. The crack propagation velocity curves for different temperatures appear to converge. When $k_b >> k_h$ and $W(\sigma) = \Delta G_b^{\ddagger}$, the crack propagation velocity Equation (3.33) reduces to

$$V_x = \frac{kT}{h} \frac{a_x}{n} \qquad D$$

The crack propagation velocity curves in Figs. 3.6 to 3.9 may sometimes appear to converge to one point, suggesting a temperature independent crack velocity value. This behaviour is only apparent and it is not expected, (from Eq. D).

It was pointed out in Section 3.3 (a) that the greater the kink spreading distance the smaller is the steady state flow of crack tips. Because the crack propagation velocity is directly proportional to the steady state flow of the crack tips, it follows that the crack propagation velocity is inversely proportional to the kink spreading distance. The greater the number of the active kink nucleation sites, therefore, the greater is the crack propagation velocity.

The results show that the mechanical energy range corresponding to the slow crack growth region varies with temperature. Table 3.1 gives a summary of the variation of the tolerance (mechanical energy range) with the temperature and the activation free energy obtained from Figs. 3.6 to 3.9. For comparison, the ratio of the mechanical energy range, $\Delta W(\sigma)$, to the mechanical energy corresponding to the Griffith equilibrium condition ($\Delta G_b^{\ddagger}/2$) is also considered. For a given activation

free energy, the tolerance first increases with an increase in the temperature to a maximum value and then decreases. In the low temperature range, the tolerance is small and the crack propagation velocity is negligible (below 10^{-10} m/s) until a certain value of the mechanical energy is reached when dynamic fracture takes place after a period of slow crack growth (time dependent crack propagation). As the temperature is increased, more thermal energy is available at the crack tip bonds so that subcritical crack growth starts at a lower mechanical energy value, while the mechanical energy corresponding to the upper limit of the slow crack growth region decreases with the increase in the temperature. The net effect, however, is an increase in the tolerance with the increase in temperature until a maximum tolerance is reached. Further increase in the temperature leads to a decrease in the tolerance.

It is of interest to note (from column 4 of Table 3.1) that in the low temperature range (200-300K) the tolerance decreases with an increase in the activation free energy. For example, when the temperature is 300K, a material with an activation free energy of 1.0 eV has a tolerance of 0.52 while a material with an activation free energy of 4.0 eV has a tolerance of 0.22. Hence at low temperature conditions stronger materials will be more brittle than weaker materials. In the high temperature range (above 1000K) the tolerance appears to increase with the increase in the activation free energy. However, because thermally activated plastic deformation takes place at the crack tip when the temperature is high, the crack tip events are more complicated than the elementary bond breaking and healing events represent. The critical crack driving force, G_{IC} (or J_{IC}) for the crack initiation has to be determined experimentally (11, 12, 13, 14).

Bond Energy, $\Delta G^{\ddagger}$ (eV)	Temp. ^{o}K	Slow crack growth range of mech. energy $\Delta W(\sigma)$ eV	Tolerance $\frac{2\,\Delta W(\sigma)}{\Delta G^{\ddagger}_{b}}$
1.0	200	0.29	0.58
	300	0.26	0.52
	400	0.16	0.32
	500	0.10	0.20
2.0	200	0.30	0.30
	300	0.41	0.41
	400	0.64	0.64
	500	0.52	0.52
	1000	0.16	0.16
3.0	200	0.30	0.20
	300	0.43	0.286
	400	0.66	0.44
	500	0.75	0.50
	1000	0.64	0.426
	1500	0.29	0.19
4.0	300	0.44	0.22
	500	0.78	0.39
	1000	1.21	0.605
	1500	0.81	0.405
	1900	0.42	0.21

Table 3.1. Summary of the variation of the slow crack growth range of the mechanical energy with the activation free energy and temperature, illustrated in Figures 3.6 to 3.9.

The fracture kinetics analysis carried out in this Chapter is generally valid when the plastic flow in front of the crack tip is negligible. No particular expression for the mechanical energy as a function of the applied stress was assumed. Both the Griffith and Irwin expressions 1.23 (a) and 1.23 (b) respectively, can be incorporated in the general crack propagation velocity Equation (3.33). Hence the effects of the applied stress, temperature and the kink spreading distance can be investigated by using the general crack propagation velocity expression that was developed in this thesis. For practical applications these investigations are incomplete without discussing the effect of the chemical environment on the crack propagation velocity.

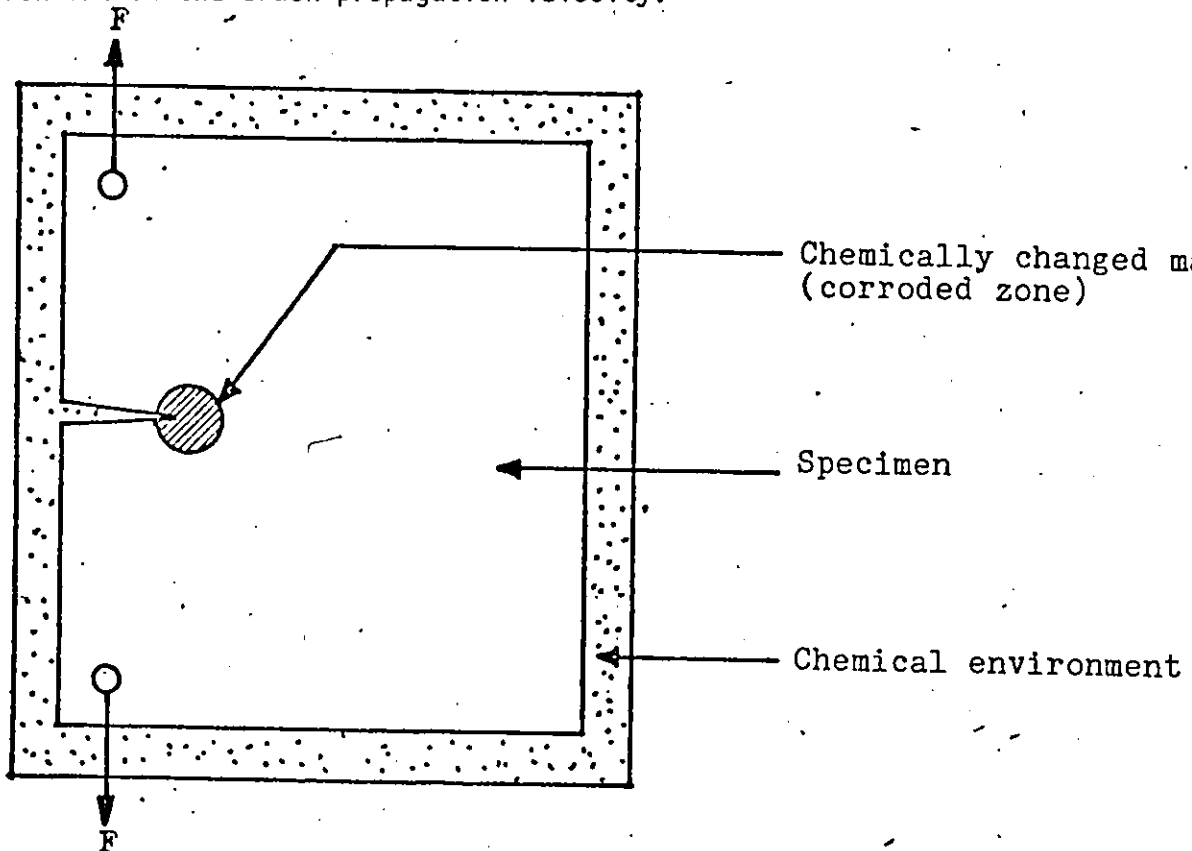

Figure 3.11 A schematic diagram showing the corroded zone in front of the crack tip.

It was suggested by Lawn [28] and others [39, 40, 41, 52, 58, 59] that the effect of the chemical environment is to weaken the material in front of the crack tip. The environmental molecules react with the crack tip bonds. The atomic bonds of the material formed during the chemical reaction are weaker than those of the parent material.

In general the stress corrosion reaction has five successive stages: (1) transport of the reactive species to the crack tip, (2) adsorption of the reactive species, (3) reaction on the surface, (4) desorption of the products, and (5) transport of the liberated products from the surface into the environment. Wiederhorn [41] suggested that the three possible limiting steps are diffusion, chemisorption and the chemical reaction. The latter two processes involve the chemical reaction with the crack tip bonds.

The schematic diagram of the typical stress corrosion cracking in most metallic and non-metallic materials is shown in Fig. 3.12. The crack propagation velocity in Regions I and III is a function of the mechanical energy, while in Region II the crack velocity appears to be independent of the applied load. It follows, therefore, that because diffusion is not stress dependent, crack propagation in Region I is controlled by the breaking (thermally activated) of the corroded zone in front of the crack tip while in Region II it is controlled by diffusion (and hence the chemical reaction) [41]. In Region III typical experimental results indicate that the crack velocity is not affected by the chemical environment. It appears that each of the three regions in Fig. 3.12 is controlled by a single energy barrier process, the rate constant of which is defined as

$$k_i = \frac{kT}{h} \exp - \frac{\Delta G_i^{\ddagger} - \alpha K_I}{kT} \qquad E$$

where the mechanical energy was expressed as

$$W(\sigma) = \alpha K_I$$

It follows from Equation E that, in general the effect of an energy barrier can be represented by a straight line in the $\log k_i$ vs. stress intensity co-ordinate system. In Fig. 3.12, the thin lines indicate the effect of each barrier on the process separately. When consecutive energy barriers control the rate of activation, the slowest process dominates. It, therefore, follows from Fig. 3.12 that Region I and II are combined in series. In parallel processes always the fastest dominates. Again, in Fig. 3.12 it is clear that Region III is controlled by a process that is parallel to barriers I and II. Thus in general, stress corrosion cracking is controlled by consecutive energy barrier system of two barriers parallel with a third barrier. It was suggested by Lawn [28,38], Brown [27] and Krausz [42] that crack propagation in Regions I and III takes place by a double kink nucleation and sideways spreading processes.

Figure 3.10 shows the experimental data in Region I of stress corrosion cracking of porcelain in water [60] by Evans and Linza. The solid line was calculated from the general crack propagation velocity Equation (3.33). For the calculation of the rate constants, the bond energy was considered to be equal to the activation free energy for the chemically changed matrix (corroded zone) at the crack tip while Irwin's expression was used in calculating the mechanical energy, i.e.,

$$W(\sigma) = \alpha K_I$$

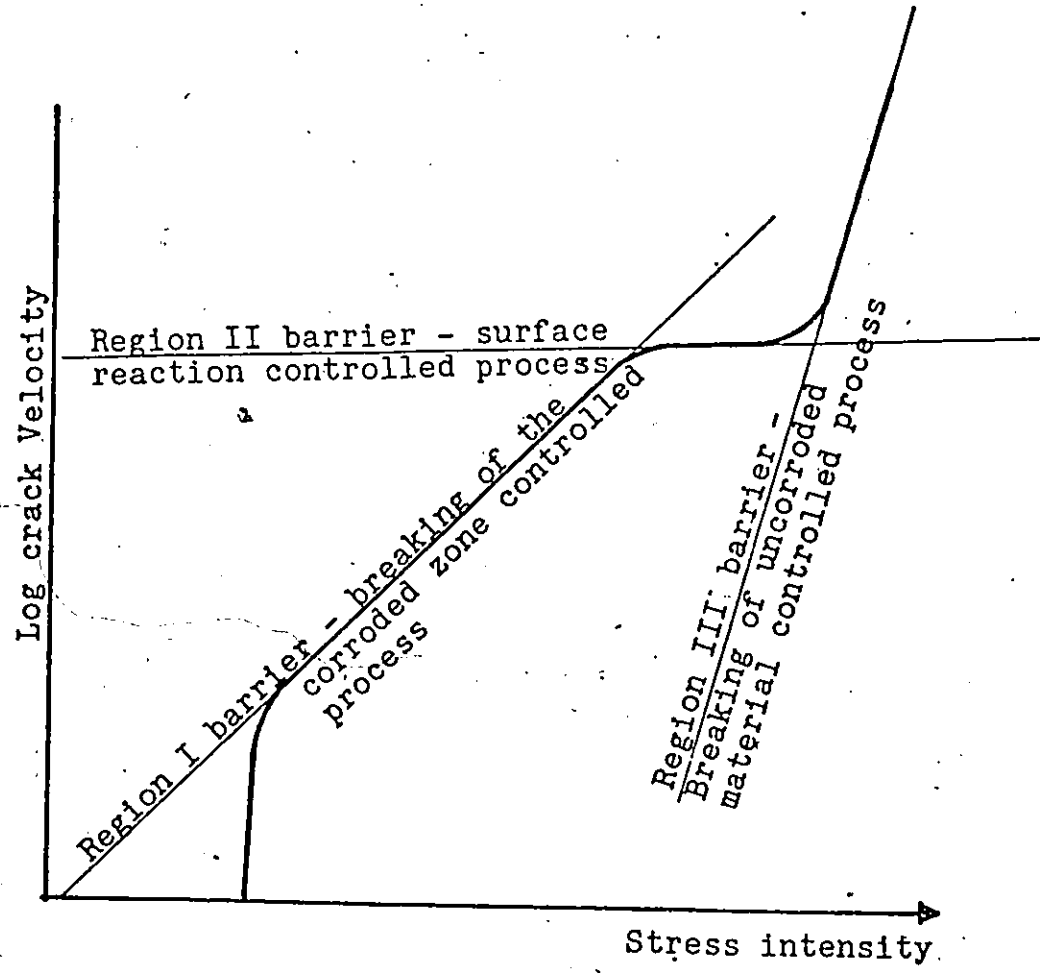

Figure 3.12 The combination of the consecutive barriers with the parallel barrier leading to the observed stress corrosion cracking behaviour.

where α is a proportionality constant controlled by the geometry of the crack |51| as well as the type of the chemical environment. The parameters used in the calculations were obtained by fitting Equation (3.33) to the experimental data. A computer subroutine ZX SSQ (Appendix 9), that is a finite difference Levenberg-Marquardt routine for solving non-linear least squares equations was used to fit Equation (3.33) to the data.

The parameters obtained from the fit are in good agreement with those obtained by Brown [27] for the same experimental data in an extensive study of stress corrosion cracking in ceramics. Table 3.2 gives a summary of the results obtained in this thesis as well as those obtained by Brown.

Table 3.2 Summary of the results obtained from curve fitting.

Parameter	Results from this analysis	Results obtained by Brown
$\Delta G_b^{\pm}$	1.05 eV	1.13 eV
α/kT	$3.015 \times 10^{-5} \frac{m^{3/2}}{N}$	$3.32 \times 10^{-5} \frac{m^{3/2}}{N}$
K_{ISCC}	$6.7 \times 10^{5} \frac{N}{m^{3/2}}$	$6.9 \times 10^{6} \frac{N}{m^{3/2}}$
$\frac{\ell}{2a_y}$	200	5 (assumed)

The free energy of activation for the corroded zone in front of the crack tip $\Delta G_b^{\ddagger}$, the proportionality constant, α/kT, and the kink spreading distance $\ell/2a_y$ were obtained from the curve fitting computer program, while the threshold stress intensity, K_{ISCC}, was obtained from the graph in Fig. 3.10. Brown obtained the threshold stress intensity value from the curve fitting program. However, Brown assumed that there were 5×10^6 kinks per cm of the crack front which is equivalent to about 10 atomic distances between two adjacent kinks. The agreement between the results from this analysis and those from Brown's analysis for $\Delta G_b^{\ddagger}$, α/kT and K_{ISCC} is within 10%. The similarity between Brown's analysis and the present kinetics is that the crack is assumed to advance by nucleation and steady state spreading of the double kinks. It was further assumed in the two analyses that there is a steady state number of active double kinks per unit length of the crack front and that the crack growth is isothermal. Brown's analysis, however, includes the effect of the chemical environment and is a complete description of stress corrosion cracking while in the present kinetics only the general model of the double kink nucleation and steady state spreading is discussed.

It was pointed out earlier that crack propagation in Regions I and II of the stress corrosion cracking process is controlled by a system of two consecutive energy barriers. However, in this analysis it has been shown that crack propagation in Region I is controlled by the breaking of the chemically changed matrix at the crack tip and that the crack propagates by double kink nucleation and spreading over a

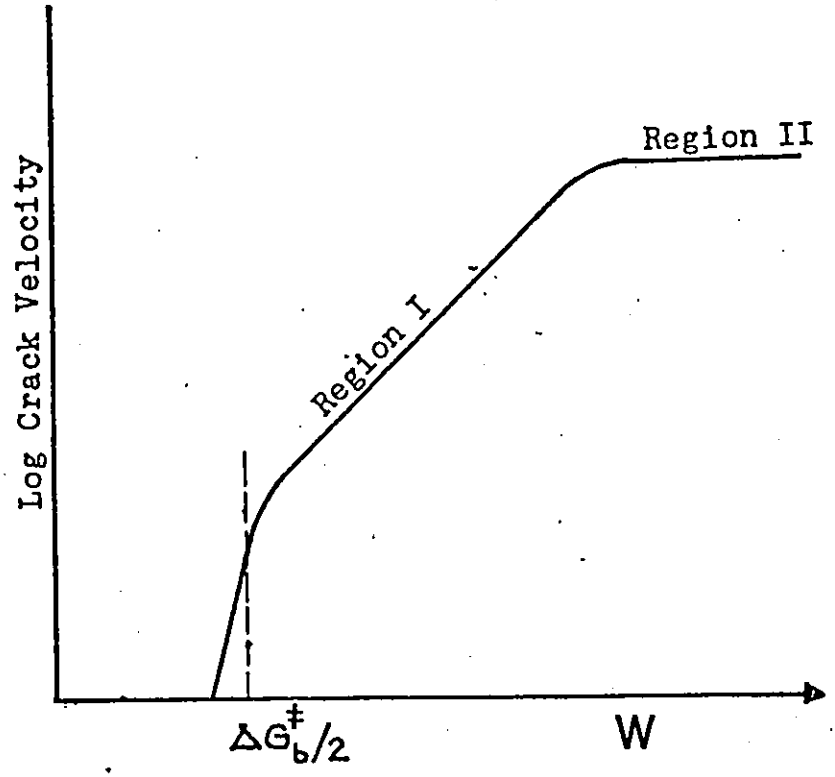

Figure 3.13 Schematic diagram of Regions I and II of stress corrosion diagram.

series of identical consecutive energy barriers. The general behaviour observed in Regions I and II is shown schematically in Fig. 3.13. This behaviour, while it appears to be controlled by a consecutive double barrier process, it is pseudo-double barrier process.

It appears from the analysis that for the threshold stress intensity, the mechanical energy is approximately equal to one half of the bond energy, i.e.,

$$W(\sigma) = \Delta G_b^{\ddagger}/2.$$

When Irwin's expression is used, the threshold stress intensity is

$$K_{ISCC} = \frac{\Delta G_b^{\ddagger}}{2\ \alpha} \qquad F$$

This is a very important result because the threshold stress intensity value can now be estimated from the material property, $\Delta G_b^{\ddagger}$ and the constant α which depends on the crack geometry. In stress corrosion cracking, $\Delta G_b^{\ddagger}$ represents the free energy of activation for the chemically changed matrix at the crack tip and is a property of the particular material and the environment. However, in some material-environment systems, the threshold stress intensity is approximately zero. In such cases, the proportionality constant, α, is very large; a condition that probably exists in aluminum alloys [25]. Equation F indicates the condition toward which the development of stress corrosion resistant alloys could be aimed.

In Region III, crack propagation is expected to be controlled by double kink formation and sideways spreading [42]. While, therefore, it appears to be controlled by a single energy barrier process, it is a consequence of a series of identical barriers.

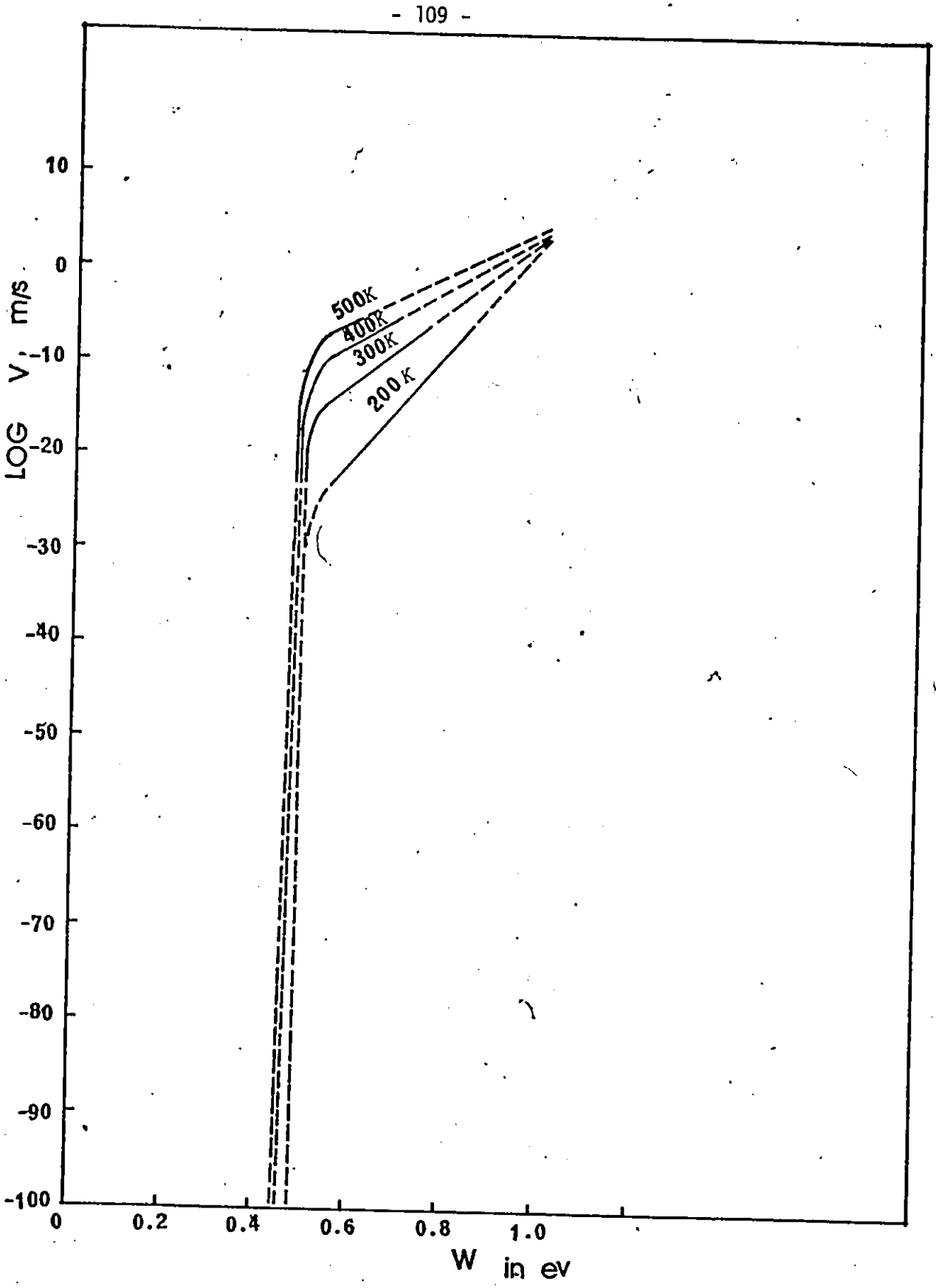
10
0
-10
-20
-30
-40
-50
-60
-70
-80
-90
-100
LOG V, m/s
500K
400K
300K
200K
0
0.2
0.4
0.6
0.8
1.0
W in ev

Figure: 3.6 (a)

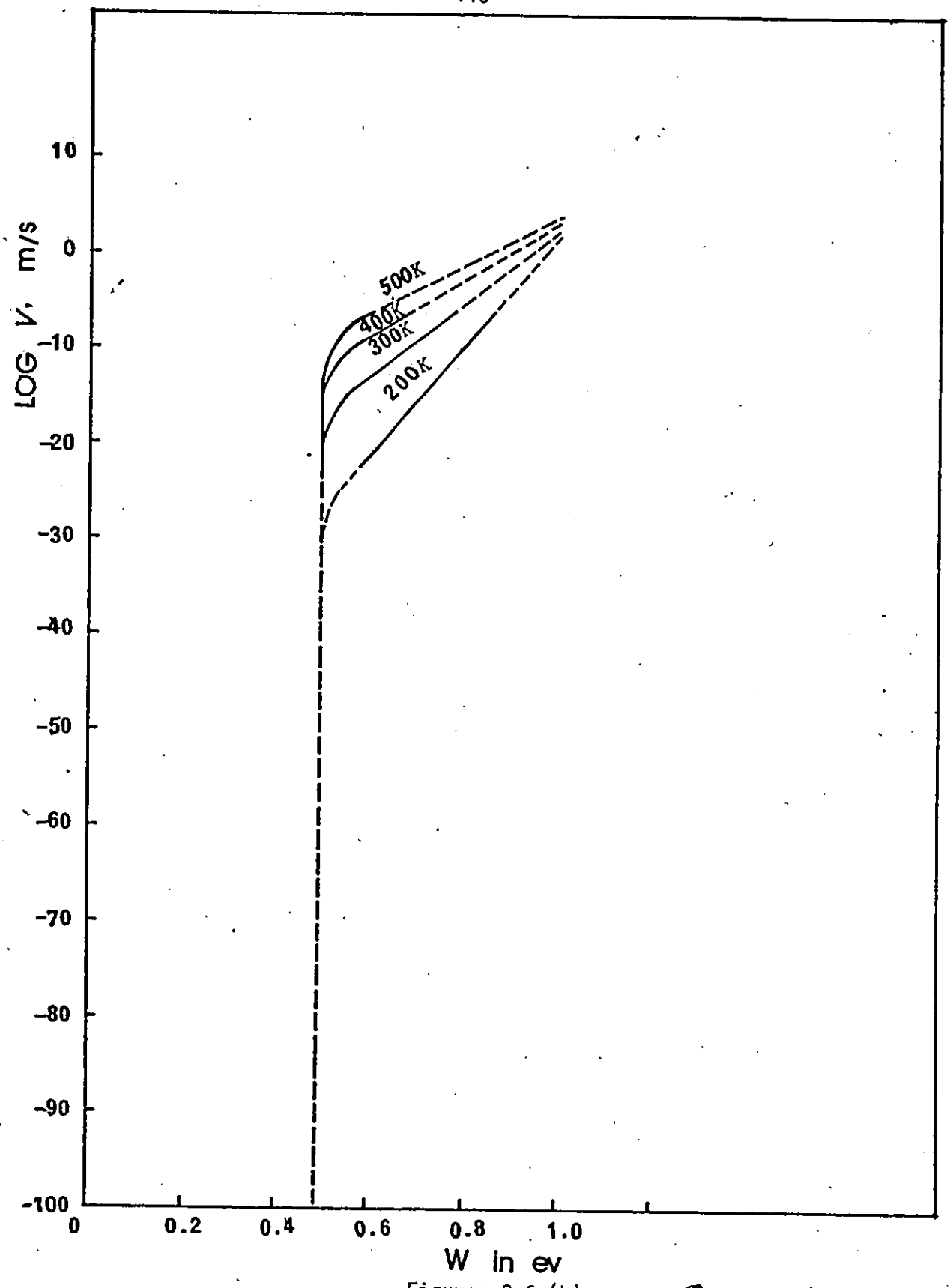

Figure: 3.6 (b)

Figure 3.6: The Figure shows the crack propagation velocity as a function of the mechanical energy, temperature and kink spreading distance for a material with bond energy of 1 eV and interatomic distance of 2 Å. The solid lines represent the slow crack growth range (10^{-10} to 10^{-3} m/s). The curves were calculated by using Eq. 3.33. (a) Kink spreading distance is 50 atomic distances. (b) Kink spreading distance is 100 atomic distances

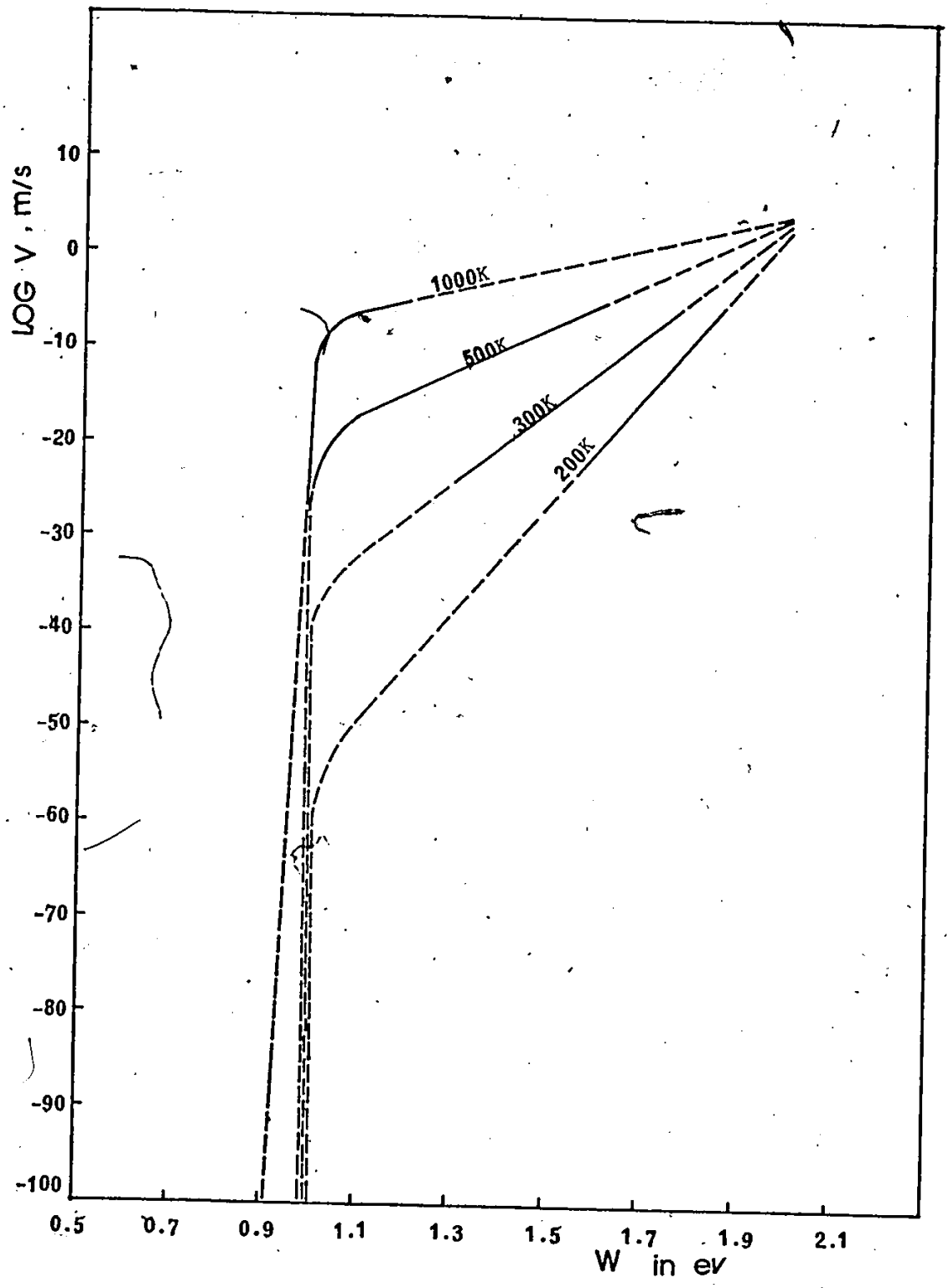
LOG V , m/s
10
0
-10
-20
-30
-40
-50
-60
-70
-80
-90
-100
1000K
500K
300K
200K
0.5
0.7
0.9
1.1
1.3
1.5
1.7
1.9
2.1
W in ev

Figure: 3.7 (a)

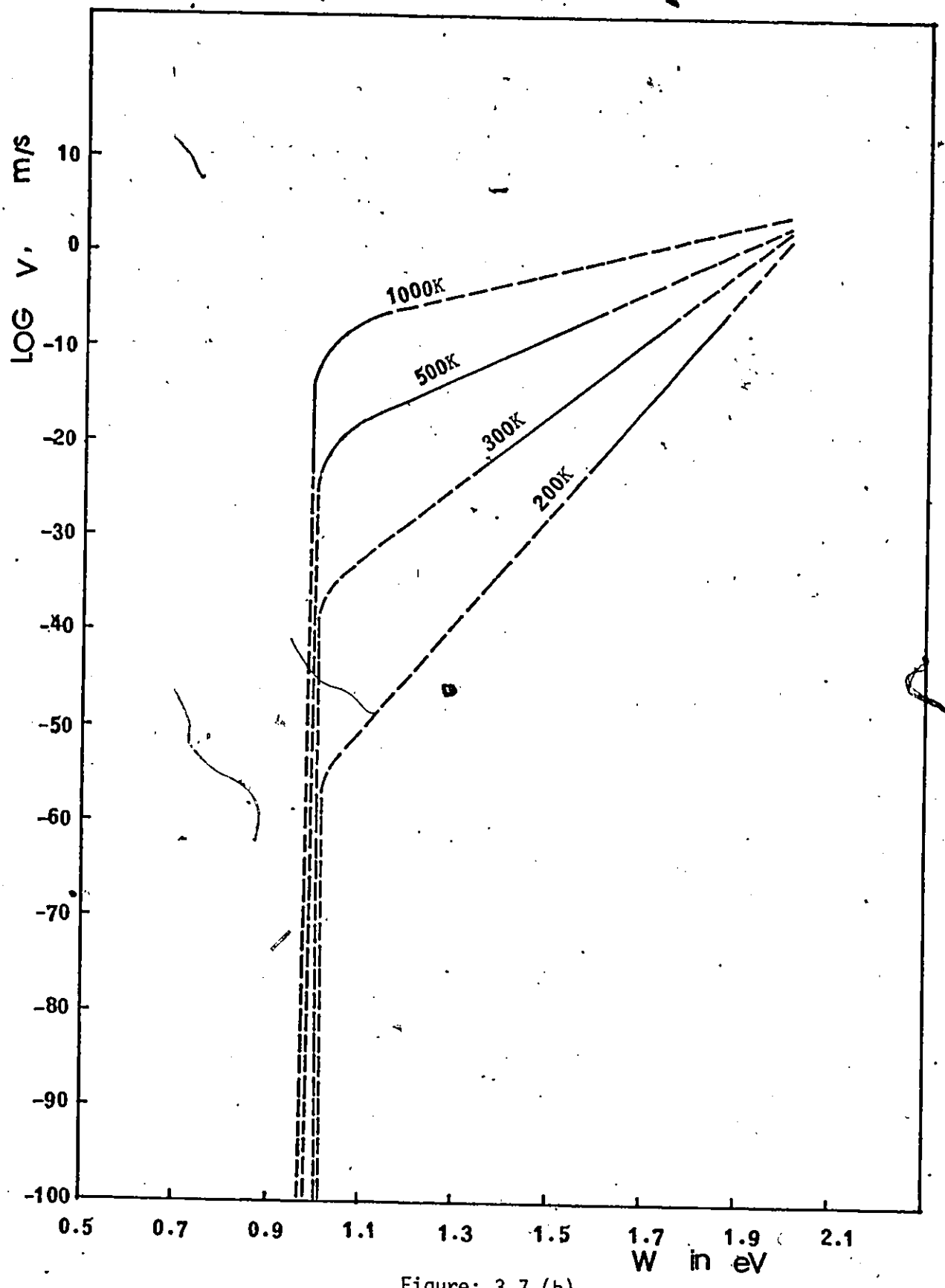

Figure: 3.7 (b)

Figure 3.7: The Figure shows the crack propagation velocity as a function of the mechanical energy, temperature and kink spreading distance for the same conditions as in Fig. 3.6 but for a material with a bond energy of 2 eV and interatomic distance of 2Å.

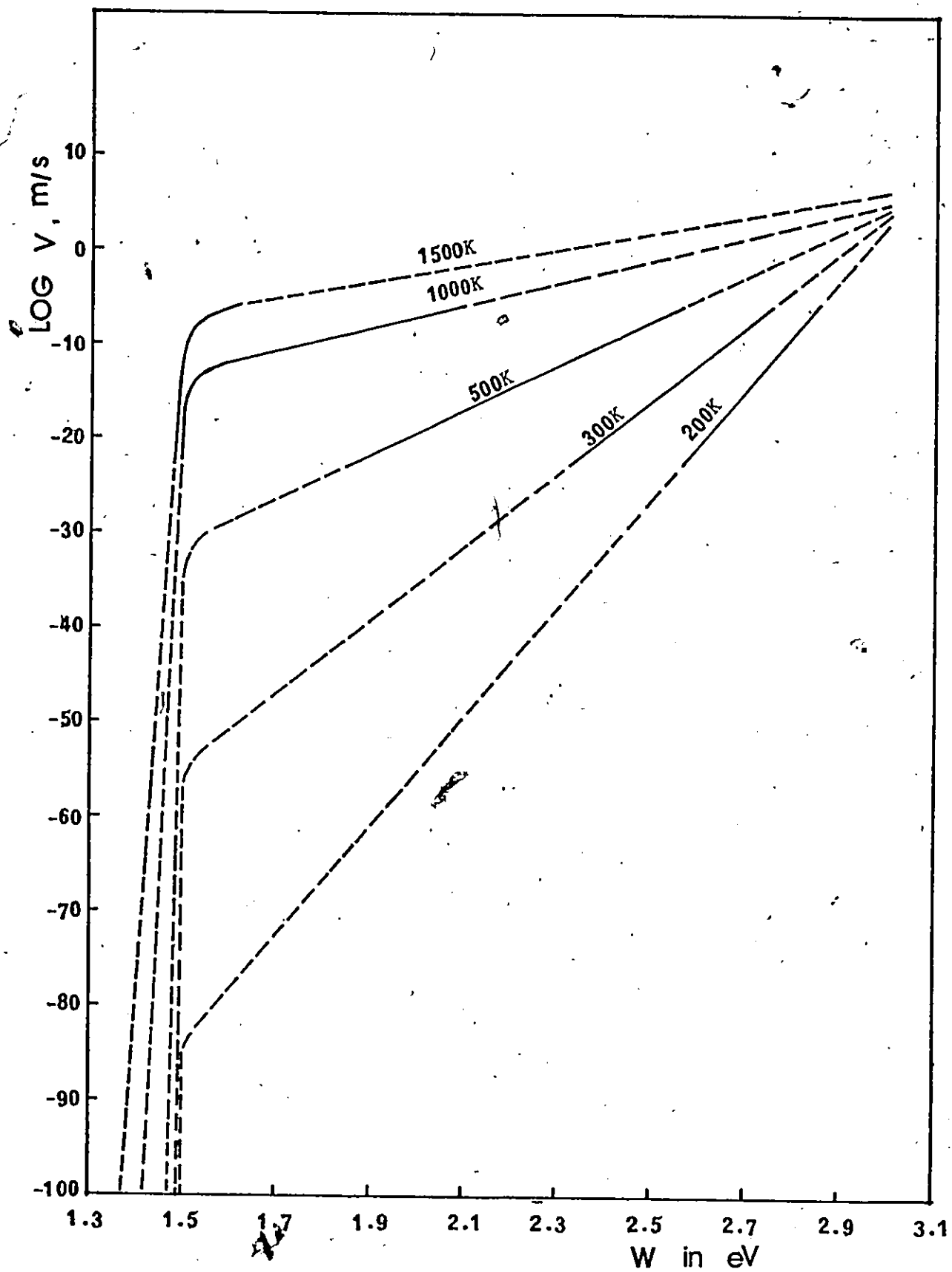
LOG V, m/s
10
0
-10
-20
-30
-40
-50
-60
-70
-80
-90
-100
1500K
1000K
500K
300K
200K
1.3
1.5
1.7
1.9
2.1
2.3
2.5
2.7
2.9
3.1
W in eV

Figure: 3.8 (a)

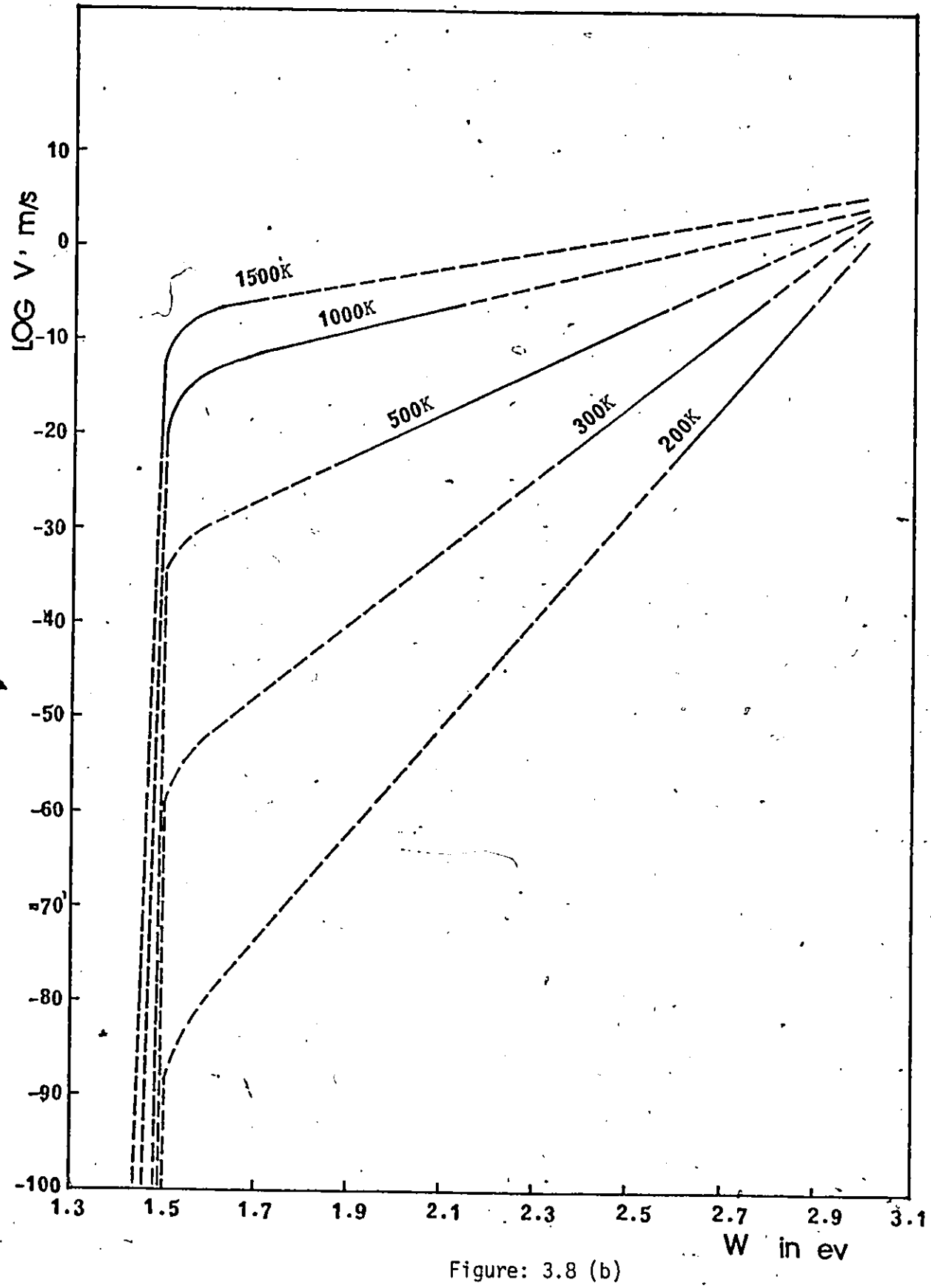

Figure: 3.8 (b)

Figure 3.8: The Figure shows the crack propagation velocity as a function of the mechanical energy, temperature and kink spreading distance for the same conditions as in Fig. 3.6 but for a material with a bond energy of 3 eV and interatomic distance of 2Å.

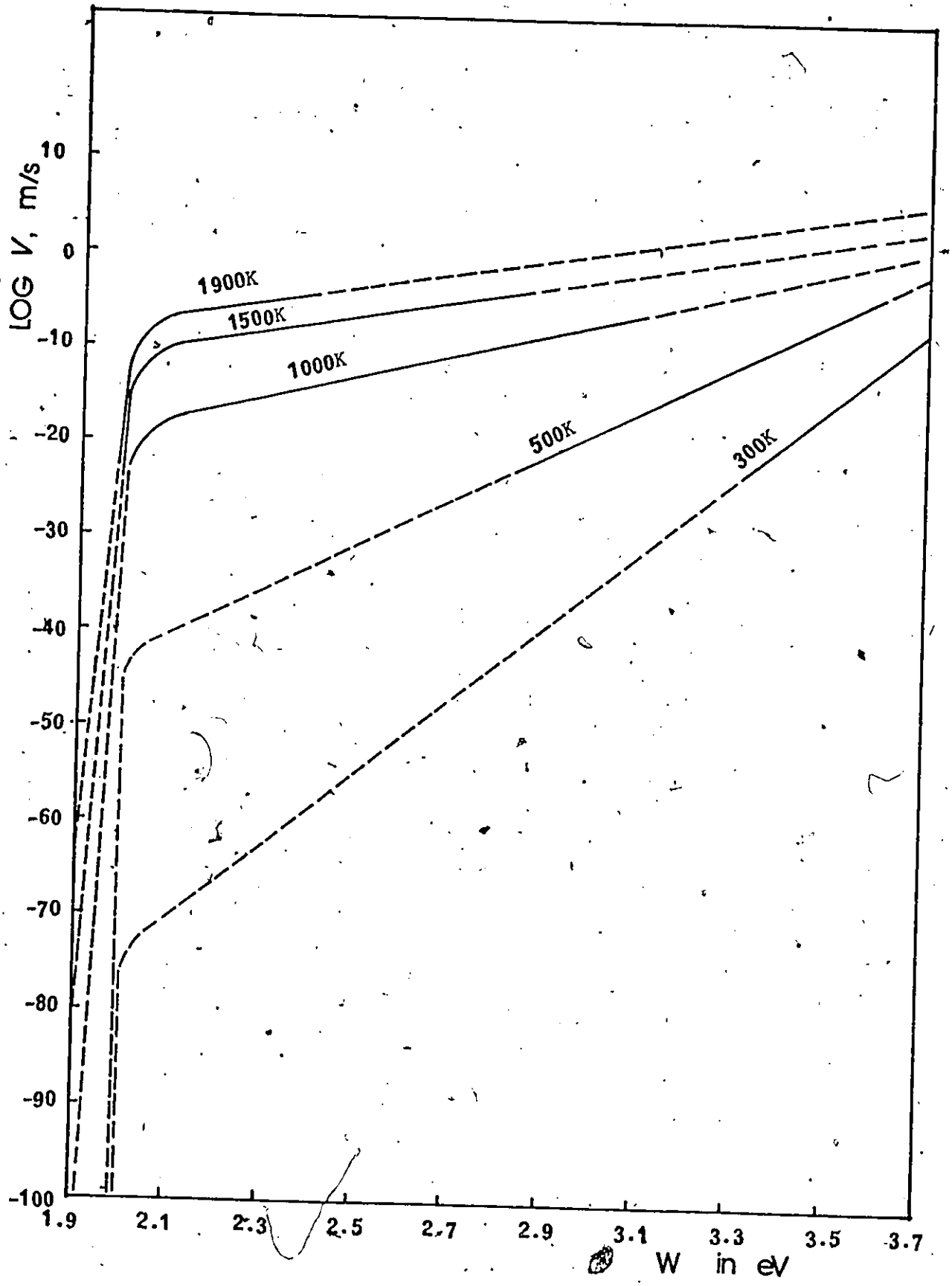
LOG V, m/s
10
0
-10
-20
-30
-40
-50
-60
-70
-80
-90
-100
1900K
1500K
1000K
500K
300K
1.9
2.1
2.3
2.5
2.7
2.9
3.1
3.3
3.5
3.7
W in eV

Figure: 3.9 (a)

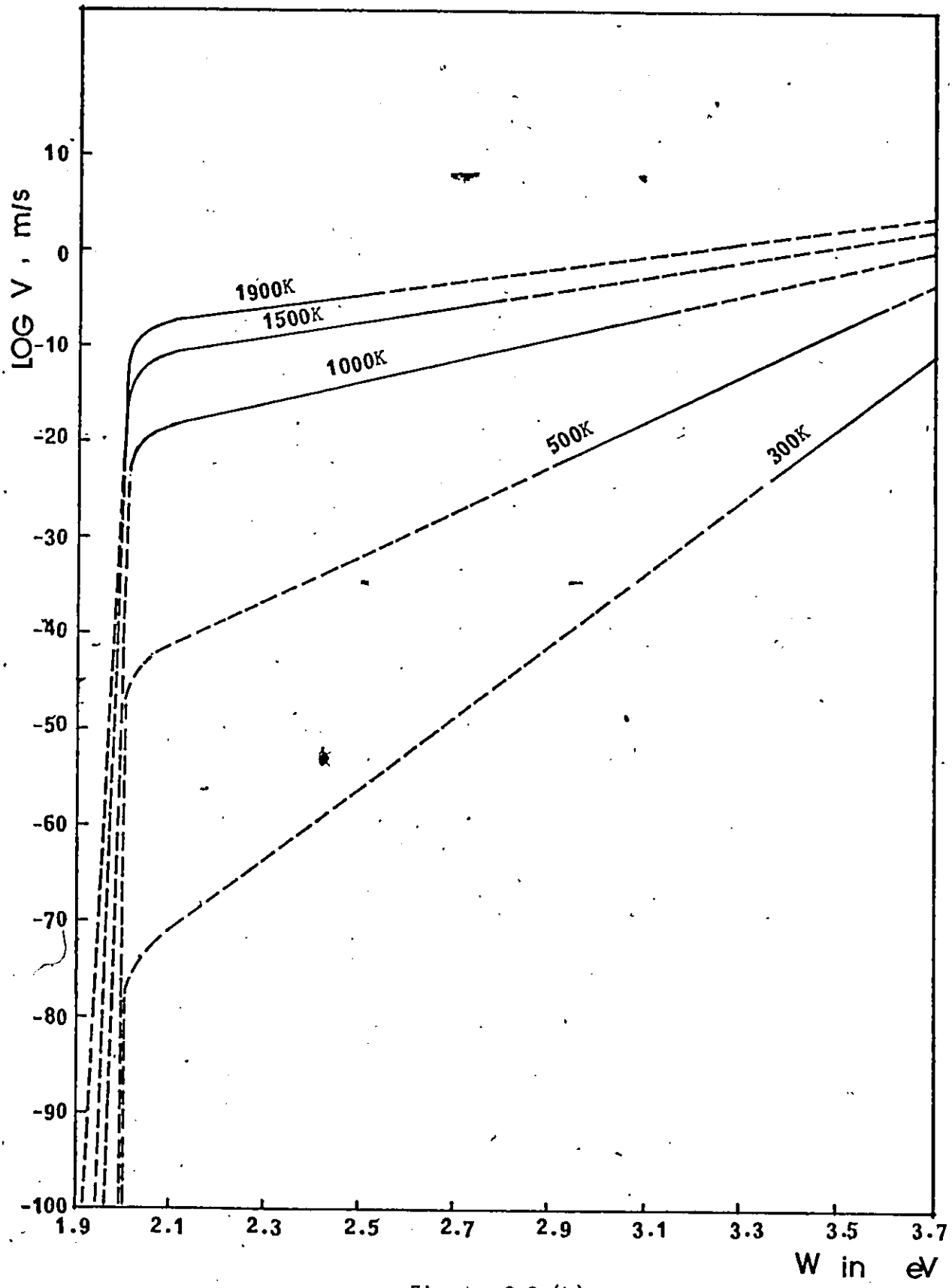

Figure: 3.9 (b)

Figure 3.9: The Figure shows the crack propagation velocity as a function of the mechanical energy, temperature and kink spreading distance for the same conditions as in Fig. 3.6 but for a material with a bond energy of 4 eV and interatomic distance of 2Å.

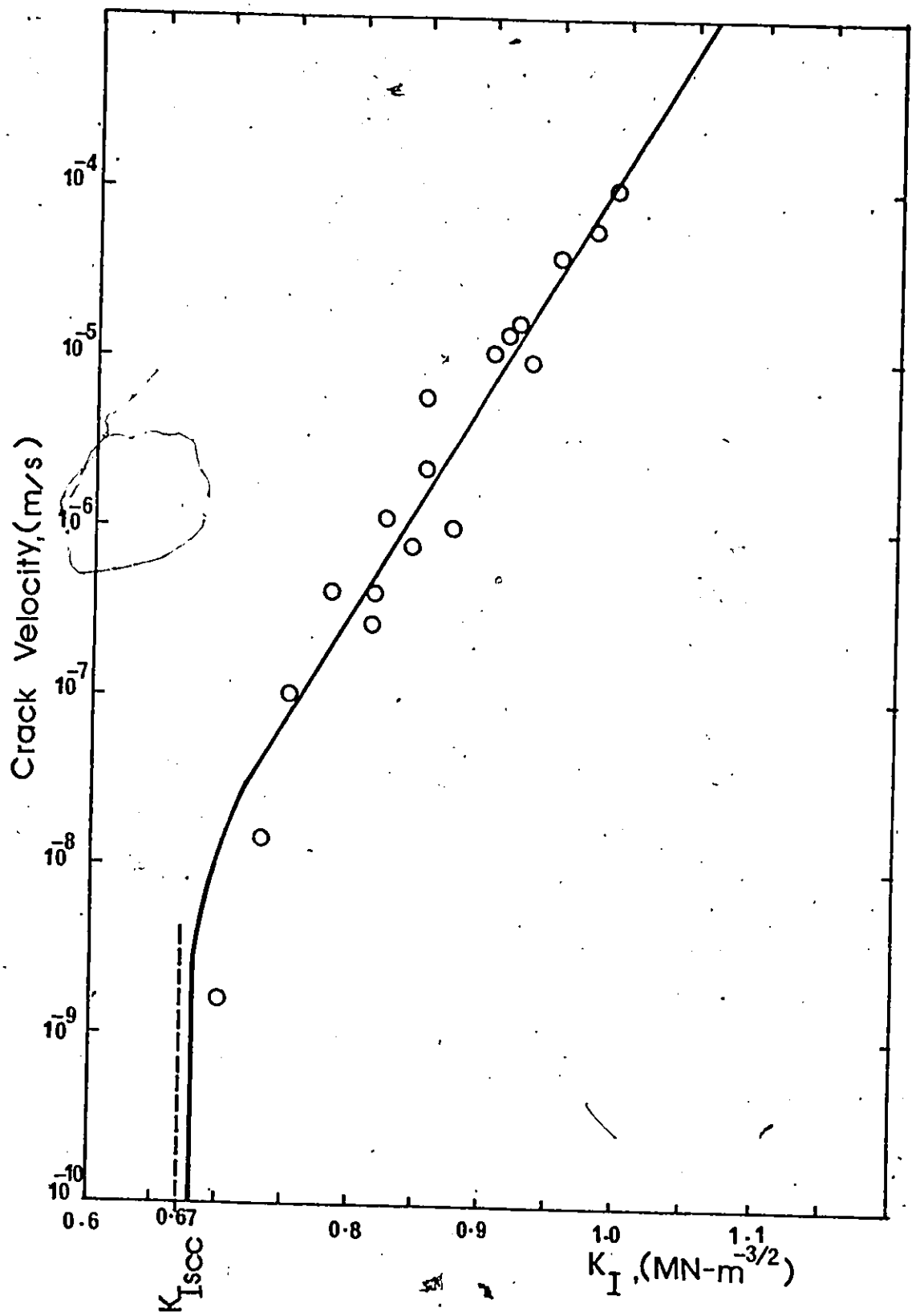

Figure: 3.10

Figure 3.10: Equation 3.33 compared with the data of Evans and Linza [60] on porcelain in water. Only Region I data of the stress corrosion cracking was considered. The circles represent the data and the solid line was calculated by using Eq. 3.33.

Chapter 4

Non-Steady State Fracture Kinetics Analysis

It was discussed in Chapters 2 and 3 that thermally activated crack propagation takes place by a bond breaking and healing process over a consecutive system of energy barriers. The continuum approach was introduced in Chapter 2 while in Chapter 3, both the continuum and discrete approaches were discussed. The discrete fracture kinetics analysis lead to the following flux equations

$$\begin{aligned} F_{i-1} &= N_{i-1}\, k_{i-1,b} - N_i\, k_{i-1,h} \\ F_i &= N_i\, k_{i,b} - N_{i+1}\, k_{i,h} \\ F_{i+1} &= N_{i+1}\, k_{i+1,b} - N_{i+2}\, k_{i+1,h} \end{aligned} \tag{4.1}$$

In Eq. 4.1, $k_{i,b}$ and $k_{i,h}$ represent the bond breaking and bond healing rate constants for the ith barrier respectively while N_i represents the concentration of the crack tips in front of the ith barrier. Studies are usually carried out for the steady state condition. Then

$$\ldots = F_{i-1} = F_i = F_{i+1} = \ldots F_{ss} \tag{4.2}$$

In this chapter, the kinetics analysis of non-steady state crack propagation where

$$\ldots \neq F_{i-1} \neq F_i \neq F_{i+1} \neq \ldots \neq F_n$$

will be introduced. The general definition of the physical condition will

be presented. However, the general method of the analysis will not be discussed and only the application of the method to stress corrosion cracking will be presented.

4.1 The Definition of the Physical Condition

Consider the propagation of a crack having an initial tip location at X_0 (Fig. 4.1 (a)) in a plate of length L. A quasi rigid crack front propagation will be assumed although the procedure could be applied to the spreading process of the double kink. Crack propagation is the net result of thermally activated bond breaking and healing steps. The crack tip, therefore, "pulsates" as it propagates. These pulsations (fluctuations), can be of any size, each with a defined probability, determined by the rate constants. However, the crack cannot shrink below the initial crack size X_0 (Fig. 4.1 (b)) where the free energy field goes to infinity presenting a non-scalable reflecting boundary. In the general case, the plate is finite and the crack tip reaching $X = L$ cannot be activated back. The last barrier n presents an infinitely large backward activation free energy as illustrated in Fig. 4.1 (b). At this end, the energy barrier system is terminated by an absorbing boundary. The analysis can be easily modified to consider an infinitely long plate.

Because in non-steady state the flux over each barrier is different the number of crack tips N_i is a function of time t as well as the location. The process has to be described by a non steady state discrete system, the rate equations of which are expressed as

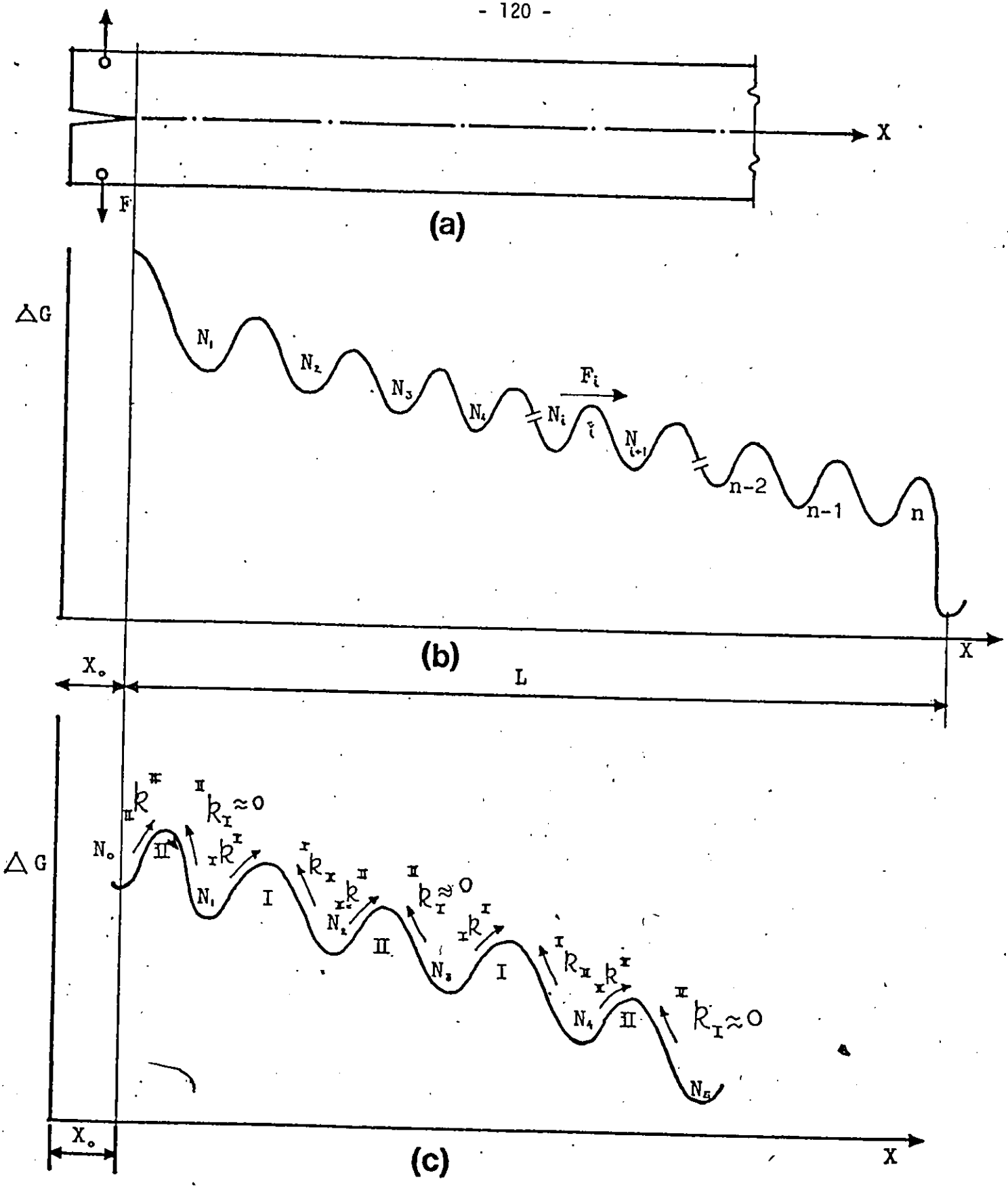

Figure 4.1 (a) Semi-infinite precracked specimen.
(b) The energy barrier system for a finite specimen of length L.
(c) The energy barrier system for stress corrosion cracking.
The dashed arrow indicates that the rate of corrosion product to reactant process is negligible.

$$\frac{dN_1}{dt} = - N_1 \, {}_1k^1 + N_2 \, {}^1k_2 + R_{n_1} - R_{im_1}$$

$$\frac{dN_2}{dt} = N_1 \, {}_1k^1 - N_2({}_2k^2 + {}^1k_2) + N_3 \, {}^2k_3 + R_{n_2} - R_{im_2}$$

$$\vdots$$

$$\frac{dN_i}{dt} = N_{i-1} \, {}_{i-1}k^{i-1} - N_i({}^{i-1}k_i + {}_ik^i) + N_{i+1} \, {}^i k_{i+1} + R_{ni} - R_{imi}$$

$$\frac{dN_n}{dt} = N_{n-1} \, {}_{n-1}k^{n-1} - N_n({}^{n-1}k_n + {}_nk^n) + R_{nm} - R_{imn} \qquad (4.3)$$

Equations (4.3) are the expression of crack conservation law similar to other transport processes such as chemical reactions [70,72,74], fluid flow, heat transfer, diffusion, electron flow, mechanical vibration, plastic flow, etc. Each equation expresses the rate of change of the number of mobile cracks N_j with the crack tips at X_j as

$\frac{dN_i}{dt}$ = flow over a unit time <u>into</u> valley i -
flow over a unit time <u>out</u> of valley i and creation of cracks -
immobilization of cracks.

In Eqs. (4.3), R_n and R_{im} expresses the rate of nucleation and immobilization respectively. The system of n differential equations has n unknowns $N_i (i = 1 \ldots n)$ and defines fully the behaviour when the initial conditions at $t = 0$ are imposed. Often two or more of the crack tip locations have identical free energy surroundings, i.e., all rate constants are identical. In these cases, the equations can be combined into a single one. For example

$$\frac{dN_\ell}{dt} = N_{\ell-1}\ {}_{\ell-1}k^{\ell-1} - N_\ell({}^{\ell-1}k_\ell + {}_\ell k^\ell) + N_{\ell+1}\ {}^\ell k_{\ell+1}$$

$$\frac{dN_m}{dt} = N_{m-1}\ {}_{m-1}k^{m-1} - N_m({}^{m-1}k_m + {}_m k^m) + N_{m+1}\ {}^m k_{m+1}$$

with $${}_{\ell-1}k^{\ell-1} = {}_{m-1}k^{m-1} = {}_{v-1}k^{v-1}$$

$${}_m k^m = {}_\ell k^\ell = {}_v k^v$$

$${}^{m-1}k_m = {}^{\ell-1}k_\ell = {}^{v-1}k_v$$

$${}^m k_{m+1} = {}^\ell k_{\ell+1} = {}^v k_{v+1}$$

Combination gives

$$\frac{d(N_\ell + N_m)}{dt} = (N_{\ell-1} + N_{m-1})_{m-1}k^{m-1} - (N_\ell + N_m)({}^{m-1}k_m + {}_m k^m) + (N_{\ell+1} + N_{m+1})^m k_{m+1}$$

$$\frac{dN_v}{dt} = N_{v-1}\ {}_{v-1}k^{v-1} - N_v({}^{v-1}k_v + {}_v k^v) + N_{v+1}\ {}^v k_{v+1}$$

In these expressions, the nucleation and immobilization rates were considered to be negligible -- a realistic and convenient condition for the explanation of the combination concept. The symbol v signifies that the combined equations provide only the combined ℓ and m but will not determine them as separate entities.

The crack size distribution relations will involve solving the differential Eqs.(4.3)to obtain N_1, N_2, N_3 ... N_n. The procedure for solving the n differential equations has been outlined by Sokolnikoff, I.S. and

Redheffer, R.M, [78] and by Krausz [61]. In the following, a system of two consecutive energy barriers controlling the crack propagation in Regions I and II of the stress corrosion cracking discussed in Chapter 3, will be considered. This is a much simpler system that can serve to illustrate the general procedure.

4.2 The Non-Steady State Fracture Kinetics of Stress Corrosion Cracking.

Consider N_t number of precracked specimens shown in Fig. 4.1 (a). At time $t = 0$, the specimens are loaded and subjected to a corrosive environment simultaneously. The corrosive environment delivers the reagent molecule that diffuses to the crack tip. A chemical reaction then takes place at the crack tip and the matrix atoms in front of the crack are replaced by a usually brittle compound. The weakened bonds are broken by the combined action of the mechanical work and the random thermal activations of the atoms at the crack tip. Both the corrosion and bond breaking steps are thermally activated and because the chemical reaction has to take place before the corroded bonds break the process is sequential over the range of Regions I and II. The free energy barrier system for this process is shown in Fig. 4.1 (c). The first barrier is associated with the chemical reaction and this is followed by the breaking of the corroded bonds. Diffusion of the reagent to the crack tip again takes place, followed by a chemical reaction and the bond breaking of the corroded matrix. Each cycle, therefore, consists of two barriers as shown in Fig. 4.1 (c). The non-steady state flux over the barriers can be written as

$$\frac{dN_o}{dt} = - N_{o\,II} k^{II} + N_1^{II} k_1 \cong - N_{o\,II} k^{II} \quad \text{initial stage}$$

$$\frac{dN_1}{dt} = N_0 \, {}_{II}k^{II} - N_1({}^{II}k_I + {}_Ik^I) + N_2 \, {}^Ik_{II}$$

$$\cong N_0 \, {}_{II}k^{II} - N_1 \, {}_Ik^I + N_2 \, {}^Ik_{II}$$

$$\frac{dN_2}{dt} = N_1 \, {}_Ik^I - N_2({}^Ik_{II} + {}_{II}k^{II}) + N_3 \, {}^{II}k_I$$

$$\cong N_1 \, {}_Ik^I - N_2({}^Ik_{II} + {}_{II}k^{II})$$

first cycle

$$\frac{dN_3}{dt} = N_2 \, {}_{II}k^{II} - N_3({}^{II}k_I + {}_Ik^I) + N_4 \, {}^Ik_{II}$$

$$\cong N_2 \, {}_{II}k^{II} - N_3 \, {}_Ik^I + N_4 \, {}^Ik_{II}$$

$$\frac{dN_4}{dt} = N_3 \, {}_Ik^I - N_4({}^Ik_{II} + {}_{II}k^{II}) + N_5 \, {}^{II}k_I$$

$$\cong N_3 \, {}_Ik^I - N_4({}^Ik_{II} + {}_{II}k^{II})$$

second cycle

(4.4)

$$\frac{dN_5}{dt} \cong N_4 \, {}_{II}k^{II} - N_5({}^{II}k_I + {}_Ik^I) + N_6 \, {}^Ik_{II}$$

.
.
.
.

For mathematical convenience in the present model, it was considered that the corrosion reaction step is irreversible, i.e. ${}^{II}k_{I} \simeq 0$. This is a physically reasonable assumption. However, it should not be considered to be a restriction on the validity of the model. Equations(4.4)can be combined as before to give

$$\frac{dN_o}{dt} = - N_o \, {}_{II}k^{II}$$

$$\frac{d(N_1+N_3+N_5\ldots)}{dt} = (N_o+N_2+N_4+N_6\ldots)\, {}_{II}k^{II} - (N_1+N_3+N_5\ldots)\, {}_{I}k^{I} + (N_2+N_4+N_6\ldots)\, {}^{I}k_{II}$$

$$\frac{d(N_2+N_4+N_6\ldots)}{dt} = (N_1+N_3+N_5\ldots)\, {}_{I}k^{I} - (N_2+N_4+\ldots)({}^{I}k_{II} + {}_{II}k^{II}) \qquad (4.5)$$

Thus

$$\frac{dN_o}{dt} = - N_o \, {}_{II}k^{II}$$

$$\frac{dN_{odd}}{dt} = N_o \, {}_{II}k^{II} + N_{even}({}^{I}k_{II} + {}_{II}k^{II}) - N_{odd} \, {}_{I}k^{I}$$

$$\frac{dN_{even}}{dt} = N_{odd} \, {}_{I}k^{I} - N_{even}({}^{I}k_{II} + {}_{II}k^{II}) \qquad (4.6)$$

The crack size distribution will, therefore, be given by the solution of Eqs. (4.6). N_o defines the number of specimens with initial crack size X_o, N_{odd} represents the number of specimens in front of type I barriers and N_{even} represents the number of specimens in front of type II barriers. ${}_{I}k^{I}$ and ${}^{I}k_{II}$ represent the forward and reverse rate constants respectively for the corroded bond breaking step while ${}_{II}k^{II}$ represents the forward rate.

constant for the corrosion (chemical reaction) process.

The general solution for Eqs. (4.6) is

$$N_o = C_o\, e^{-\lambda t} + \phi_o$$

$$N_{odd} = C_{odd}\, e^{-\lambda t} + \phi_{odd} \qquad (4.7)$$

$$N_{even} = C_{even}\, e^{-\lambda t} + \phi_{even}$$

Substituting Eqs. (4.7) in Eqs. (4.6) results in

$$({}_{II}k^{II} - \lambda)\, C_o\, e^{-\lambda t} = \phi_o\, {}_{II}k^{II}$$

$$-{}_{II}k^{II} C_o\, e^{-\lambda t} + ({}_{I}k^{I} - \lambda)\, C_{odd}\, e^{-\lambda t} - C_{even}({}^{I}k_{II} + {}_{II}k^{II}) e^{-\lambda t} = \phi_o\, {}_{II}k^{II}$$

$$-\phi_{odd}\, {}_{I}k^{I} + \phi_{even}({}^{I}k_{II} + {}_{II}k^{II})$$

and

$$-{}_{I}k^{I}\, e^{-\lambda t}\, C_{odd} + ({}^{I}k_{II} + {}_{II}k^{II} - \lambda) C_{even}\, e^{-\lambda t} = \phi_{odd}\, {}_{I}k^{I}$$

$$-({}^{I}k_{II} + {}_{II}k^{II})\, \phi_{even} \qquad (4.8)$$

In Eqs. (4.8), the L.H.S. represents the time dependent terms and the R.H.S. represents the time independent terms. Each of the Eqs. in (4.8) must be satisfied separately by the time dependent terms and by the time independent terms. Therefore, it follows for the time dependent terms that

$$\begin{bmatrix} ({}_{II}k^{II} - \lambda) & 0 & 0 \\ -{}_{II}k^{II} & ({}_{I}k^{I} - \lambda) - ({}^{I}k_{II} + {}_{II}k^{II}) & \\ 0 & -{}_{I}k^{I} & ({}^{I}k_{II} + {}_{II}k^{II} - \lambda) \end{bmatrix} \begin{bmatrix} C_o \\ C_{odd} \\ C_{even} \end{bmatrix} = 0 \qquad (4.9)$$

and for the time independent terms that

$$\begin{bmatrix} {}_{II}k^{II} & 0 & 0 \\ {}_{II}k^{II} & -{}_{I}k^{I} & ({}^{I}k + {}_{II}k^{II}) \\ 0 & {}_{I}k^{I} & -({}^{I}k_{II} + {}_{II}k^{II}) \end{bmatrix} \begin{bmatrix} \phi_o \\ \phi_{odd} \\ \phi_{even} \end{bmatrix} = 0 \qquad (4.10)$$

The set of algebraic equations given by (4.9) has non trivial solutions if the determinant of the coefficients, that are formed by the rate constants and λ, is zero.

Therefore,

$$\begin{vmatrix} {}_{II}k^{II} - \lambda & 0 & 0 \\ -{}_{II}k^{II} & ({}_{I}k^{I} - \lambda) & -({}^{I}k_{II} + {}_{II}k^{II}) \\ 0 & -{}_{I}k^{I} & ({}^{I}k_{II} + {}_{II}k^{II} - \lambda) \end{vmatrix} = 0 \qquad (4.11)$$

On expanding the determinant 4.11,

$$(\lambda - {}_{II}k^{II})\{(\lambda - {}_{I}k^{I})[\lambda - ({}^{I}k_{II} + {}_{II}k^{II})] - {}_{I}k^{I}({}^{I}k_{II} + {}_{II}k^{II})\} = 0$$

$$\lambda(\lambda - {}_{II}k^{II})\left[\lambda - ({}^{I}k_{II} + {}_{I}k^{I} + {}_{II}k^{II})\right] = 0$$

Leading to

$$\lambda_1 = 0$$

$$\lambda_2 = {}_{II}k^{II} \qquad (4.12)$$

$$\lambda_3 = {}^{I}k_{II} + {}_{I}k^{I} + {}_{II}k^{II}$$

Case (a): $\lambda_1 = 0$

Substituting $\lambda_1 = 0$ in the algebraic Eqs. (4.9), we obtain

$$C_o \; {}_{II}k^{II} = 0$$

$$C_o \; {}_{II}k^{II} - C_{odd} \; {}_{I}k^{I} + ({}^{I}k_{II} + {}_{II}k^{II}) \; C_{even} = 0 \qquad (4.13)$$

$$C_{odd} \; {}_{I}k^{I} - ({}^{I}k_{II} + {}_{II}k^{II}) \; C_{even} = 0.$$

Solving for C_o, C_{odd} and C_{even}, we have

$$C_o = 0$$

$$\frac{C_{odd}}{C_{even}} = \frac{{}^{I}k_{II} + {}_{II}k^{II}}{{}_{I}k^{I}} = \beta$$

If $C_{even} = a$, then $C_{odd} = a\beta$. On substituting these results in Eqs. (4.7) together with $\lambda_1 = 0$

$$N'_o = 0 + \phi_o$$

$$N'_{odd} = a\beta + \phi_{odd} \qquad (4.14)$$

$$N'_{even} = a + \phi_{even}$$

Case (b): $\lambda_2 = {}_{II}k^{II}$

In this case, the algebraic Eqs. (4.9) become

$$C_o \; X \; 0 = 0$$

$$C_o \; {}_{II}k^{II} + ({}_{II}k^{II} - {}_{I}k^{I}) \; C_{odd} + ({}^{I}k_{II} + {}_{II}k^{II}) \; C_{even} = 0$$

$${}_{I}k^{I} \; C_{odd} - {}^{I}k_{II} \; C_{even} = 0$$

thus $\frac{C_{odd}}{C_{even}} = \frac{{}_{I}k_{II}}{{}_{I}k^{I}} = \psi$

and $\frac{C_o}{C_{even}} = -\frac{{}_{I}k^{I} + {}_{I}k_{II}}{{}_{I}k^{I}} = \gamma$

If C_{even} is chosen arbitrarily again, say $C_{even} = b$

then $C_o = \gamma b$

$C_{odd} = \psi b$

Thus, from Eqs. 4.7,

$$N_o'' = \gamma b\, e^{-{}_{II}k^{II}t} + \phi_o$$

$$N_{odd}'' = \psi b\, e^{-{}_{II}k^{II}t} + \phi_{odd} \qquad (4.15)$$

$$N_{even}'' = b\, e^{-{}_{II}k^{II}t} + \phi_{even}$$

Case (c): $\lambda_3 = {}_{I}k^{I} + {}_{I}k_{II} + {}_{II}k^{II}$

Again, from the algebraic Eqs. (4.9) we have

$$({}_{I}k^{I} + {}_{I}k_{II})\, C_o = 0$$

$$C_o\, {}_{II}k^{II} + ({}_{I}k_{II} + {}_{II}k^{II})\, C_{odd} + ({}_{I}k_{II} + {}_{II}k^{II})\, C_{even} = 0$$

$$C_{odd}\, {}_{I}k^{I} + C_{even}\, {}_{I}k^{I} = 0$$

which gives

$C_o = 0$ since $({}_{I}k^{I} + {}_{I}k_{II}) \neq 0$

$C_{odd} = - C_{even}$

Letting $C_{even} = d$, then $C_{odd} = - d$

hence

$$N_o''' = \phi_o$$

$$N_{odd}''' = - d\ e^{-\lambda_3 t} + \phi_{odd} \qquad (4.16)$$

$$N_{even}''' = d\ e^{-\lambda_3 t} + \phi_{even}$$

The general solution is obtained by summing all the particular integrals, thus

$$N_i = N_i' + N_i'' + N_i'''$$

Hence, from Eqs. (4.14), (4.15) and (4.16), we obtain,

$$N_o = \gamma\ b\ e^{-\lambda_2 t} + \phi_o$$

$$N_{odd} = \psi\ b\ e^{-\lambda_2 t} - d\ e^{-\lambda_3 t} + a\ \beta + \phi_{odd} \qquad (4.17)$$

$$N_{even} = b\ e^{-\lambda_2 t} + d\ e^{-\lambda_3 t} + a + \phi_{even}$$

From the first of Eqs. (4.10) we get

$$\phi_o = 0,$$

and from the last two of Eqs. (4.10), we obtain

$$\phi_{odd} = \frac{I_{k_{II}} + {}_{II}k^{II}}{I k^{I}}\ \phi_{even} = \beta \cdot \phi_{even}$$

At time $t = 0$, $N_o = N_t$ and $N_{even} = N_{odd} = 0$

Hence from Eqs. (4.17) we get

$$N_o = N_t = \gamma\ b$$

$$N_{odd} = 0 = a\ B + \beta\ \phi_{even} + \psi\ b - d$$

$$N_{even} = 0 = a + \phi_{even} + b + d \qquad (4.18)$$

It follows from the first of Eqs. (4.18) that

$$b = \frac{N_t}{\gamma}$$

Eqs. (4.17) then becomes

$$N_o = N_t\, e^{-\lambda_2 t}$$

$$N_{odd} = N_t \frac{\psi}{\gamma} e^{-\lambda_2 t} - d\, e^{-\lambda_3 t} + B(a + \phi_{even})$$

$$N_{even} = N_t \frac{1}{\gamma} e^{-\lambda_2 t} + d\, e^{-\lambda_3 t} + a + \phi_{even} \qquad (4.19)$$

At time $t = 0$, the last two Eqs. of Eqs. (4.19) become

$$0 = B(a + \phi_{even}) - d + N_t \frac{\psi}{\gamma}$$

$$0 = a + \phi_{even} + d + N_t \frac{1}{\gamma}\,.$$

If we let $a + \phi_{even} = \varepsilon$, then from the first Eq. we get

$$d = \beta\varepsilon + N_t \frac{\psi}{\gamma}$$

Substituting the value of d into the second Eq. results in

$$\varepsilon = -\frac{N_t(1 + \psi)}{\gamma(1 + B)}$$

$$\text{Hence } d = \frac{N_t(\psi - B)}{\gamma(1 + B)} \qquad (4.20)$$

Finally, the number of crack tips in front of each of the two barriers is given by

$$\frac{N_o}{N_t} = e^{-\lambda_2 t}$$

$$\frac{N_{odd}}{N_t} = f\, e^{-\lambda_2 t} - g\, e^{-\lambda_3 t} + q \qquad (4.21)$$

$$\frac{N_{even}}{N_t} = \ell\, e^{-\lambda_2 t} + g\, e^{-\lambda_3 t} + p$$

where

$$f = \frac{-{}_{I}k_{II}}{{}_{I}k^{I} + {}_{I}k_{II}}$$

$$g = \frac{{}_{II}k^{II}\,{}_{I}k^{I}}{({}_{I}k^{I} + {}_{II}k^{II} + {}_{I}k_{II})({}_{I}k^{I} + {}_{I}k_{II})}$$

$$\ell = -\frac{{}_{I}k^{I}}{{}_{I}k^{I} + {}_{I}k_{II}}$$

$$p = \frac{{}_{I}k^{I}}{{}_{I}k^{I} + {}_{II}k^{II} + {}_{I}k_{II}}$$

$$q = \frac{{}_{II}k^{II} + {}_{I}k_{II}}{{}_{I}k^{I} + {}_{II}k^{II} + {}_{I}k_{II}}$$

4.3 Discussion

Figure 4.2 shows the crack size distribution as a function of the mechanical energy and time. The curves were calculated by using Eqs. (4.21). The parameters are those for the stress corrosion cracking of polycrystalline alumina in toluene [27]. The free energy of activation for the corroded zone in front of the crack tip is 1.4 eV. The temperature is 300K while the rate constant for the diffusion process is 350/s (considered to be independent of the mechanical work). The procedure that was used to calculate the rate constants ${}_{I}k^{I}$ and ${}^{I}k_{II}$ was similar to that for calculating k_h and k_b, outlined in Chapter 2. The dashed and solid curves represent the number of crack tips in front of type II barriers, $\frac{N_{even}}{N_t}$ and the number of crack tips in front of type I barriers, $\frac{N_{odd}}{N_t}$, respectively.

The number of the crack tips at the initial crack size X_o decreases sharply from $N_o = N_t$ at $t = 0$ to almost zero within 2×10^{-2} seconds while the number of the crack tips in front of type II barriers, $\frac{N_{even}}{N_t}$, and the number of the crack tips in front of type I barriers, $\frac{N_{odd}}{N_t}$, increases from zero to the steady state values $\frac{N^s_{even}}{N_t}$ and $\frac{N^s_{odd}}{N_t}$ respectively, for a given mechanical energy. When the mechanical energy is increased, N^s_{even}/N_t increases while N^s_{odd}/N_t decreases. Because ${}_{II}k^{II}$ was assumed to be independent of the mechanical energy, N_o/N_t is not a function of the mechanical energy.

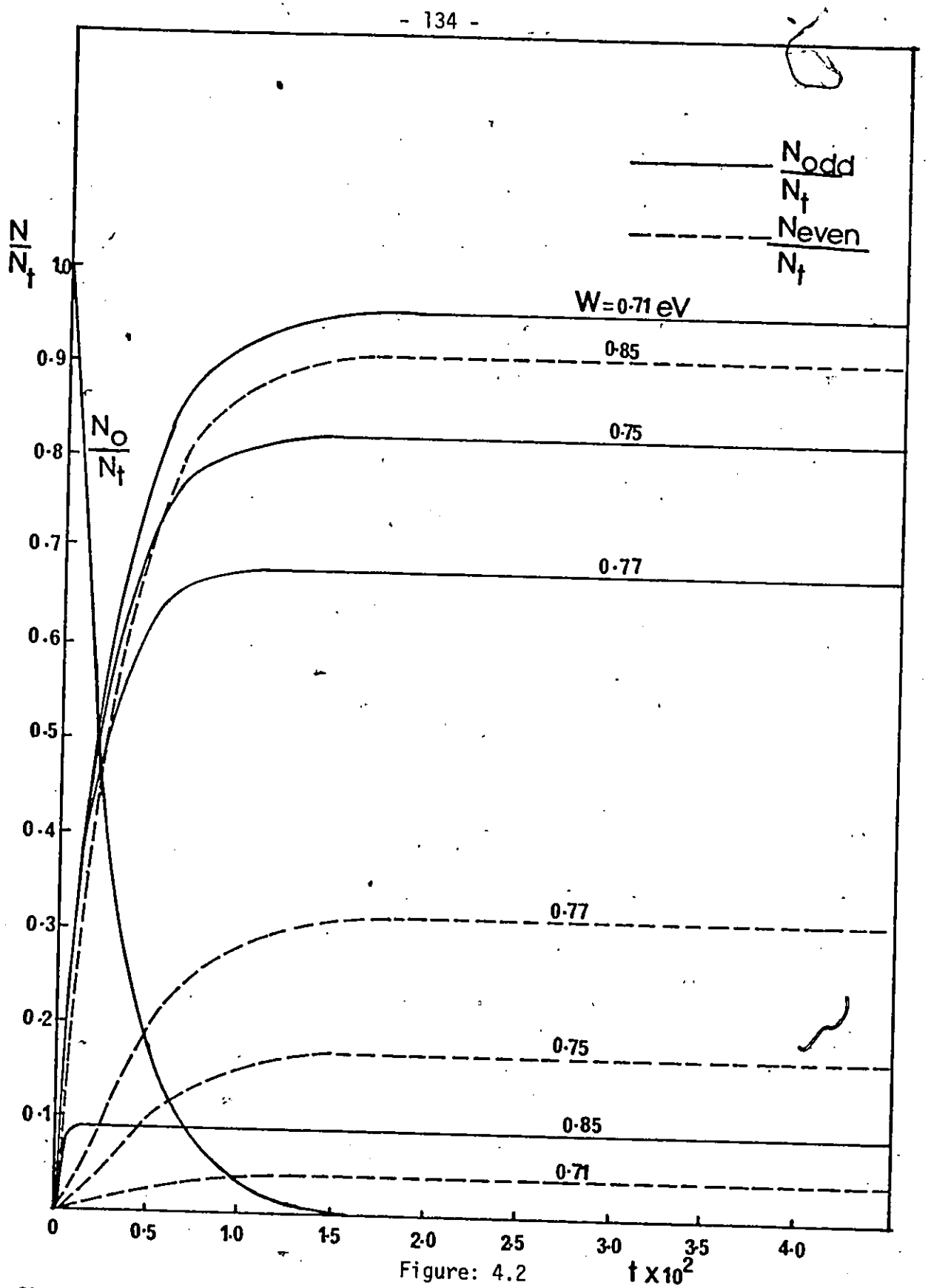

Figure: 4.2

Figure 4.2: The figure shows the variation of the number of crack tips in front of barriers I and II with the mechanical energy and time. The dashed and solid curves represen t the number of crack tips in front of the type II barriers, (N_{even}) and the number of crack tips in front of type I barriers (N_{odd}) respectively. The number on each curve represents the mechanical energy value. The other parameters are |27|; $\Delta G^{\ddagger} = 1.4$ eV, T = 300K and ${}_{II}k^{II} = 350/s$. ${}_{I}k^{I}$ and ${}^{I}k_{II}$ were calculated by using Eqs. 1.22.

Chapter 5

Conclusions

5.1 Crack Distribution in Homogeneous Solids

The non-steady state fracture kinetics analysis for a quasi-rigid crack front (that is double kink nucleation controlled) propagation in semi-infinite plate specimens lead to a crack size distribution function. The analysis shows that the crack size distribution function is controlled by the mechanical energy, temperature, time and the activation free energy of the material. The following are concluded from the analysis.

1. When the rate of bond breaking is less than the rate of bond healing, incipient cracks develop in the specimen to a steady state crack size distribution of a few atomic distances. The existing microcracks may heal back to the same steady state crack size distribution if the physical conditions are favourable. One of these conditions is that there should be no plastic deformation of the crack tip because such deformation may cause geometrical mismatch of the atomic bonds. Another physical condition is that the crack surfaces must be free from chemical contamination.

2. The crack size is normally distributed when the rate of bond breaking is greater than or equal to the rate of bond healing. The shape of the crack size distribution is controlled by the value of $(k^{+}t)$ while the average crack size or the location of the crack tip is controlled by the value of $(k^{-}t)$. When the stress level corresponds to that of the Griffith equilibrium condition, i.e. the rate of bond breaking is equal to the rate of bond healing, the average crack size is $a_x(2k^{+}t)^{\frac{1}{2}}$.

The typical crack size distribution that was predicted in the analysis is in the order of one tenth of a millimeter (10^6Å). In crack propagation velocity measurements, however, a larger scatter is usually observed. Although there could be other factors affecting the crack size distribution, one of the main reasons could be that the cracks probably propagate by the double kink nucleation and sideways spreading mechanism rather than the quasi-rigid crack front (that is double kink nucleation controlled) mechanism that was assumed in the analysis. That the rate constants remain constant during crack propagation may not necessarily be true because the change in crack length usually leads to a change in the stress intensity and hence a change in the rate constants. The structural inhomogeneities, scatter in loading, temperature fluctuations and scatter in the geometry of the crack are some of the possible causes of the observed large scatter in crack propagation experiments.

5.2 The Steady State Fracture Kinetics of Crack Propagation

The steady state fracture kinetics analysis of the double kink nucleation and spreading leads to the kink distribution and crack propagation velocity expressions.

Both are controlled by the applied stress, temperature, the activation energy of the material and the kink spreading distance. The analysis leads to the following conclusions.

1. The kink concentration distribution is determined by the ratio of k_h/k_b (or k^-/k^+), for a given kink spreading distance. The larger the kink spreading distance the smaller is the kink concentration and hence, the steady state flow of kinks. Thus, the crack propagation velocity is inversely proportional to the kink spreading distance.
2. The continuous function description approach and the discrete analysis approach lead to the same kink distribution and crack propagation velocity results when the rate of bond breaking is greater than or equal to the rate of bond healing. It appears that when the rate of bond breaking is less than the rate of bond healing, the residue of the Taylor series is high. In this range, therefore, the first order term approximation in the Taylor expansion is less satisfactory and higher order terms need to be included. For the slow crack growth range (10^{-10} - 10^{-3} m/s) however, this extension is not necessary because the two approaches lead to the same results.
3. In the low temperature range (< 300K), the mechanical energy range (tolerance) corresponding to the slow crack growth range is small.

The observed low tolerance in the low temperature range leads to the conclusion that components operating under low temperature conditions will fail in brittle manner. Stronger materials, however, are more brittle than weaker materials in the low temperature range.

4. In Region I of stress corrosion cracking, the crack propagation velocity is controlled by thermally activated bond breaking and healing of the chemically changed matrix (corroded zone) in front of the crack tip. The crack propagates by double kink nucleation and steady state sideways spreading over a series of identical consecutive energy barriers. When the kink spreading distance is large (approximately greater than 100 atomic distances) the threshold stress intensity (K_{ISCC}) is approximately equal to one half of the activation free energy for the corroded zone in front of the crack tip. Thus, in crack-environment systems, where the threshold effect is observed, the threshold stress intensity can be estimated from the material properties, the crack geometry and the chemical environment.

5.3 Non-Steady State Fracture Kinetics of Stress Corrosion Cracking

Stress corrosion cracking was considered to be controlled by a system of two consecutive free energy barriers. The non-steady state fracture kinetics analysis was used to describe the crack size distribution. The analysis shows that the crack size distribution is controlled by the mechanical energy, temperature, time, the activation free energy for the corroded material in front of the crack tip and by the concentration of the chemical environment. Typical results show that the time needed for the system to reach steady state is in the order of a few hundredths of a second.

Chapter 6

Recommendations for Further Research

6.1 Crack Size Distribution in Homogeneous Solids

In the present analysis, crack propagation in semi-infinite plate specimens was considered. However, in most cases, the plates are of finite size. The present study should, therefore, be extended to describe the crack size distribution in finite plate specimens; say of length L. In addition to the reflecting boundary at $X = 0$ that was discussed in Chapter 2, an absorbing boundary at $X = L$ should be introduced. Together with the absorbing boundary, the change in the rate constants with the crack length [51,64], may be incorporated in the model. It is, however, anticipated that the mathematics involved in the extension will be complicated. Simplifying assumptions may be necessary.

6.2 The Steady State Fracture Kinetics of Crack Propagation

The extension of the analysis of steady state fracture kinetics of crack front spreading to include cyclic loading conditions (fatigue) would lead to results that are applicable to fracture problems in industry. Fatigue failure is caused by the elmentary fracture processes [73], i.e. thermally activated bond breaking and healing processes. The extension of the present work to describe fatigue failure would, therefore, require a functional relationship between the rate constants and time. Further extensions to include corrosion fatigue failure processes would be even more applicable because in most cases fatigue and stress corrosion cracking take place simultaneously.

APPENDICES

Appendix 1

The second term in the R.H.S. of Eq. (2.16) is

$$\frac{C}{2K(\pi Kt)^{\frac{1}{2}}} \int_{X_o}^{\infty} \exp\left[-\frac{(\alpha + X)^2}{4Kt} + \frac{C(\alpha - X_o)}{2K} \right] d\alpha$$

Rewriting the term under the integral sign as

$$\exp -\frac{(X + \alpha - Ct)^2}{4Kt} \exp\left[\frac{Ct}{4K} - \frac{C(X + X_o)}{2K} \right]$$

leads to

$$\frac{C}{2K(\pi Kt)^{\frac{1}{2}}} \exp\left[\frac{Ct}{4K} - \frac{C(X + X_o)}{2K} \right] \int_{X_o}^{\infty} \exp\left[\frac{-(X + \alpha - Ct)^2}{4Kt} \right] d\alpha$$

Transforming the exponential term as,

$$y = \frac{X + \alpha - Ct}{2(Kt)^{\frac{1}{2}}}$$

leads to $dy\ 2(Kt)^{\frac{1}{2}} = d\alpha$

The transformed integral, together with the corresponding integration limits are

$$\frac{C}{K\sqrt{\pi}} \exp\left[\frac{Ct}{4K} - \frac{C(X + X_o)}{2K} \right] \int_{\frac{X+X_o-Ct}{2(Kt)^{\frac{1}{2}}}}^{\infty} \exp(-y^2)\, dy. \qquad \text{A 1.1}$$

Appendix 2

The average crack propagation distance $\bar{X}$ is

$$\bar{X} = \left[\frac{\int_0^\infty X^2\, N(X,t)dx}{\int_0^\infty N(X,t)\, dx}\right]^{\frac{1}{2}} \qquad A\ 2.1$$

From Eq. (2.25)

$$\int_0^\infty X^2\, N(X,t)\, dX = \frac{N_t}{(\pi Kt)^{\frac{1}{2}}} \int_0^\infty X^2 \exp\left(\frac{-X^2}{4Kt}\right) dX,$$ and from the table of standard integrals,

$$= (2Kt)^{\frac{1}{2}}\, N_t$$

Also $$\int_0^\infty N(X,t)\, dX = \frac{N_t}{(\pi Kt)^{\frac{1}{2}}} \int_0^\infty \exp\left(\frac{-X^2}{4Kt}\right) dX.$$

$$= N_t$$

$$\therefore\ \bar{X} = (2Kt)^{\frac{1}{2}} = (2Kt)^{\frac{1}{2}}$$

$$= a_x(2kt)^{\frac{1}{2}} \qquad A\ 2.2$$

Appendix 3

Eq. (2.19) is

$$\frac{N(X,t)}{N_t} = \frac{1}{(\pi Kt)^{\frac{1}{2}}} \exp \frac{-(X + Ct)^2}{4Kt} + \frac{C}{2K} \exp\left(\frac{-Ct}{K}\right) \operatorname{erfc} \frac{(X - Ct)}{2(Kt)^{\frac{1}{2}}}$$

Let $$\frac{1}{(\pi Kt)^{\frac{1}{2}}} \exp - \frac{(X + Ct)^2}{4Kt} = B \qquad \text{A 3.1}$$

and

$$\frac{C}{2K} \exp\left(-\frac{CX}{K}\right) \operatorname{erfc} \frac{(X - Ct)}{2(Kt)^{\frac{1}{2}}} = \alpha$$

The ratio $$\frac{B}{\alpha} = \frac{2}{\sqrt{\pi}} \left(\frac{K}{t}\right)^{\frac{1}{2}} \frac{1}{C} \frac{\exp - \frac{(X + Ct)^2}{4Kt}}{\exp\left(-\frac{CX}{K}\right) \operatorname{erfc} \frac{(X - Ct)}{2\sqrt{Kt}}}$$

Consider the ratio, B/α when $X = - Ct$. So that $X + Ct = 0$

$$\frac{B}{\alpha} = + \frac{2}{\sqrt{\pi}} \left(\frac{K}{t}\right)^{\frac{1}{2}} \frac{1}{C \exp. \frac{C^2 t}{K} . \operatorname{erfc}\left(\frac{-Ct}{\sqrt{Kt}}\right)} \qquad \text{A 3.2}$$

If $Z = C\left(\frac{t}{K}\right)^{\frac{1}{2}}$, then

$$\frac{B}{\alpha} = \frac{2}{\sqrt{\pi}} \frac{1}{Z} \frac{1}{\exp(Z^2) \operatorname{erfc}(-Z)}$$

Let $Z = - Z$, (when $k_b > k_h$, C is - Ve)

$$\frac{B}{\alpha} = - 2 \frac{1}{\sqrt{\pi}} \frac{1}{Z e^{Z^2} \operatorname{erfc}(Z)}$$

as $t >> 0$, $Z >> 0$,

From error Function and Fresnel Integrals (complementary error function table),

$$Ze^{Z^2} \operatorname{erfc} Z = 0.5641896$$

$$\lim \; Z >> 0$$

$$= \frac{1}{\sqrt{\pi}}$$

So that

$$\frac{B}{\alpha} = -2 \quad \text{or} \quad \alpha = -\frac{B}{2} \qquad \text{A 3.3}$$

Hence

$$\frac{N(X,t)}{N_t} = \alpha + B$$

$$= \frac{B}{2}.$$

Thus,

$$\frac{N(X,t)}{N_t} = \frac{1}{2(\pi Kt)^{\frac{1}{2}}} \exp - \frac{(X + Ct)^2}{4Kt} \qquad \text{A 3.4}$$

Appendix 4

Table A 4.1 Typical values of bond energies [69].

Bond	Bond energy $\Delta G_b^{\ddagger}$ (eV)	Bond	Bond energy $\Delta G_b^{\ddagger}$ (eV)
H - H	4.52	C - C	6.247
Si - Si	3.297	Fe - Br	2.56
Li - F	5.965	C - Si	4.51
C - N	7.98	Na - Cl	4.14
Ni - Ni	2.407	Fe - Au	1.95
Cu - Cu	2.01	H - Vinyl	> 4.68
Al - Al	1.735	$(CH_3)_3$ Si - $Si(CH_3)_3$	2.90

Table 4.2 Typical values for free energy of activation for the chemically changed matrix in front of the crack tip (corroded zone).

	Material	Chemical Environment	Free energy of Activation (eV)
1.	Porcelain	Water, at 300K	1.13 [27]
2.	Commercial soda lime silica glass	Octanol at 300K	0.73 [27]
3.	Soda Lime Silicate Glass	Distilled Water	1.13 [66]
4.	Soda-Lime Silicate	Vacuum	6.24 [67]

Table A 4.3 Typical mechanical energy corresponding to different stress intensities.

This table is meant to illustrate how the mechanical energy is related to stress intensity; using Irwin's relation $W = \alpha K_I$

Stress Intensity K_I MN - $m^{-3/2}$	Stress Proportionality factor α, eV/MN - $m^{-3/2}$	Mechanical energy $W = \alpha K_I$ (eV)
0.7	0.78	0.546
0.9	0.78	0.72
0.5	0.75	0.375
0.7	0.75	0.525

The proportionality constant α is obtained experimentally for a given material and crack geometry.

Appendix 5

The number of kinks in front of the first barrier is given by

$$N_1 = F\left(\frac{1}{{}_1k^1} + \frac{{}^1k_2}{{}_1k^1\ {}_2k^2} + \ldots + \frac{{}^1k_2\ {}^2k_3 \ldots\ {}^{i-1}k_i}{{}_1k^1\ {}_2k^2 \ldots\ {}_ik^i} + \frac{{}^1k_2\ {}^2k_3\ \ldots {}^{i-1}k_i\ \ldots {}^{n-1}k_h}{{}_1k^1\ {}_2k^2\ {}_3k^3\ \ldots\ {}_nk^n} \right)$$

Each of the terms in the brackets is a complete rate constant, as illustrated in Fig. A 5.1.

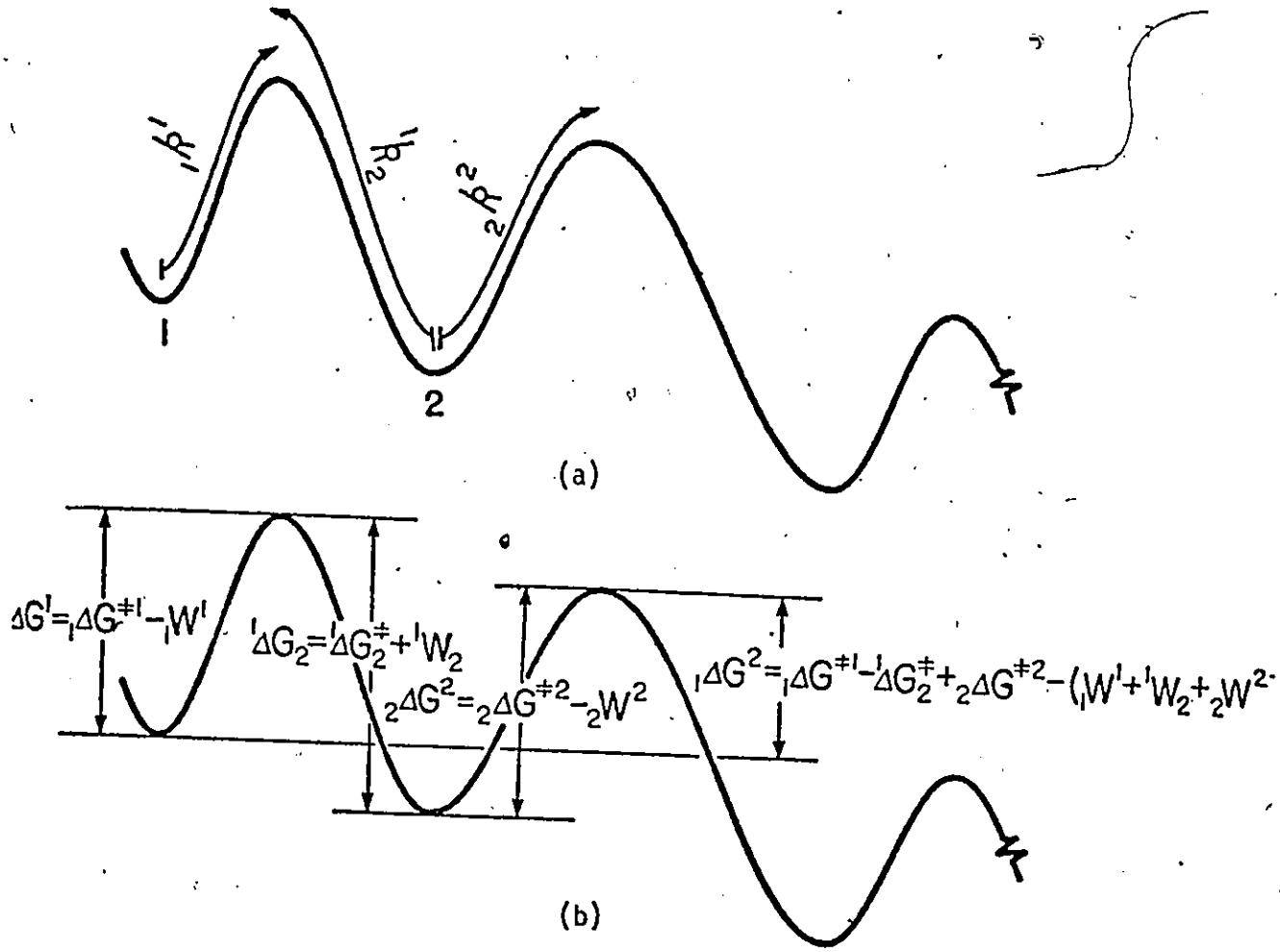

Figure A 5.1 Illustrates the meaning of the complex rate constants.

(a) the rate constants of activation
(b) the apparent free energies of activation and the true free energies.

$$ {}_1\Delta G^1 = {}_1\Delta G^{\ddagger 1} - {}_1W^1(\sigma) $$

$$ {}^1\Delta G_2 = {}^1\Delta G^{\ddagger}{}_2 + {}^1W_2(\sigma) $$

$$ {}_2\Delta G^2 = {}_2\Delta G^{\ddagger 2} - {}_2W^2(\sigma) $$

$$ {}_1\Delta G^2 = {}_1\Delta G^{\ddagger 1} - {}^1\Delta G^{\ddagger}{}_2 + {}_2\Delta G^{\ddagger 2} - ({}_1W^1(\sigma) + {}^1W_2(\sigma) + {}_2W^2(\sigma)) $$

Thus

$$ \frac{{}^1k_2}{{}_1k^2\ {}_2k^2} = \frac{\frac{kT}{h}\exp - \frac{({}^1\Delta G^{\ddagger}{}_2 + {}^1W_2(\sigma)}{kT}}{\frac{kT}{h}\exp\left(-\frac{\Delta G^{\ddagger 1} - {}_1W^1}{kT}\right)\frac{kT}{h}\exp\left(-\frac{{}_2\Delta G^{\ddagger 2} - {}_2W^2}{kT}\right)} $$

$$ = \frac{h}{kT}\exp\left[\frac{({}_1\Delta G^{\ddagger 1} - {}^1\Delta G^{\ddagger}{}_2 + {}_2\Delta G^{\ddagger 2}) - ({}_1W^1 + {}^1W_2 + {}_2W^2)}{kT}\right] $$

$$ = \frac{h}{kT}\exp\left(\frac{{}_1\Delta G^2}{kT}\right) = \frac{1}{{}_1k^2} $$

where for convenience $W(\sigma) = W$ was written and the symbol ${}_1\Delta G^2$ was introduced to indicate the apparent activation energy from the first valley to the top of the second barrier.

Appendix 6

The expression $\frac{1}{{}_{i}k^{i+j}}$ can be written as

$$\frac{1}{{}_{i}k^{i+j}} = \frac{{}_{i}k_{i+1}\ {}_{i+1}k_{i+2} \cdots {}_{i+j-1}k_{i+j}}{{}_{i}k^{i}\ {}_{i+1}k^{i+1} \cdots {}_{i+j}k^{i+j}}$$

$$= \frac{\exp - \frac{{}_{i}\Delta G^{\ddagger}_{i+1} + {}_{i+1}\Delta G^{\ddagger}_{i+2} + \ldots + {}_{i\ j-1}\Delta G^{\ddagger}_{i+j} + ({}_{i}W_{i+1} + {}_{i+1}W_{i+2} + \ldots + {}_{i+j}W_{i+j})}{kT}}{\frac{kT}{h} \cdot \exp - \frac{({}_{i}\Delta G^{\ddagger i} + {}_{i+1}\Delta G^{\ddagger i+1} \ldots + {}_{i+j}\Delta G^{\ddagger i+j}) - ({}_{i}W^{i} + {}_{i+1}W^{i+j} + \ldots + {}_{i+j}W^{i+j})}{kT}}$$

An approximation is made that [28]

$${}_{i}\Delta G^{\ddagger}_{i+1} = {}^{1}\Delta G^{\ddagger}_{2} = \ldots = 0$$

$${}_{i}\Delta G^{\ddagger i} = {}_{i+1}\Delta G^{\ddagger i+1} = \ldots = \Delta G^{\ddagger}_{b}$$

and

$${}_{i}W^{i} = {}_{i+1}W^{i+1} = {}^{i}W_{i+1} = {}^{dk}W_{1} = W. \quad \text{so that}$$

$$\frac{1}{{}_{i}k^{i+j}} = \frac{h}{kT} \exp \frac{(j+1)\ \Delta G^{\ddagger}_{b} - (2j+1)W}{kT}$$

$$= \frac{h}{kT} \exp \frac{\Delta G^{\ddagger} - W}{kT} \quad \exp \frac{(\Delta G^{\ddagger} - 2W)j}{kT}$$

$$= \left(\frac{k_h}{k_b} \right)^{j} \quad \frac{1}{k_b}$$

Appendix 7

Eq. (3.16) is

$$\frac{a_y N}{N_t} = \frac{1 - \left(\frac{k_h}{k_b}\right)^{n+1-i}}{\frac{k_h}{k_b}\left[\frac{1 - \left(\frac{k_h}{k_b}\right)^{n}}{1 - \frac{k_h}{k_b}}\right]\left[\frac{h\bar{k}}{kT} - 1\right] + n + \frac{h\bar{k}}{kT}}$$

which can be written as

$$\frac{a_y N}{N_t} = \frac{\left[1 - \left(\frac{k_h}{k_b}\right)^{n+1-i}\right](1 - \frac{k_h}{k_b})}{\frac{k_h}{k_b}\left[1 - \left(\frac{k_h}{k_b}\right)^{n}\right]\left[\frac{h\bar{k}}{kT} - 1\right] + (n + \frac{h\bar{k}}{kT})(1 - \frac{k_h}{k_b})}$$

The numerator can be written in series form as ($k_h/k_b = \exp(\Delta G^{\ddagger} - 2W)/kT$)

$$\left[1 - 1 - (n+1-i)\frac{(\Delta G^{\ddagger} - 2W)}{kT} - \frac{(n+1-i)^2}{2}\left(\frac{\Delta G^{\ddagger} - 2W)^2}{kT} - \ldots\right]\right] x$$

$$\left[1 - 1 - \frac{\Delta G^{\ddagger} - 2W}{kT} - \frac{1}{2}\left(\frac{\Delta G^{\ddagger} - 2W)^2}{kT} - \ldots\right]\right]$$

$$= (n+1-i)\left(\frac{\Delta G^{\ddagger} - 2W}{kT}\right)^2 + \frac{(n+1-i)^2}{2}\left(\frac{\Delta G^{\ddagger} - 2W}{kT}\right)^3 + \ldots$$

Because $\frac{h\bar{k}}{kT} \ll 1$ when $W \to \Delta G^{\ddagger}/2$, the first term in the denominator can be written in series form as

$$\left[1 + \frac{\Delta G^{\ddagger} - 2W}{kT} + \frac{1}{2}\left(\frac{\Delta G^{\ddagger} - 2W}{kT}\right) + \ldots\right]\left[n\frac{\Delta G^{\ddagger} - 2W}{kT} + \frac{n^2}{2}\left(\frac{\Delta G^{\ddagger} - 2W}{kT}\right)^2 + \ldots\right]$$

$$= n \frac{\Delta G^{\ddagger} - 2W}{kT} + \frac{n^2 + 2n}{2} \left(\frac{\Delta G^{\ddagger} - 2W}{kT} \right) + \frac{n + n^2}{2} \left(\frac{\Delta G^{\ddagger} - 2W}{kT} \right)^3 + \ldots \qquad \text{A 7.2}$$

and the second term in the denominator can be written in series form as

$$n \left[- \frac{\Delta G^{\ddagger} - 2W}{kT} - \left(\frac{\Delta G^{\ddagger} - 2W}{kT} \right)^2 \frac{1}{2} - \frac{1}{6} \left(\frac{\Delta G^{\ddagger} - 2W}{kT} \right)^3 - \ldots \right] \qquad \text{A 7.3}$$

Combining Eqs. A 7.1, A 7.2 and A 7.3 for the denominator and numerator terms of Eq. (3.16) we get

$$\frac{a_y N}{N_t} = \frac{(n+1-i) \left(\frac{\Delta G^{\ddagger} - 2W}{kT} \right)^2 + \frac{(n+1-i)^2}{2} \left(\frac{\Delta G^{\ddagger} - 2W}{kT} \right)^3 + \ldots}{\left(\frac{\Delta G^{\ddagger} - 2W}{kT} \right)^2 \left(\frac{n + n^2}{2} \right) + \frac{2n + 3n^2}{6} \left(\frac{\Delta G^{\ddagger} - 2W}{kT} \right)^3 + \ldots}$$

$$= \frac{n+1-i + \frac{(n+1-i)^2}{2} \left(\frac{\Delta G^{\dagger} - 2W}{kT} \right) + \ldots}{\frac{n + n^2}{2} + \frac{2n + 3n^2}{6} \left(\frac{\Delta G^{\dagger} - 2W}{kT} \right) + \ldots} \qquad \text{A 7.4}$$

When $W \to \Delta G^{\ddagger}/2$, $\Delta G^{\ddagger} - 2W \to 0$, thus

$$\frac{a_y N}{N_t} = 2 \frac{(n+1-i)}{n+n^2} = \frac{2}{n} \left[1 - \frac{i}{n+1} \right] \qquad \text{A 7.5}$$

Appendix 8

Eq. (3.33) can be written as

$$v_x = \frac{\frac{kT}{h} \cdot a_x}{1 + \left(\frac{k_h}{k_b}\right)^n \frac{1 - \left(\frac{k_h}{k_b}\right)}{1 - \frac{k_h}{k_b}} + \frac{\exp\left(\frac{(\Delta G^{\ddagger} - W)}{kT}\right)}{1 - \frac{k_h}{k_b}} \cdot n - \frac{k_h}{k_b} \cdot \frac{1 - \left(\frac{k_h}{k_b}\right)^n}{1 - \frac{k_h}{k_b}}}$$

The second term in the denominator can be written in series form as

$$\left[1 + \frac{\Delta G^{\ddagger} - 2W}{kT} + \frac{1}{2!}\left(\frac{\Delta G^{\ddagger} - 2W}{kT}\right)^2 + \cdots\right]\left[\frac{n\frac{\Delta G^{\ddagger} - 2W}{kT} + n^2\left(\frac{\Delta G^{\ddagger} - 2W}{kT}\right) + \cdots}{\frac{\Delta G^{\ddagger} - 2W}{kT} + n^2\left(\frac{\Delta G^{\ddagger} - 2W}{kT}\right) + \cdots}\right]$$

$= n$ when $2W \to \Delta G^{\ddagger}$ A 8.1

Similarly, the third term in the denominator can be written in series form as

$$\left[\frac{\exp\left(\frac{\Delta G^{\ddagger} - W}{kT}\right)}{\frac{k_h}{k_b} - 1}\right]\left[\frac{\frac{n+n^2}{2}\left(\frac{\Delta G^{\ddagger} - 2W}{kT}\right) + \frac{n}{2}\frac{\Delta G^{\ddagger} - 2W}{kT}}{1 + \frac{1}{2}\left(\frac{\Delta G^{\ddagger} - 2W}{kT}\right) + \cdots}\right]$$

$$= \frac{\frac{n+n^2}{2} + \frac{n+n^2}{2}\left(\frac{\Delta G^{\ddagger} - 2W}{kT}\right)}{1 + \frac{1}{2}\frac{\Delta G^{\ddagger} - 2W}{kT} + \cdots} \exp\frac{\Delta G^{\ddagger} - W}{kT}$$

as $2W \to \Delta G^{\ddagger}$,

$$= \frac{n+n^2}{2}\exp\left(\frac{\Delta G^{\ddagger} - W}{kT}\right) \quad \text{A 8.2}$$

Combining Eqs. A 8.1 and A 8.2 for the denominator of Eq. (3.33), the crack propagation velocity when $W \to \frac{\Delta G^{\ddagger}}{2}$ is

$$v_x = \frac{\frac{a_x kT}{h}}{1+n+\frac{n+n^2}{2}\exp((\Delta G^{\ddagger} - W)/kT)}$$

Because $(1 + n) \exp - \left(\frac{\Delta G^{\ddagger} - W}{kT} \right) << \frac{n+n^2}{2}$

and $\frac{n(1+n)}{2} \approx \frac{n^2}{2}$, the crack propagation velocity is

$$v_x = \frac{2a_x k}{n^2}, \qquad \text{A 8.3}$$

Appendix 9

Non-Linear Least-Square Curve Fitting

Experimental data for the Region I of stress corrosion cracking of porcelain in water environment was obtained by Evans and Linza |60|. The activation parameters were obtained by fitting the crack propagation velocity equation 3.33 to the data. A Fortran program was written to fit equation 3.33 to the data. The basic subroutine of this program includes an algorithm whose function is to estimate the activation parameters so that the residual sum of the squares is minimized, in the usual least square sense. This subroutine is Z X SSQ and is part of a commercial software package known as IMSL |68|. The following was the Fortran program and the output parameters. Other computer programs that were used in the thesis are also included.

```
      COMPILER OPTIONS - NAME=  MAIN,OPT=02,LINECNT=64,SIZE=0000K,
                         SOURCE,EBCDIC,NOLIST,NODECK,LOAD,MAP,NOEDIT,ID,NCXREF
ISN 0002              EXTERNAL FUNC
ISN 0003              DIMENSION X(4),F(19),XJAC(19,4),XJTJ(10),WORK(68)
ISN 0004              COMMON/PSQ/Y(19),ST(19)
ISN 0005              REAL K
ISN 0006              K=8.6164E-05
ISN 0007              TEMP=300.0
ISN 0008              B=1.9
ISN 0009              N=4
ISN 0010              IXJAC=19
ISN 0011              NSIG=3
ISN 0012              EPS=0.0
ISN 0013              DELTA=0.0
ISN 0014              MAXFN=4000
ISN 0015              IOPT=0
ISN 0016              B=1/(K*TEMP)
ISN 0017              X(1)=EXP(1.05/(K*TEMP))
ISN 0018              X(2)=0.78
ISN 0019              X(3)=200
ISN 0020              X(4)=200*B*1.05
ISN 0021              DO 20 I=1,19
ISN 0022           40 FORMAT (E16.3,4X,E16.3)
ISN 0023              READ(5,40) V,SK
ISN 0024              ST(I)=SK
ISN 0025              Y(I)=V
ISN 0026           20 CONTINUE
ISN 0027              CALL ZXSSQ(FUNC,M,N,NSIG,EPS,DELTA,MAXFN,IOPT,PARM,X,SSQ,F,XJAC,IX
                     9JAC,XJTJ,WORK,INFER,IER)
ISN 0028              GBR=(ALOG(X(1)))*K*TEMP
ISN 0029              RG=(X(4)/X(3))*1/B
ISN 0030              PRINT 69,RG
ISN 0031           69 FORMAT ('1',6X,F6.3)
ISN 0032              ALPHA=X(2)*B
ISN 0033              NI=IFIX(X(3))
ISN 0034              PRINT 71
ISN 0035              PRINT 72,GBR
ISN 0036              PRINT 73,ALPHA
ISN 0037              PRINT 74,X(3)
ISN 0038              PRINT 75,SSQ
ISN 0039              PRINT 76,IER
ISN 0040              PRINT 77,INFER
ISN 0041           77 FORMAT('0',6X,'CONVERGENCE CRITERIA IS',I3)
ISN 0042           71 FORMAT('1',20X,'OUTPUT PARAMETERS')
ISN 0043           72 FORMAT('0',6X,'FREE ENERGY OF ACTIVATION IS',F6.3,2X,'EV')
ISN 0044           73 FORMAT('0',6X,'STRESS CON. ALPHA/(K*TEMP)IS',F6.3,2X,'M**1.5/MN')
ISN 0045           74 FORMAT('0',6X,'KINK SPREADING DISTANCE L/2*A IS',F7.2)
ISN 0046           75 FORMAT('0',6X,'SUM OF RESIDUAL SQUARES IS',E12.4)
ISN 0047           76 FORMAT('0',6X,'ERROR PARAMETER IS',I3)
ISN 0048              STOP
ISN 0049              END
```

```
      COMPILER OPTIONS - NAME=  MAIN,OPT=02,LINECNT=64,SIZE=0000K,
                         SOURCE,EBCDIC,NOLIST,NODECK,LOAD,MAP,NOEDIT,ID,NOXREF
ISN 0002              SUBROUTINE FUNC (X,M,N,F)
ISN 0003              DIMENSION TA(19),TB(19),TD(19)
ISN 0004              DIMENSION X(N),F(M)
ISN 0005              COMMON/PSQ/Y(19),ST(19)
ISN 0006              REAL K
ISN 0007              K=8.6164E-05
ISN 0008              RT=0.2084E11
ISN 0009              TEMP=300.0
ISN 0010              B=1/(K*TEMP)
ISN 0011              A=RT*(0.2E-09)*TEMP
ISN 0012              DO 5  I=1,M
ISN 0013              TA(I)=X(1)*EXP((-2*B*X(2)*ST(I)))
ISN 0014              TB(I)=X(1)*(EXP(-B*X(2)*ST(I)))/(TA(I)-1.0)
ISN 0015              TH=X(4)-2*X(3)*B*X(2)*ST(I)
ISN 0016              IF (TH.LT.-174) GO TO 7
ISN 0018              TD(I)=EXP(X(4)-2*X(3)*X(2)*B*ST(I))
ISN 0019              F(I)=Y(I)-A/(1.0+TA(I)*(1.0-TD(I))/(1.0-TA(I))+TB(I)*(TA(I)*(1.0-
                     2TD(I))/(1.0-TA(I)))-TB(I)*X(3))
ISN 0020              GO TO 5
ISN 0021            7 CONTINUE
ISN 0022              F(I)=Y(I)-A/(1.0+TA(I)/(1.0-TA(I))+TB(I)*TA(I)/(1.0-TA(I))-X(3)*
                     1TB(I))
ISN 0023            5 CONTINUE
ISN 0024              RETURN
ISN 0025              END
```

OUTPUT PARAMETERS

FREE ENERGY OF ACTIVATION IS 1.050 EV

STRESS CON. ALPHA/(K*TEMP)IS30.152 M**1.5/MN

KINK SPREADING DISTANCE L/2*A IS 200.00

SUM OF RESIDUAL SQUARES IS 0.2510E-08

ERROR PARAMETER IS 0

CONVERGENCE CRITERIA IS 1

```
      $JOB  SH872541,MSHANA,PAGES=60,TIME=20
C     THIS IS A PROGRAM FOR CALCULATING THE CRACK SIZE DISTRIBUTION
C
      REAL KB
      REAL KP
      REAL KM
      REAL K
      K=8.6164E-5
      RT=0.2084E 11                                                    07
      A=2.35E-8                                                        04
      GBR=1.0
      W=0.49
       TEMP=200.0
   17 CONTINUE
      GM=W
      GB=GBR-W
   10 KB=RT*TEMP*(EXP((-GB)/(K*TEMP)))                                 10
      KM=RT*TEMP*(EXP((-GM)/(K*TEMP)))
C     CALCULATE THE CRACK PROPAGATION CONSTANT  KP                     11
      V=KM-KB
      KP=(KB+KM)/2.0
      PRINT 9                                                          14
       T=0.1E-7
   14 CONTINUE
C     PRINT THE VALUES OF  TEMP, , KB, KP, TIME, AND TITLES            13
    9 FORMAT (15X,'THERMALLY  ACTIVATED  CRACK  PROPAGATION')          15
    8 PRINT 11,TEMP,KB,KM,KP,V,T
      VE=V*T
   11 FORMAT (' ',' TEMP=',F6.2,' ','KB=',E12.5,' ','KM=',E12.5,' ','KP=
     8,E12.5,' ','V=',E12.5,' ','TIME=',E12.4,'SECS')
       VE=-0.20E08
   70 CONTINUE
      PRINT 12                                                         22
   12 FORMAT (' ',2X,'CRACK SIZE      ',4X,'CRACK SIZE DISTRIB.')
C                                                                      20
C                                                                      21
C                                                                      24
C     CALCULATE CRACK SIZE DISTRIBUTION 'P'                            25
      C=1.0/((3.142*KP*T)**0.5)
      X=0.0
   13 CONTINUE
      QD=((X+V*T)**2)/(4.0*KP*T)
      IF (QD.GT.174) GO TO 100
      QE=(X-V*T)/(2.0*((KP*T)**0.5))
      IF (QE.LE.-13) GO TO 101
       QN=V*X/KP
       IF (QN.GT.174) GO TO 59
       P=C*EXP(-QD)+(V/(2.0*KP))*EXP(-QN)*ERFC(QE)
       GO TO 57
   59 CONTINUE
      P=C*EXP(-QD)
       GO TO 57
  101 CONTINUE
      QM=V*X/KP
      IF (QM.GT.174) GO TO 61
      P=C*EXP(-QD)+(V/KP)*EXP(-QM)
       GO TO 57
   61 CONTINUE
      P=C*EXP(-QD)
       GO TO 57
```

```
      100 CONTINUE
          QL=V*X/KP
          IF (QL.GT.174) GO TO 58
          QF=(X-V*T)/(2.0*((KP*T)**0.5))
           IF (QF.LT.-13) GO TO 102
           IF (QF.GT.13) GO TO 58
          P= (V/(2.0*KP))*(EXP(-V*X/KP))*ERFC(QF)
          GO TO 57
      102 CONTINUE
          QG=V*X/KP
          IF (QG.GT.174) GO TO 58
           P=(V/KP)*EXP(-V*X/KP)
       57 CONTINUE
           PRINT 15,X,P
          IF (P.LT.0.1E-4) GO TO 58
       15 FORMAT (' ',6X,E15.6,6X,E15.6)
          X=X+1
           GO TO 13
       58 CONTINUE
           T=T*10
           IF (T.LE.0.1E07) GO TO 14
          TEMP=TEMP+100
          IF (TEMP.LE.400) GO TO 17
           R=0.05
      201 CONTINUE
          PRINT 202,R
      202 FORMAT (' ',6X,'RATIO EQUALS ',F12.4)
           X=0
      200 CONTINUE
           P=2.0*R*EXP(-2*R*X)
           PRINT 203,X,P
      203 FORMAT (' ',6X,F12.4,6X,E15.4)
           IF (P.LT.0.1E-4) GO TO 204
          X=X+2
          GO TO 200
      204 CONTINUE
           R=R+0.05
          IF (R.LE.0.4) GO TO 201
          STOP
          END
```

```
$JOB  SH872541,MSHANA,PAGES=60,TIME=60
C     THIS IS A PROGRAM FOR CALCULATING THE KINK DISTRIBUTION USING
C     CONTINUOUS FUNCTION DESCRIPTION APPROACH
      REAL K,KB,KM
      K=8.6164E-05
      RT=0.2084E11
       GBR=1.0
       RN=50
  104 CONTINUE
      TEMP=300.0
      PRINT 30
   30 FORMAT (' ',20X,'CRACK SIZE DISTRIBUTION')
   14 CONTINUE
      PRINT 31,TEMP,GBR
   31 FORMAT (' ',10X,'TEMP=',F10.3,6X,'BOND ENERGY=',F10.3)
      PRINT 32
   32 FORMAT (' ',6X,'CRACK SIZE',10X,'CONCENTRATION',10X,'LOG CONC',6X,
     1'MECH. ENERGY')
       W=0.49
   12 CONTINUE
      GM=W/(K*TEMP)
      GB=(GBR-W)/(K*TEMP)
      VO=RT*TEMP
        KM=VO*EXP(-GM)
        KB=VO*EXP(-GB)
      RM=KM/KB
        VY=KB-KM
        VP=KB+KM
       R=2*VY/VP
       X=0
   13 CONTINUE
       IF (W.EQ.GBR/2) GO TO 50
      IF (R.LT.0.0) GO TO 40
         CONTINUE
      IF (R.EQ.0.0) GO TO 50
         CONTINUE
      RA=1.0/(RN*R)
      T=RN*R
       IF (T.GT.174) GO TO 61
       TB=R*(X-RN)
       IF (TB.LT.-174.0) GO TO 62
         TA=EXP(TB)
       T=-T
        TN=(1.0-TA)/(RN*(1.0-RA*(1.0-EXP(T))))
      TN=TN*RN
       GO TO 80
   62 CONTINUE
       T=-T
       TN=1.0/(RN*(1.0-RA*(1.0-EXP(T))))
       TN=TN*RN
      GO TO 80
   61 CONTINUE
         TB=R*(X-RN)
       IF (TB.LT.-174.0) GO TO 63
       TN=(1.0-EXP(TB))/(RN*(1.0-RA))
        TN=TN*RN
       GO TO 80
   63 CONTINUE
         TN=1.0/(RN*(1.0-RA))
        TN=TN*RN
```

```
      GO TO 80
   50 CONTINUE
   40 CONTINUE
      T=-RN*R
      IF (T.GT.174) GO TO 20
      TB=R*(X-RN)
      RA=1.0/(RN*R)
      IF (TB.GT.174.0)GO TO 21
      TN=(1.0-EXP(TB))/(RN*(1.0-RA*(1.0-EXP(T))))
      TN=TN*RA
      GO TO 80
   20 CONTINUE
      TN=-R*RN*EXP(R*X)
   80 CONTINUE
      TN=TN/RN
      TL=ALOG(TN)
      PRINT 70,X,TN,TL,W
   70 FORMAT(' ',8X,F10.3,9X,E15.4,7X,E15.4,5X,F10.3)
   21 X=X+2
      IF (X.LT.RN) GO TO 13
      W=W+0.05
      IF (W.LE.0.54) GO TO 12
      TEMP=TEMP+100.0
      IF (TEMP.LE.600.0) GO TO 14
      RN=RN+50
      IF (RN.LE.100) GO TO 104
      STOP
      END
```

```
$JOB   SH872541,MSHANA,PAGES=60,TIME=60,NOWARN
C      THIS IS A PROGRAM FOR CALCULATING  THE KINK DISTRIBUTION AND THE
C      CRACK VELOCITY USING THE DISCRETE ANALYSIS
       REAL K
       REAL KP
       REAL KB
       REAL KI
       REAL KM
       RT=0.2084E11
       K=8.6164E-5
       A=2.35E-8
        GBR=1.0
       GO TO 32
       CONTINUE
       RN=50
  200  CONTINUE
        TEMP=300
  205  CONTINUE
        PRINT 201,TEMP,RN
  201  FORMAT (' ',10X,'TEMP=',F15.4,10X,'KINK LENGTH=',F10.3)
       W=0.505
   12  CONTINUE
       ALPHA=0.78
   21  CONTINUE
       GM=W
       GB=GBR-W
   10  KB=RT*TEMP*(EXP((-GB)/(K*TEMP)))
       KM=RT*TEMP*(EXP((-GM)/(K*TEMP)))
       RM=KM/KB
       F=(GBR-2*W)/(2*K*TEMP)
       VY=KB-KM
       VP=KB+KM
       R=2*(KB-KM)/(KB+KM)
       GBD=GBR-2*W
        X=0
   13  CONTINUE
        XA=(RN-X)
       S=-2*RN*VY/VP
        Q=XA*(GBR-2*W)/(K*TEMP)
        IF (W.EQ.GBR/2) GO TO 100
       IF (Q.GT.170) GO TO 11
       IF (Q.LT.-170) GO TO 41
        QE=(RN-1)*(GBR-2*W)/(K*TEMP)
        IF (QE.LE.-174) GO TO 101
       CONTINUE
        IF (QE.GT.174) GO TO 300
        FC=RM*(1.0-RM**(RN-1))/(1.0-RM)
        DQ=RN*(1.0-RM**(RN-X))/(RN-1.0-FC)
       DM=ALOG(DQ)
         GO TO 42
  101  CONTINUE
        FC=RM/(1.0-RM)
       DQ=RN*(1.0-RM**(RN-X))/(RN-1.0-FC)
       DM=ALOG(DQ)
       GO TO 42
   41  CONTINUE
        QF=(RN-1.0)*(GBR-2*W)/(K*TEMP)
        IF (QF.LE.-174) GO TO 102
        FC=RM*(1.0-RM**(RN-1))/(1.0-RM)
        DQ=RN/(RN-1.0-FC)
```

```
      DM=ALOG(DQ)
       GO TO 42
  102 CONTINUE
       FC=RM*1.0/(1.0-RM)
       DG=RN/(RN-1.0-FC)
      DM=ALOG(DQ)
       GO TO 42
  100 CONTINUE
      DQ=2.0*(1.00-X/RN)
       DM=ALOG(DQ)
   42 CONTINUE
       DG=DQ/RN
       DM=ALOG(DQ)
      PRINT 17,X,DQ,DM,W
   17 FORMAT(' ',4X,F15.4,6X,E15.5,6X,E15.5,6X,F15.4)
   11 X=X+2
       IF (X.LT.RN) GO TO 13
  300 CONTINUE
       W=W+0.05
      IF (W.LE.0.505) GO TO 12
      RN=RN+50
       IF (RN.LE.100) GO TO 200
   32 CONTINUE
      GBR=1.05
      RN=201
  120 CONTINUE
      RN=RN-1
      TEMP=300.0
  110 CONTINUE
       PRINT 19,TEMP,RN
   19 FORMAT (' ',6X,'TEMP=',F15.5,6X,'KINK LENGTH=',F15.5)
      ALPHA=(3.015E-05)*K*TEMP
      ST=0.65E06
   31 CONTINUE
      W=ST*ALPHA
      GBD=GBR-2*W
      GB=GBR-W
      GBA=GB/(K*TEMP)
      IF (GBA.GT.10) GO TO 50
      PRINT 51,W
   61 FORMAT (' ','GBA=',F15.5)
   50 CONTINUE
      DB=EXP(-W/(K*TEMP))
       PQ=GBD/(K*TEMP)
       IF (PQ.GE.174) GO TO 33
      DG=EXP((GBD)/(K*TEMP))
      DC=EXP((GB)/(K*TEMP))
      DK=RT*TEMP
      DH=DC/(DG-1)
      DL=(DC/(DG-1))*RN
      DZ=DG/(1-DG)
      QA=(RN*GBD)/(K*TEMP)
      IF (QA.GT.170) GO TO 33
      IF (QA.LT.-170) GO TO 35
      QB=(GB+GBD*(1+RN))/(K*TEMP)
      IF (QB.GT.170) GO TO 33
      DE=EXP((RN*GBD)/(K*TEMP))
      DF=DB*DC*(1-DE)/(1-DG)
      DJ=(DC/(DG-1))*(DG*(DE-1)/(DG-1))
      VX=DK/(1+DF+DJ-DL)
```

```
      VX=(2E-10)*VX
      VM=ALOG(VX)
      GO TO 36
   35 CONTINUE
      VX=DK/(1+DZ*(1+DH)-DL)
      VX=(2E-10)*VX
      VM=ALOG(VX)
   36 CONTINUE
        IF (VX.GE.0.01) GO TO 52
      PRINT 18,VX,VM,ST
   18 FORMAT (' ',6X,E15.5,6X,E15.5,6X,E15.5)
   33 ST=ST+0.01E06
      IF (ST.LE.1.0E06) GO TO 31
   52 CONTINUE
      GO TO 202
      CONTINUE
      TEMP=TEMP+100
      IF (TEMP.LE.1500) GO TO 110
C       RN=RN+51
  202 CONTINUE
      STOP
      END
```

```
$JOB  SH872541,MSHANA,PAGES=60,TIME=20
C     THIS IS A  PROGRAM FOR CALCULATING THE NON STEADY STATE CRACK SIZE
C     DISTRIBUTION IN STRESS CORROSION CRACKING
      REAL KB,KM,K,KP
      K=8.6164E-05
      RT=0.2084E11
      A=2.35E-08
      GBR=1.4
      TEMP=300.0
      VO=RT*TEMP
   16 CONTINUE
   51 FORMAT (' ',6X,'TEMP=',F12.4)
      PRINT 51,TEMP
      W=0.75
   15 CONTINUE
      GM=W/(K*TEMP)
      GB=(GBR-W)/(K*TEMP)
      KB=VO*EXP(-GB)
      KM=VO*EXP(-GM)
      VA=350.0
      BK=VA
      RK=0.0
      B=-(3*BK+2*KM+2*RK+2*KB)/2.0
      CK=(KM*KB+3*BK*RK+3*KB*BK+BK**2-RK**2-KB*RK)/2.0
      ALMJ=KM+KB+BK
      ALMEI=BK
      PRINT 600,ALMEI,ALMJ
  600 FORMAT (' ',6X,'FIRST ROOT=',E15.4,6X,'SECOND ROOT=',E15.4)
      ALPHA=0
      TM=(2.0*KM+BK-2.0*RK-2.0*KB-2.0*ALPHA)/(4.0*(RK+KB))
      TB=-(1.0+KB/KM)
      TN=KB/(KB+KM)
      PRINT 110,TB,TM,TN
  110 FORMAT (' ',3X,'TB=',E15.4,3X,'TM=',E15.4,3X,'TN=',E15.4)
      H=(BK+KM+(KM**2)/KB+KM*BK/KB)/((1.0+KM/KB+BK/KB)*(KB+KM))
      DL=-KB/(KB+KM)
      P=KB/(BK+KM+KB)
      F=-KM/(KB+KM)
      G=-(KB*BK)/((KB+KM)*(KM+KB+BK))
      PRINT 1000,W
 1000 FORMAT (' ',6X,'MECH. ENERGY=',F10.3)
      T=0
  108 CONTINUE
      TK=ALMEI*T
      TJ=ALMJ*T
      IF (TJ.GT.174) GO TO 100
      IF (TK.GT.174) GO TO 101
      PB=DL*EXP(-TK)-G*EXP(-TJ)+P
      PA=F*EXP(-TK)+G*EXP(-TJ)+H
      TO=EXP(-TK)
      GO TO 106
  101 CONTINUE
      TO=0.0
      PB=-G*EXP(-TJ)+P
      PA=G*EXP(-TJ)+H
      GO TO 106
  100 CONTINUE
      TO=EXP(-TK)
      PB=DL*EXP(-TK)+P
      PA=F*EXP(-TK)+H
```

```
      106 CONTINUE
          PRINT 107,T,PA,PB,TO
           IF (PB.EQ.P) GO TO 109
      107 FORMAT (' ',6X,E15.4,3X,E15.4,3X,E15.4,3X,E15.4)
           T=T+0.001
          GO TO 108
      109 CONTINUE
          W=W+0.02
           IF (W.LE.0.9) GO TO 15
          T=0.0
          R=2.0*(KB+KM)
          PRINT 10,R
       10 FORMAT (' ',10X,'RATIO=',F15.4)
       70 FORMAT (' ',6X,E15.4,6X,F12.4,6X,F12.4)
       14 CONTINUE
           QA=R*T
          IF (QA.GT.174) GO TO 30
          PI=0.50*(EXP(-QA)-1.0)+1.0
          PJ=0.50*(1.0-EXP(-QA))
          PRINT 70,T,PI,PJ
           IF (PJ.EQ.0.500) GO TO 30
          T=T+0.1E-04
           GO TO 14
       30 CONTINUE
          STOP
          END
```

```
$ENTRY
```

Appendix 10

The comparison between the kink distribution calculation results obtained from the discrete and the differential equation analysis is shown in the following tables. The corresponding curves were shown in Figures 3.2(a) and 3.2(c).

Table A 10.1, W = 0.49 eV

Kink length $(\frac{y}{a_y})$	Discrete analysis $(\frac{aN}{N_t})$	Differential Equation analysis $(\frac{aN}{N_t})$
0	0.11678 E 01	0.7373 E 00
2	0.2485 E 00	0.1687 E 00
4	0.5288 E-01	0.3862 E-01
6	0.11253 E-01	0.8839 E-02
8	0.23945 E-02	0.2023 E-02
10	0.50954 E-03	0.4630 E-03
12	0.10843 E-03	0.1060 E-03
14	0.23073 E-04	0.2426 E-04
16	0.49099 E-05	0.5551 E-05
18	0.10448 E-05	0.1271 E-05
20	0.22233 E-06	0.2908 E-06
22	0.47310 E-07	0.6656 E-07
24	0.10067 E-07	0.1523 E-07
26	0.21423 E-08	0.3486 E-08
28	0.45587 E-09	0.7979 E-09
30	0.97008 E-10	0.1826 E-09
32	0.20643 E-10	0.4180 E-10
34	0.43927 E-11	0.9567 E-11
36	0.93473 E-12	0.2189 E-11
38	0.19889 E-12	0.5011 E-12
40	0.42309 E-13	0.1146 E-12
42	0.89886 E-14	0.2618 E-13
44	0.18982 E-14	0.5936 E-14
46	0.38939 E-15	0.1303 E-14
48	0.68322 E-16	0.2427 E-15
50	0.000	0.000

Table A 10.2, W = 0.499 eV

Kink length $(\frac{y}{a_y})$	Discrete analysis $(\frac{aN}{N_t})$	Differential Equation analysis $(\frac{aN}{N_t})$
0	0.8799 E-01	0.8431 E-01
2	0.751113 E-01	0.7197 E-01
4	0.64075 E-01	0.6139 E-01
6	0.54619 E-01	0.5234 E-01
8	0.46519 E-01	0.4458 E-01
10	0.39580 E-01	0.3793 E-01
12	0.33636 E-01	0.3224 E-01
14	0.28545 E-01	0.2736 E-01
16	0.24183 E-01	0.2318 E-01
18	0.20447 E-01	0.1960 E-01
20	0.17246 E-01	0.1653 E-01
22	0.14504 E-01	0.1391 E-01
24	0.12156 E-01	0.1165 E-01
26	0.10144 E-01	0.9726 E-02
28	0.84203 E-02	0.8074 E-02
30	0.69439 E-02	0.6659 E-02
32	0.56793 E-02	0.5447 E-02
34	0.45959 E-02	0.4408 E-02
36	0.36679 E-02	0.3518 E-02
38	0.28729 E-02	0.2756 E-02
40	0.21919 E-02	0.2103 E-02
42	0.16086 E-02	0.1543 E-02
44	0.11089 E-02	0.1064 E-02
46	0.68081 E-03	0.6531 E-03
48	0.31412 E-03	0.3014 E-03
50	0.000	0.000

Table A 10.3, W = 0.501 eV

Kink length ($\frac{y}{a_y}$)	Discrete analysis $\frac{aN}{N_t}$	Differential Equation analysis $\frac{aN}{N_t}$
0	0.26570 E-01	0.2622 E-01
2	0.26475 E-01	0.2613 E-01
4	0.26365 E-01	0.2602 E-01
6	0.26235 E-01	0.2589 E-01
8	0.26084 E-01	0.2574 E-01
10	0.25908 E-01	0.2557 E-01
12	0.25703 E-01	0.2536 E-01
14	0.25463 E-01	0.2513 E-01
16	0.25182 E-01	0.2485 E-01
18	0.24855 E-01	0.2453 E-01
20	0.24473 E-01	0.2415 E-01
22	0.24028 E-01	0.2371 E-01
24	0.23507 E-01	0.2320 E-01
26	0.22900 E-01	0.2260 E-01
28	0.22191 E-01	0.2190 E-01
30	0.21363 E-01	0.2108 E-01
32	0.20397 E-01	0.2012 E-01
34	0.19268 E-01	0.1901 E-01
36	0.17951 E-01	0.1771 E-01
38	0.16414 E-01	0.1619 E-01
40	0.14619 E-01	0.1442 E-01
42	0.12524 E-01	0.1236 E-01
44	0.10079 E-01	0.9943 E-01
46	0.72237 E-02	0.7126 E-02
48	0.38907 E-02	0.3838 E-02
50	0.0000	0.0000

Table A 10.4, W = 0.54 eV

Kink length ($\frac{y}{a_y}$)	Discrete analysis $\frac{aN}{N_t}$	Differential Equation analysis $\frac{aN}{N_t}$
0	0.20428 E-01	0.2022 E-01
2	0.20428 E-01	0.2022 E-01
4	0.20428 E-01	0.2022 E-01
6	0.20428 E-01	0.2022 E-01
8	0.20428 E-01	0.2022 E-01
10	0.20428 E-01	0.2022 E-01
12	0.20428 E-01	0.2022 E-01
14	0.20428 E-01	0.2022 E-01
16	0.20428 E-01	0.2022 E-01
18	0.20428 E-01	0.2022 E-01
20	0.20428 E-01	0.2022 E-01
22	0.20428 E-01	0.2022 E-01
24	0.20428 E-01	0.2022 E-01
26	0.20428 E-01	0.2022 E-01
28	0.20428 E-01	0.2022 E-01
30	0.20428 E-01	0.2022 E-01
32	0.20428 E-01	0.2022 E-01
34	0.20428 E-01	0.2022 E-01
36	0.20428 E-01	0.2022 E-01
38	0.20428 E-01	0.2022 E-01
40	0.20428 E-01	0.2022 E-01
42	0.20428 E-01	0.2022 E-01
44	0.20428 E-01	0.2022 E-01
46	0.20428 E-01	0.2021 E-01
48	0.20386 E-01	0.1970 E-01
50	0.0000	

The kink spreading distance for the kink distribution in the above calculations is 50 atomic distances.

References

1. Griffith, A.A., Phil. Trans. R. Soc. London A 221, 163 (1921).

2. Inglis, C.E., (1913), "Stresses in a Plate Due to the Presence of Cracks and Sharp Corners", Trans. Inst. Naval Archit. 55, 219.

3. Orowan, E. (1955), "Energy Criteria of Fracture", Weld. Res. Supp. 34, 157-s.

4. Irwin, G.R. (1958), "Fracture", Hanbuch der Physik, Springer-Verlag, Berlin, Vol. 6, p. 551.

5. Irwin, G.R., "The Crack Extension Force for a Part-Through Crack in a Plate", Trans. ASME, J. Appl. Mech. (1962), pp. 651-654.

6. Paris, P.C. and Sih, G.C., "Stress Analysis of Cracks", ASTM STP 391, (1965), pp. 30-81.

7. Irwin, G.R., "Plastic Zone Near a Crack and Fracture Toughness", Proc. 7th Sagamore Conf., p. IV-63 (1960).

8. Dugdale, D.S., "Yielding of Steel Sheets Containing Slits", J. Mech. Phys. Sol., 8 (1960), pp. 100-108.

9. Barenblatt, G.I., "The Mathematical Theory of Equilibrium of Cracks in Brittle Fracture", Advances in Appl. Mech. 7 (1962), pp. 55-129.

10. Burdekin, F.M. and Store, D.E.W., "The Crack Opening Displacement Approach to Fracture Mechanics in Yielding Materials", J. Strain Analysis, 1 (1966), pp. 145-153.

11. Rice, J.R. (1968a), "A Path Independent Integral and The Approximate Analysis of Strain Concentration by Notches and Cracks", J. Appl. Mech. 35, pp. 379-386.

12. Rice, J.R. (1968b), "Mathematical Analysis in the Mechanics of Fracture", Fracture (ed. H. Liebowitz), Academic Press, New York, Vol. 2, Chapter 3.

13. Landes, J.D. and Begley, J.A., "The Effect of Specimen Geometry on J_{IC} ASTM, STP 514, (1972), pp. 24-39.

14. Begley, J.A. and Landes, J.D., "The J Intergral as a Fracture Criteria", ASTM STP 514 (1972), pp. 1-20.

15. Cekirge, H.M., Tyson, W.R. and Krausz, A.S., "Static Corrosion and Static Fatigue of Glass", Jour. Amer. Ceram. Soc., Vol. 58, No. 5-6, May-June 1976.

16. Anderson, W.E., "An Engineer Views Brittle Fracture History", Boeng Rept. (1969).

17. Biggs, W.D., "The Brittle Fracture of Steel", McDonald and Evans LTD (1960), pp. 13-39.

18. Wiederhorn, S.M., "Fracture Mechanics of Ceramics", Conference Proceedings, edited by R.C. Bradt, D.P.H. Hasselman and F.F. Lange (Plenum, New York, 1974) p. 613.

19. Thomson, R., Hsieh, C. and Rana, V., "Lattice Trapping of Fracture Cracks", J. Appl. Phys. 42, 3145, (1971).

20. Hsieh, C. and Thomson, R., (1963), "Lattice Theory of Fracture and Crack Creep", J. Appl. Phys. 44, p. 2051.

21. Krausz, A.S. and Eyring, H., "Deformation Kinetics", Wiley, New York, 1975.

22. Krausz, A.S., "Time Dependent Crack Propagation in Linear Elastic Solids", J. Appl. Phys. 49(7), p. 3774 (1978).

23. Gilman, J.J., Bull. Am. Phys. Soc. 15, p. 374 (1970).

24. Tobolsky, A. and Eyring, H., J. Chem. Phys. 11(1943) p. 125.

25. Speidel, M.O., "The Theory of Stress Corrosion Cracking in Alloys", (Ed. J.C. Scully), North Atlantic Treaty Organization Scientific Affairs Division, Brussels (1971).

26. Speidel, M.O., "Stress Corrosion Cracking of Aluminium Alloys", Met. Trans. A, 6, pp. 613-651 (1975).

27. Brown, S.D., "The Multibarrier Kinetics of Subcritical Brittle Crack Growth", Proc. 6th Cong. Appl. Mech. pp. 257-258, (1977).

28. Lawn, B.R., "An Atomistic Model of Kinetic Crack Growth in Brittle Solids", J. Mat. Sci. 10, pp. 469-480, (1975).

29. Swain, M.V. and Lawn, B.R., "A Microprobe Technique for Measuring Slow Crack Velocities in Brittle Solids", Int. J. Fracture Mech. 9, pp. 481-483, (1973).

30. Tyson, W.R., Cekirge, H.M. and Krausz, A.S., "Thermally Activated Fracture of Glass", J. Mates. Sci. 11, pp. 780-782, (1976).

31. Hsiao, C.C., Phys. Today, 19 (1966) p. 49.

32. Robinson, C.N., Report UTEC MSE 71-151, College of Eng; Univ. of Utah, 1971.

33. Zhurkov, S.N., Int. J. Fracture Mech. 1 (1965), p. 311.

34. Krausz, A.S., "The Theory of Non-Steady State Fracture Propagation Rate", Int. Jour. of Fracture, 12 (1976) pp. 239-242.

35. Krausz, A.S., "Crack Size Distribution in Homogenous Solids", Int. Jour. of Fracture (in press).

36. Kusenko, V.S., Ryskin, V.S., Betekhtin, V.I. and Slutsker, A.I., "Nucleation of Submicroscopic Cracks in Stressed Solids", Int. Jour. of Fracture, 11 (1975), pp. 829-840.

37. Regel, V.R. and Leksovsky, A.M., "A Study of Fatigue Within the Framework of the Kinetic Concept of Fracture", Int. Jour. of Fracture Mech. Vol. 3, No. 2, p. 99, (1967).

38. Lawn, B.R. and Wilshaw, T.R., "Fracture of Brittle Solids", Cambridge Solid State Science Series, 1975.

39. Charles, R.J., "Static Fatigue of Glass II", Jour. of Appl. Phys. 29, 11(1958), p. 1554.

40. Hillig, W.B.,"Modern Aspects of the Vitreous State", Vol. 2, pp. 152-194, Edited by J.D. Mackenzie, Butterworth, Inc., Washington, D.C., 1962.

41. Wiederhorn, S.M., "Influence of Water Vapour on Crack Propagation in Soda-Lime Glass", J. Amer. Ceram. Soc. 50 (1967), p. 407.

42. Krausz, A.S., "The Theory of Thermally Activated Processes in Brittle Stress Corrosion Cracking", Eng. Fract. Mech. 11 (1979), pp. 33-42.

43. Krausz, A.S., "The Deformation and Fracture Kinetics of Stress Corrosion Cracking", Int. Jour. Fracture 14, 1 (1978), pp. 5-15.

44. Jost, W., "Diffusion in Solids, Liquids and Gasses", Academic Press, New York (1960).

45. Crank, J., "The Mathematics of Diffusion", Oxford University Press, London 1970.

46. Shewmon, P.G., "Diffusion in Solids", McGraw-Hill, New York (1963).

47. Orowan, E., Z. Physik, 82, 235 (1933).

48. Wiederhorn, S.M. and Townsend, P.R., "Crack Healing in Glass", J. Amer. Cer. Soc. 53, p. 486, (1970).

49. Chandrasekhar, S., "Selected Papers on Noise and Stochastic Processes", Edited by Nelson Wax, Dover Publications, Inc., New York 19, New York (1954), pp. 4-92.

50. Carslaw and Jaeger, "Conduction of Heat in Solids", Oxford University Press, Second Edition, (1959).

51. Regel, V.R., Leksovski, A.M. and Sakiev, S.N., "The Kinetics of the Thermofluctuation-Induced Micro and Macrocrack Growth in Plastic Metals", Int. Jour. of Fracture 11 (1975), pp. 841-850.

52. Schonert, K., Umhauer, H. and Klemm, W., "The Influence of Temperature and Environment on the Slow Crack Propagation", Fracture 1969 (Proceedings of the 2nd Conference on Fracture, Brighton, April 1969) Chapman and Hall Ltd., London (1969), p. 474.

53. Zhurkov, S.N., Kusenko, V.S. and Slutsker, A.I., "Submicrocrack Formation Under Stress", Fracture 1969 (Proceedings of the 2nd Conference on Fracture, Brighton, April 1969) Chapman and Hall Ltd., London, pp. 531-543.

54. Krausz, A.S., "The Random Walk Theory of Crack Propagation", Eng. Fracture Mech. (in Press).

55. Pollet, J.C. and Burns, S.J., "An Analysis of Slow Crack Propagation Data in PMMA and Brittle Materials", Int. Jour. of Fracture, 13 (1977), pp. 775-768.

56. Pollet, J.C. and Burns, S.J., "Thermally Activated Crack Propagation Theory", Int. Jour. of Fracture 13 (1977), pp. 667-679.

57. Gladstone, Samuel, Laider, K.J. and Eyring, H., "Theory of Rate Processes", p. 369, McGraw-Hill Book Co., New York, 1941.

58. Charles, R.J. and Hillig, W.B., pp. 511-527 in Symposium on Mechanical Strength of Glass and Ways of Improving It, Italy, September 1961, Union Scintifique Continentale du Verre, Charleroi, Belgium 1962.

59. Hillig, W.B. and Charles, R.J., pp. 682-705 in High Strength Materials Edited by V.R. Zackey, John Wiley and Sons Inc., New York, 1965.

60. Evans, A.G. and Linza, M., "Failure Prediction in Structural Ceramics Using Acoustic Emission", J. Amer. Ceram. Soc. 56 |11|, pp. 575-81,(1973).

61. Krausz, A.S., "The Theory of Non-Steady State Fracture Kinetics Analysis", (to be published).

62. Freiman, S.W., "Effect of Alcohol on Crack Propagation in Glass", J. Amer. Ceram. Soc. 57 |8|, pp. 350-353 (1974).

63. Krausz, A.S. and Faucher, B., "The Steady-State Kinetics of Double-Kink Spreading", Scripta Met. Vol. 13, No. 2, pp. 91-94.

64. Krausz, A.S., "The Statistical Mechanics Theory of Griffith Crack Behavior", (to be published).

65. Carlaw, H.S. and Jaeger, J.C., "Operational Methods in Applied Mathematics", Oxford University Press, Amen House, London E.C. 4, Second Edition (1947).

66. Wiederhorn, S.M. and Boltz, L.H., "Stress Corrosion and Static Fatigue of Glass", J. Amer. Ceram. Soc. 50 (1970), pp. 543-548.

67. Wiederhorn, S.M., Johnson, H., Diness, A.M. and Heuer, A.H., "Fracture of Glass in Vacuum", Jour. of Amer. Ceram. Soc. 57, 8(1974), pp. 336-341.

68. Reference Manual, IMSL Library 1, 5th Edition, International Mathematics and Statistical Libraries Inc., Houston, Texas, U.S.A., 1975.

69. Handbook of Chemistry and Physics, Weast 53rd Edition 1972-1973, CRC.

70. Benson, W.S., "The Foundations of Chemical Kinetics", McGraw-Hill series in Advanced Chemistry, McGraw-Hill Book Co. Inc. (1960), p. 14.

71. Petrov, V.A. and Orlov, A.N., "Statistical Kinetics of Thermally Activated Fracture", Int. Jour. of Fracture, 12 (1976), pp. 231-238.

72. Matsen, F.A. and Franklin, J.L., "A General Theory of Coupled Sets of First Order Reactions", J. Am. Chem. Soc. 72, p. 3337 (1950).

73. Broek, David, "Elementary Engineering Fracture Mechanics", Sijhoff and Noordhoff (1978), Alphen aan den Rijn, The Netherlands.

74. Zwolinski, B.J. and Eyring, H., "The Non-Equilibrium Theory of Absolute Rates of Reaction", J. Am. Chem. Soc. 69, p. 2702 (1947).

75. Lewis, E.S. and Johnson, M.D., "The Reactions of p-Phenylene-bis-diazonium Ion With Water", J. Amer. Chem. Soc. 82, p. 5399 (1960).

76. Erying, H. and Zwolinski, B.J., Rec. Chem. Progra., 87 (1947).

77. Prigogine, I., Nicolis, G. and Allen, P.M., in "Chemical Dynamics", J.O. Hirsch-felder and D. Henderson, Eds., Wiley, New York, 1971.

78. Sokolnikoff, I.S. and Redheffer, R.M., "Mathematics of Physics and Modern Engineering", Second Edition, 1966, McGraw-Hill Book Co., N.Y., p. 148.

79. Kreyszig, E., "Advanced Engineering Mathematics", John Wiley and Sons, Inc., New York (1972), Third Edition, p. 734.